The Pennsylvania State University

The Graduate School

College of Earth and Mineral Sciences

A QUANTITATIVE ASSESSMENT OF THE EFFECTS OF BASE LEVEL FALL AND BASIN DEPTH ON RIVER-DOMINATED DELTAS

A Thesis in

Geosciences

by

James A. Cederberg

Submitted in Partial Fulfillment
of the Requirements
for the Degree of

Master of Science

December 2014

The thesis of James A. Cederberg was reviewed and approved* by the following:

Rudy L. Slingerland
Professor of Geology
Thesis Adviser

Elizabeth Hajek
Assistant Professor of Geosciences

Michael Arthur
Professor of Geosciences

Demian Saffer
Professor of Geosciences
Interim Associate Head of Graduate Programs

*Signatures are on file in the Graduate School.

Abstract

A better understanding of how deltas form and their resulting morphologic and stratigraphic characteristics is needed to improve geoscientist's abilities to manage deltas and their wetland systems as well as explore and develop hydrocarbon resources. Inherently, deltas form as shoreline regressions, making sea level cycle interpretation difficult. Here we seek to quantify the effects of relative base level fall (BLF) and basin depth on the morphology and internal geometry of river-dominated deltas in order create a model that can be applied to distinguish between deltas experiencing forced regressions and normal regressions. Doing so will allow us to more accurately interpret the sequence stratigraphic record. We propose measuring the relative influence of BLF and basin depth on delta formation through the shoreline trajectory. The shoreline trajectory is defined as the locus of points defined by the shoreline in the vertical plane. We find that as basin depth increases, the number of active distributaries decreases because river mouth bars take longer to aggrade leading to fewer bifurcations. Increased basin depth increases the avulsion period because it takes longer for enough sediment to be deposited such that a distributary channel becomes super-elevated and can avulse. Fewer active distributaries and longer avulsion periods lead to deposition being focused in one region for greater periods of time which results in more rugose shorelines and more variability in foreset dip directions. Deeper basin depths are associated with smaller average lobe areas because more sediment is required to form a lobe of equal areal extent in a deep basin than in a shallow basin. We find that the greater volume of sediment required in deeper basins outweighs the more focused deposition also associated with a deeper basin, thereby forming smaller delta lobes on average. We find that the thickness of topset deposits varies little with basin depth while the foreset thickness varies greatly. This leads to decreased volumetric topset/foreset ratios in deeper basins. Deeper basins have delta fronts that are less affected by tractional sediment transport resulting in larger clinoform average dip magnitudes. Higher rates of BLF results in elongate a deltas with greater topset roughness caused by down-stepping lobes. Higher rates or BLF are also associated with larger total topset areas. Twelve deltas simulated deltas are formed under different rates of BLF and basin depths using Delft3D, an engineering-grade, 2D vertically integrated hydrodynamic and morphodynamic model. The model is an improvement over earlier models because it accounts for multiple grain size fractions, cohesive sediment fractions, and bed stratigraphy. The model findings are validated with data collected from the Goose River Delta, sandy, fjord-style delta prograding into the 30m deep basin of Goose Bay, Labrador, Canada and experiencing 5 mm of BLF per year for the last 8000 years. A re-interpretation of the Cretaceous Panther Tongue Member of the Starr Point Formation in the Book Cliffs of Utah, USA is based on clinoform dip and dip direction variability data. We propose that the southern lobe of the Panther Tongue Delta, near Crandall Canyon, has higher clinoform dips due to it prograding into deeper water as opposed to BLF because clinoform heights increase from proximal (north) to distal (south) indicating deeper water depths in the south.

Table of Contents

List of Figures

List of Tables

Introduction

A better understanding of how deltas form and their resulting morphologic and stratigraphic characteristics is needed to improve geoscientist's abilities to manage deltas and their wetland systems as well as explore and develop hydrocarbon resources. To this end we seek to improve current predictive tools by modeling deltas forming under varying rates of base level fall and initial basin depths, validating model results with the modern Goose River Delta in Labrador, Canada which is experiencing 5 mm yr^{-1} of base level fall, and applying validated model results to the Panther Tongue Member of the Star Point Formation near Helper, Utah as a case study.

Sequence stratigraphy has become the de facto predictive tool for interpreting the relationships between facies successions and base level changes, yet much work must still be done to fully quantify these relationships. At the heart of sequence stratigraphy is the balance of sediment supply and the change in accommodation, and deltas represent an environment where this balance is inherently complex. Quantification of how deltas form in different base level conditions will help refine sequence stratigraphic principles for these complex systems and create a more robust predictive tool.

Background

There are two contrasting views on how relative base level fall (BLF) affects deltas. Some researchers think that BLF causes deltas to elongate and develop incised valleys because lateral migration of channels and avulsions are suppressed (Suter and Berryhill 1985; Sala and Long 1989; Corner et al., 1990; Walker 1992; Posamentier and Allen 1992a; Posamentier and Allen 1992b; Hart and Long 1996; Posamentier and Morris 2000; Howell and Flint 2003; Porebski and Steel 2003; Porebski and Steel 2006). Whereas others think deltas can remain in an aggradational regime during BLF such that their planforms and stratigraphies give no indication that accommodation space is decreasing (Muto and Steel

2004; Muto and Swenson 2005; Muto and Swenson 2006; Swenson and Muto 2007; Petter and Muto 2008; Lorenzo-Trueba et al. 2013; Prince and Burgess 2013).

The former view arose in early conceptual stratigraphic models of deltas. Falling base level was thought to form elongate deltas with incised valleys and suppressed lobe and channel switching (Walker 1992; Posamentier and Allen 1992a), and create channelized sediment bypass zones cutting across older delta lobes (Fig.1) (Posamentier and Allen 1992a; Posamentier and Allen 1992b). Later workers modified this view, arguing that the formation of incised valleys was confined to shelf-edge deltas (Suter and Berryhill 1985; Porebski and Steel 2003; Porebski and Steel 2006). Posamentier and Morris (2000) and later Howell and Flint (2003) formalized these earlier ideas in a set of 8 characteristic features that should be seen in the stratigraphic record for both inner-shelf and shelf-edge, forced-regressive deltas (i.e., deltas subject to BLF, also referred to as falling-stage deltas):

1) presence of a significant zone of lateral separation between successive shoreface deposits;
2) sharp-based shoreface/delta front deposits;
3) progressively lower relief clinoforms going from proximal to distal;
4) occurrence of long-distance regression;
5) absence of fluvial and/or coastal plain/delta plain facies capping the proximal portion of regressive deposits;
6) presence of a seaward-dipping upper bounding surface;
7) increased average sediment grain size in regressive deposits going from proximal to distal due to lack of accommodation for coarse grains on the topset; and
8) presence of “foreshortened” stratigraphic successions where the measured thickness of parasequences is considerably less than estimates of paleowater depth (i.e., there is a subaqueous

clinform rollover some distance away from the shoreline), suggesting coeval relative sea-level fall.

Based upon these criteria, both Posamentier and Morris (2000) and Howell and Flint (2003) argued that the Panther Tongue Mbr. of the Starr Point Fm. near Helper, UT, USA is a forced-regressive delta.

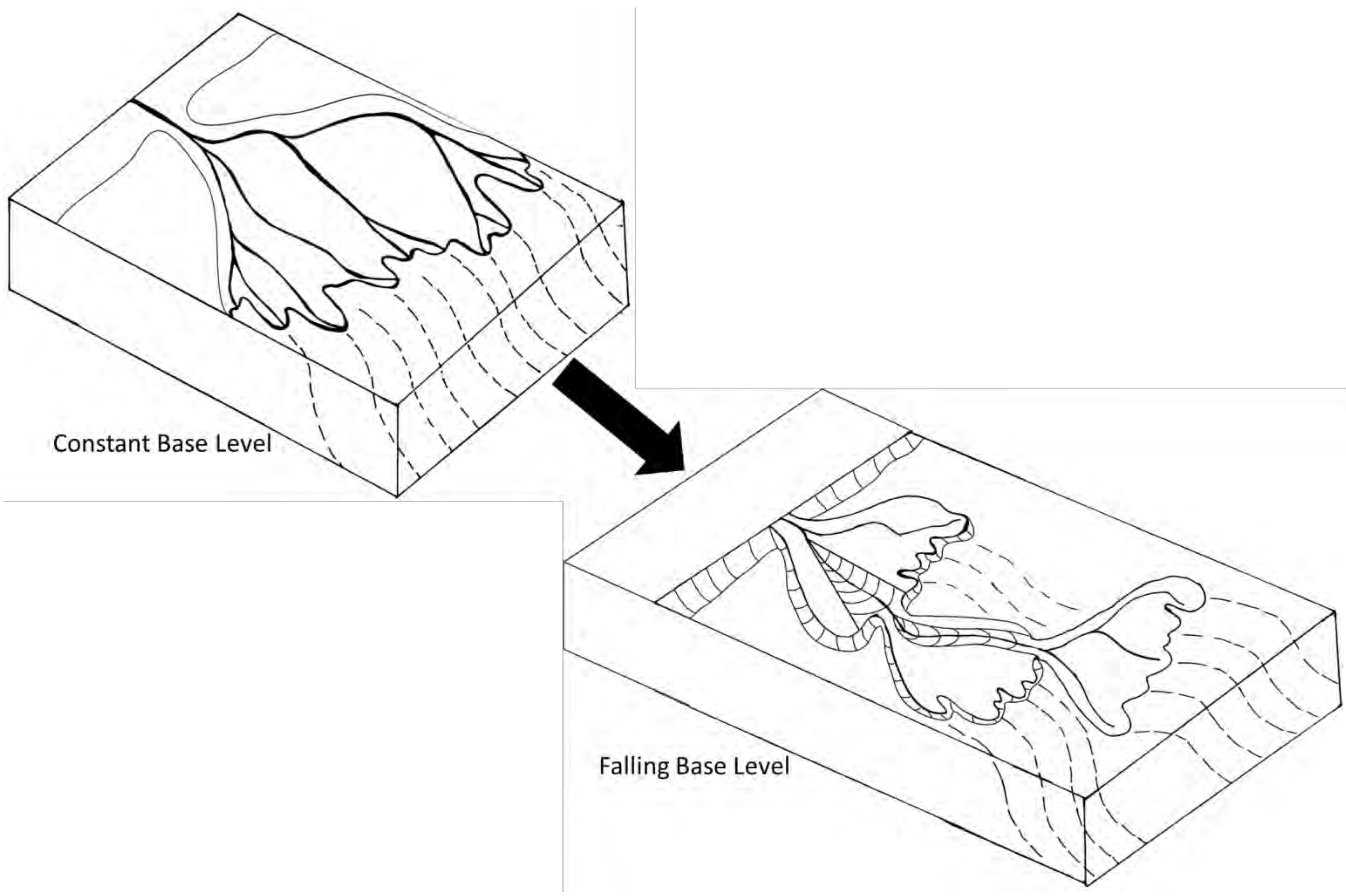

Figure 1. Early conceptual models suggested that BLF forms elongate deltas with down-stepping lobes, incised valleys, and suppressed lobe and channel switching, as well as creates channelized sediment bypass zones cutting across older delta lobes. Dotted lines indicate the delta front.

Studies of modern deltas in areas of glacial rebound generally supported this earlier view of delta response to BLF (Corner et al., 1990; Sala and Long, 1989; Hart and Long, 1996). Researchers pointed out their terraced paleoshorelines, abandoned delta lobes, and distributary incision (Hart and Long 1996). The latter prevents lateral fluvial erosion of the topset until base level begins to rise during early lowstand. This observation suggests that criterion 5 of Posamentier and Morris (2000) is likely the result of subsequent base level rise rather than occurring during BLF.

That deltas can remain in an aggradational regime during BLF was first suggested by numerical and physical models. Muto and Steel (2004) formed unscaled flume deltas experiencing varying dimensionless base level fall rates, water discharge to sediment discharge ratios, and basin slope. They found that numerical and experimental deltas experiencing BLF remain aggradational until an intrinsic response time has been met, at which time the first major incision of the distributary channels form. Muto and Steel (2004) called this type of downcutting “auto-incision.” The intrinsic response time, τ (yr), was defined by Swenson and Muto (2007) as $\tau = \frac{q_{so}^2}{v}|\dot{r}|^{-2}$ where q_{so} is the sediment supply ($m^2\ yr^{-1}$), $\dot{r}$ is the rate of BLF ($m\ yr^{-1}$), and v is the fluvial diffusivity ($m^2\ yr^{-1}$). The intrinsic response time represents a threshold time at which point the channel abandons its former floodplain and incises due to continued steady BLF. Prior to this time the delta continues to prograde seaward and as a consequence, the whole channel network up to the mountain front must aggrade to maintain its energy slope. Thus the alluvial-bedrock transition migrates progressively landward and the alluvial plain continues to rise, even after the initiation of BLF. After the intrinsic response time, a wave of incision sweeps up the system. Rivers then reach grade, or create a sediment bypass zone in which no net erosion or deposition is occurring, if the rate of BLF varies with the square root of time (Muto and Steel 2005). This behavior arises as the result of the linearly sloping basin used in their experiment which causes the shoreline and delta-toe to advance basinward at a constantly decreasing rate. Muto and Swenson (2006) built upon this work and found that rivers can attain grade via an autogenic response to steady BLF, regardless of the rate of BLF, if the initial basin slope is the same as the slope of the graded reach. In that study, the authors conducted flume experiments fed only with sand to form deltas. These flume experiments were unscaled in that they did not account for Froude-scaling. This study contradicts Muto and Steel’s (2005) theory that base level fall must vary with the square root of time in order for a river to attain grade. In a numerical modeling and unscaled flume experiment, Swenson and Muto (2007) determined that deltas are unable to attain grade while experiencing steady BLF and actually remain aggradational until the intrinsic response time is reached, and then the deltas become incisional. Lorenzo-Trueba et al. (2013) use a geometric, mass-balance model that treats the shoreline and the alluvial-bedrock transition as moving boundaries to support the idea that BLF is not a sufficient condition for incision.

The studies summarized above underscore the roles played during BLF by the relative magnitudes of the initial fluvial slope and the basin floor slope. If the fluvial slope is greater than the slope of the receiving basin, the alluvial river aggrades faster during BLF, resulting in sediment starvation of its delta and retreat of the delta shoreline. Petter and Muto (2008) called this phenomenon "auto-detachment." Petter and Muto (2008) observed "auto-detachment" in an unscaled flume experiment and a diffusion-based forward numerical model in which cohesive sediment was ignored. Even the characteristic features in the list above may not be indicative of forced regressive deltas. Prince and Burgess (2013) report that topset/foreset ratios are not indicative of BLF and are non-unique. They arrived at this conclusion by conducting numerical experiments using the diffusion-based numerical model, named Dionisos, in which they varied the rate of BLF and the basin slope.

In summary, there are two contrasting views on delta response to BLF. Some workers argue that deltas experiencing BLF will become elongate and incised, whereby lateral channel migration and distributary avulsions are suppressed (Suter and Berryhill 1985; Sala and Long 1989; Corner et al., 1990; Walker 1992; Posamentier and Allen 1992a; Posamentier and Allen 1992b; Hart and Long 1996; Posamentier and Morris 2000; Howell and Flint 2003; Porebski and Steel 2003; Porebski and Steel 2006). On the other hand, others argue that falling-stage deltas will remain aggradational for a time, and then experience a variety of phenomena including graded, "auto-incision", and "auto-detachment".

This varied response may produce non-unique stratigraphies (Muto and Steel 2004; Muto and Swenson 2005; Muto and Swenson 2006; Swenson and Muto 2007; Petter and Muto 2008; Lorenzo-Trueba et al. 2013; Prince and Burgess 2013).

The effects of water depth on delta morphology and internal geometry have been typically considered by categorizing deltas from shallowest to deepest as bayhead, inner shelf, mid-shelf, and shelf-margin deltas (Porebski and Steel, 2006). Conceptual models (Porebski and Steel 2006, Kolla et al. 2000) predict that bayhead deltas will possess many distributaries, be river-dominated, and be confined and funnel-shaped. Inner-shelf deltas are commonly thought to have shallow clinoform slopes (Reading and Collison 1996) and to fall within the Galloway et al. (1975) tripartite regime of river-, wave-, and tide dominated deltas. Mid-shelf deltas are predicted to possess steeper clinoforms (Posamentier and Morris 2000), and be either river- or wave- dominated. Porebski and Steel (2006), Kolla et al. (2000) suggested that mid-shelf deltas are often associated with BLF and therefore should have thin to absent topsets due to incision during BLF. It is unclear whether the authors recognize any mid-shelf deltas that are not experiencing BLF. Shelf-margin deltas are thought to be elongate deltas that possess the steepest clinoforms (Porebski and Steel 2006, Kolla et al. 2000). In summary, conceptual models predict that shelf-margin deltas in deep water will become more elongate and form steeper clinoforms than shallow-water, bayhead and inner-shelf deltas. It is important to note that many conceptual models are underlain by sequence stratigraphic logic which tends to conflate basin depth and rate of BLF, failing to acknowledge that deltas may prograde into deep-water without regard to the rate of base level rise or fall.

The goal of this paper is to help resolve these debates by quantifying the effect of varying rates of relative base level fall and basin depths on the planform and internal geometry of properly scaled deltas formed with multiple grain size fractions and cohesive sediments. Quantification allows for a better understanding of the relative influence of different amounts of forcings on delta planforms and internal geometries. Consequently, our quantification provides a more widely applicable predictive tool for the interpretation of deltas experiencing BLF.

Statement of the Problem

Previous studies have focused on either the morphology of modern systems (Sala and Long 1989; Corner et al. 1990; Hart and Long 1996), the stratigraphy of ancient systems (Suter and Berryhill 1985; Walker 1992; Posamentier and Allen 1992a; Posamentier and Allen 1992b; Posamentier and Morris 2000; Howell and Flint 2003; Porebski and Steel 2003; Porebski and Steel 2006), or in some cases highly simplified modeling of both (Muto and Steel 2004; Muto and Swenson 2005; Muto and Swenson 2006; Swenson and Muto 2007; Petter and Muto 2008; Lorenzo-Trueba et al. 2013; Prince and Burgess 2013). Here we hope to better understand delta response to falling base level and basin depth by using Delft3D modelling. No previous modelling study has thus far been a 2D vertically-averaged flow model accounting for multiple grain sizes, cohesive sediment, and bed stratigraphy, so this paper represents a significant improvement over previous models. Here, we define base level fall as any relative drop in sea or lake level, regardless of the origin of the relative fall. We attempt to answer two questions: 1) when and under what conditions of base level fall rate and basin depth will a delta switch from progradation and aggradation to downstepping and degradation; and 2) what morphological features and internal geometries if any, are characteristic of a falling-stage delta?

A useful non-dimensional parameter incorporating both BLF and basin depth is the shoreline trajectory, S_T:

$$S_T = \frac{\dot{r}}{PR}, \qquad (1)$$

where $\dot{r}$ is the rate of relative base level fall (mm yr^{-1}) and PR is the time-averaged progradation rate of the delta (mm yr^{-1}) spatially averaged over the delta perimeter, defined as

$$PR = (A/P)/t \tag{2}$$

where A equals topset area (mm^2), P equals delta shoreline length (mm), and t is time (yr). Note that if the rates of BLF and sediment fluxes of two deltas are equal, then the progradation rate is set solely by the basin depth.

We hypothesize that deeper initial basin depths will result in fewer active distributaries, longer avulsion periods, a more rugose shoreline, greater foreset dip azimuth variability, larger clinoform dip magnitudes, lower topset/foreset ratios, and smaller average delta lobe areas while higher rates of base level fall should result in greater topset roughness. We predict that deeper initial basin depth will result in longer time periods for river mouth bars to aggrade to a height at which they can bifurcate distributaries which in turn causes fewer active distributaries. With deeper initial basin depths channels must aggrade more in order to become super-elevated and avulse, therefore longer time periods are required for a channel to become super-elevated and avulse. This process results in an increased avulsion period. Fewer active distributaries and longer avulsion periods should focus sediment deposition in fewer locations for longer periods of time thereby creating irregular, rugose shorelines. Based on this logic we expect deltas with deeper initial basin depths to have more rugose shorelines than deltas forming in shallow basins. The more focused deposition associated with deeper initial basin depths should also result in reduced foreset dip azimuth variability. Delta lobes in deeper basins require more sediment per unit of area; therefore deeper basin depths should result in smaller delta lobe areas on average. Deeper basin depths result in tractional sediment transport occurring over a smaller portion of the delta front than in shallower basins. Tractional sediment transport tends to create shallower clinoform slopes than suspended transport; therefore we expect deeper initial basin depths to result in tractional transport accounting for less of the total sediment transport along the delta front and larger clinoform dip magnitudes. We predict that deeper basins will result in lower topset/foreset ratios because while the thickness of topset deposits, set by the height of levees and point bars in distributary channels, should be relatively constant across basin depths, the foreset thicknesses must be larger in deeper basins. Higher rates of BLF should have lobes that downstep by larger amounts leading to greater topset roughness. In contrast to Posamentier and Morris (2000), we expect no change in mean grain size across delta lobes from proximal to distal because any change in the amount of coarse-grained sediment in the total sediment load of a given distributary channel should be small in relation to the total sediment load delivered to that distributary channel by the main channel feeding the delta.

Our approach is to build deltas under various boundary conditions using Delft3D, a high-complexity numerical model often used in engineering studies, and perform an in-depth validation study of the model by testing those model predictions against morphological and stratigraphical data from the modern Goose River Delta, Labrador where relative base level has fallen at the rate of at least 5 mm yr^{-1} over the last 7,000 yrs. We then attempt to better understand the origin of the Panther Tongue Member of the Starr Point Formation near Helper, UT, USA using the results of the modeling study. This approach allows us to validate model predictions with a modern delta and test those predictions against a delta in the rock record as a case study.

The rest of this paper is structured such that it brings the reader through the model development, validation, and application. To this end, the variables of interest will first be defined. The Delft3D modelling approach and methods will be described, followed by model results and a discussion of their significance. Next, an overview of the Goose River Delta and the methods employed to study it will be presented, followed by results from the Goose River Delta. A discussion of the Goose River Delta validation study will follow. Validated model results will then be applied to the Panther Tongue Member as a case study. Finally, the key findings and conclusions of this study will be presented.

Variables

Nine variables (Fig. 2) are used to characterize deltas in this study: (1) number of active distributaries, (2) avulsion period, (3) shoreline rugosity, (4) foreset dip-azimuth uniformity statistic, (5) average clinoform dip magnitude, (6) topset/foreset thickness ratio, (7) topset roughness, (8) coefficient of determination for degree of coarsening or fining of delta lobes from oldest to youngest, and (9) the average delta lobe subaerial area. These variables were chosen to characterize the general planform and stratigraphy of because they are process-focused, and test existing conceptual models of deltas experiencing BLF.

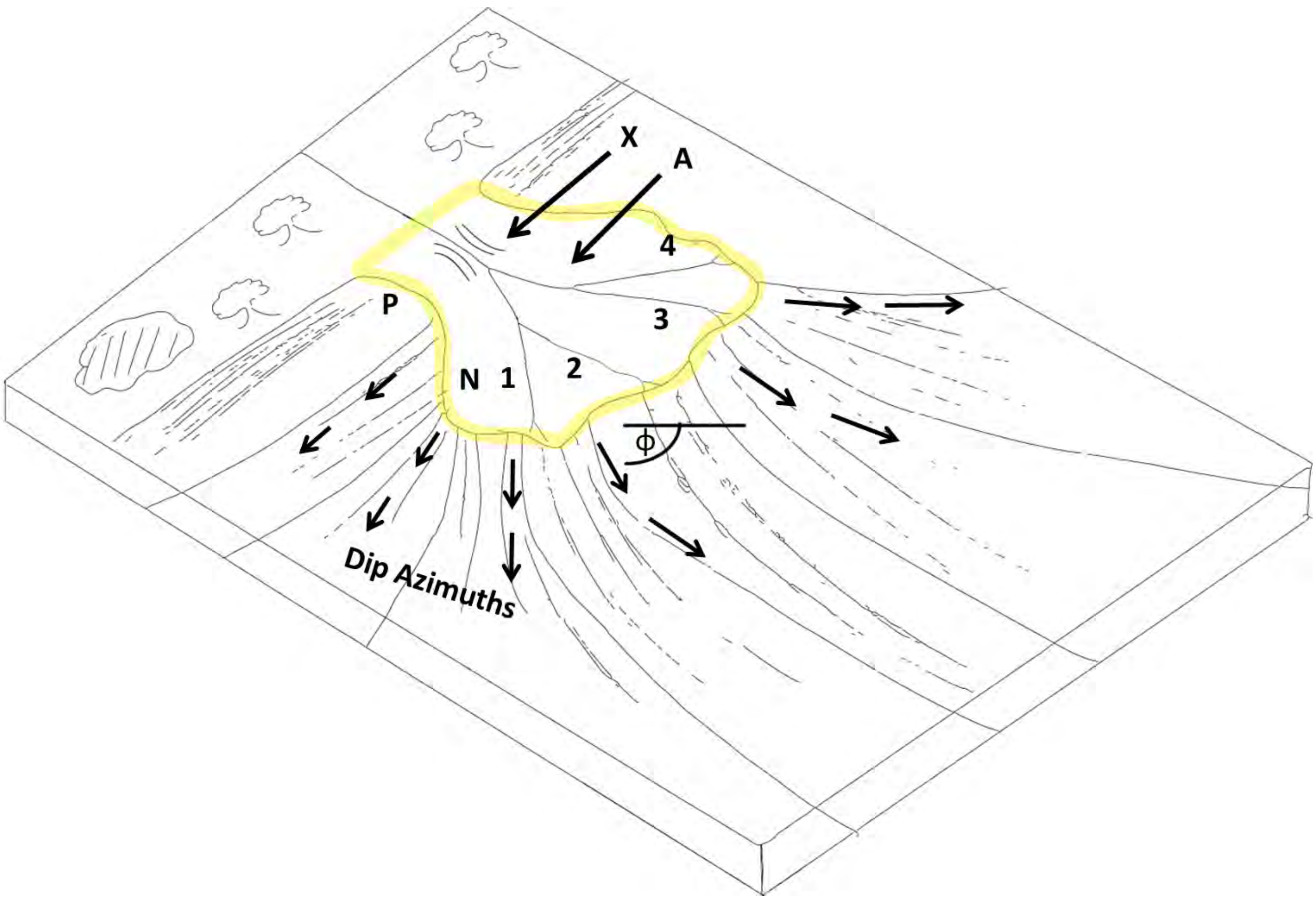

Figure 2. In the schematic delta above, there are four active distributaries; therefore N = 4. The shoreline rugosity is defined as $R=P^2/4\pi A$, where P is the topset perimeter (highlighted in yellow) and A is the topset area (the area within the yellow polygon). Clinoform dip magnitudes, ϕ,are averaged across the whole delta foreset. The dip azimuths at grid points on the foreset are used to compute the foreset dip azimuth variance, $\bar{\boldsymbol{R}}$. The topset roughness, X, is defined as the standard deviation of surface elevations within the yellow polygon.

The number of active distributaries in the modeled deltas, N, is defined as the time-averaged number of simultaneously active distributaries that are at least 50 m wide at their widest point and have a depth-averaged flow velocity greater than 0.8 m s^{-1}. 0.8 m s^{-1} is the flow velocity that allows the user to clearly differentiate between overland and channelized flow in the Delft3D models. Flow velocities less than 0.8 m s^{-1} are commonly associated with overland flow or small distributaries. For the modern Goose River Delta, we counted distributaries that were at least 50 m wide at their widest point in aerial photographs taken in 1951, 1970, 1975, 1987, 1998, and 2012. Values from each year were given equal weight and averaged. No flow velocity criterion was used. This variable could not be measured in the Panther Tongue Delta. The number of active distributaries is of interest because it is a strong control on a number of other delta morphometries including shoreline rugosity.

The avulsion period, T, is defined as the average recurrence interval for major avulsions or channel reoccupations of former channels. A major avulsion is defined operationally as a shift in locus of deposition of more than 5 channel widths (i.e., a lobe switching event). For the modeled deltas the intervals between avulsions were noted and averaged. We calculated the avulsion period for the Goose River Delta by dividing the number of identifiable, active, and abandoned lobes by the time it took to form the identified lobes. We identified five lobes, and were able to determine the duration of lobe formation from radiocarbon dates. Avulsion period was not measured in the Panther Tongue Mbr. The avulsion period is important because it dictates how long sediment deposition is focused at one location and therefore the shape of the delta.

Shoreline rugosity is measured in the model simulations and the modern Goose River Delta following Burpee et al. (in review). The shoreline rugosity, R, is defined as:

$$R = P^2/4\pi A \tag{3}$$

where P is the delta's shoreline perimeter (km) and A is the delta's topset area (km^2). Higher values of R correspond to more complex shorelines. The shoreline is delineated in the modeled deltas using the open angle method with a threshold angle of 25° (Shaw et al. 2008). For the Goose River Delta, the shoreline of the whole delta complex, including paleoshorelines of abandoned lobes, was delineated by interpreting aerial photographs and a digital elevation model. Shoreline rugosity was not measured in the Panther Tongue Mbr. Shoreline rugosity is a valuable statistic because it gives a sense of how the delta is shaped which could be useful in delta management and oil and gas exploration.

Foreset dip azimuth variance, $\bar{R}$, is measured by calculating the length of the mean resultant vector from the azimuthal data and normalizing for the number of samples (Jones 2006). The length of the resultant vector, R, is defined by:

$$R = \sqrt{X^2 + Y^2} \tag{4}$$

where X and Y are the summed x and y components (L) of each foreset dip azimuth, respectively. $\bar{R}$ is defined as:

$$\bar{R} = R/N \tag{5}$$

where N is the sample size. $\bar{R}$ varies between 0-1. A value of 1 means that the length of the resultant vector length is equal to the sample size indicating the foreset dip azimuths have little variance and are all oriented in the same direction. A value of 0 indicates a large variance in foreset dip azimuths with the vectors oriented more equally around the compass. The foreset dip azimuth variance provides insight into both how complex the delta front is (a low $\bar{R}$ value) and how elongate a delta is (a high $\bar{R}$ value) (Fig. 3).

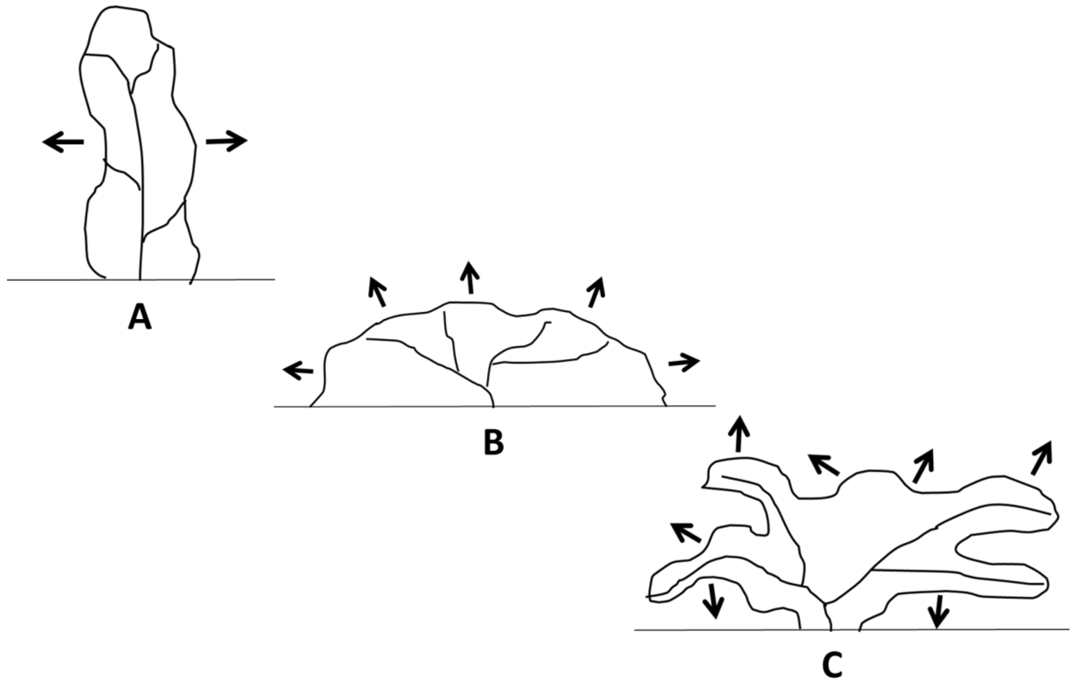

Figure 3. Foreset dip azimuth variance increases ($\bar{\boldsymbol{R}}$ decreases) from A to C. Elongate deltas (A) have less variance in foreset dip azimuths with most dips oriented perpendicular to the direction of progradation. Fan deltas (B) have a moderate amount of variance in foreset dip azimuths, but tend not to have any azimuths in oriented in the southern hemisphere (90° - 270°). Irregularly-shaped deltas (C) have the most variability in foreset dip azimuths because they have dips oriented equal proportion around the entire compass (0°-360°).

Aspect ratio is measured to convey a sense of how elongate a delta is. The aspect ratio is defined as the ratio between the width of the delta perpendicular to the main channel and the length of the delta from proximal to distal. The width and length are measured by fitting a rectangle to the shoreline of the delta such that the most extreme locations in each direction are just encompassed by the rectangle (Fig. 4). A high aspect ratio indicates that the delta does not extend very far into the basin, but rather extends parallel to the pre-existing beach. A low aspect ratio indicates an elongate delta prograding far into the basin in relation to its width, and could be useful for hydrocarbon exploration.

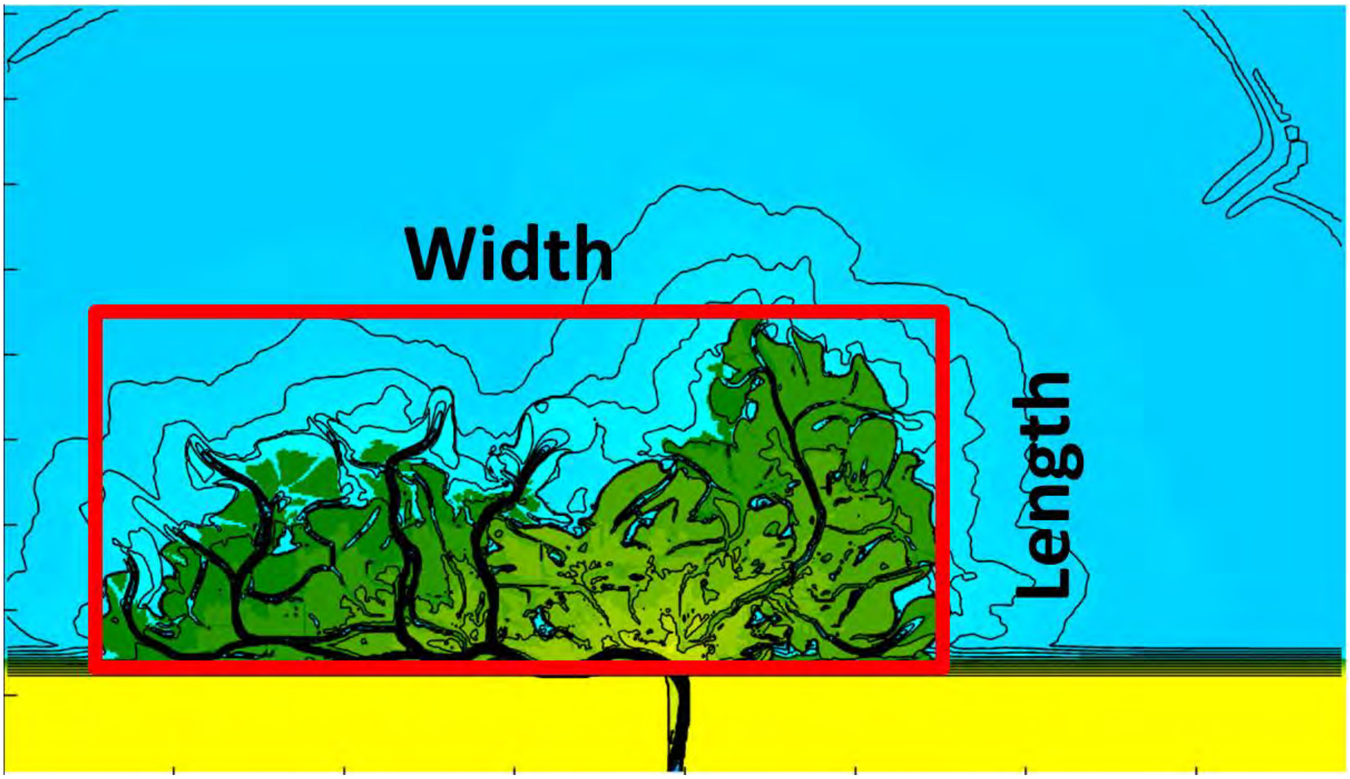

Figure 4. Aspect ratios are calculated by dividing the width or a delta by the length. Width and length are defined by drawing a rectangle that completely encompasses the delta. High aspect ratios indicate wide deltas like the one shown here, while low aspect ratios indicate elongate deltas.

The average clinoform dip magnitude, ϕ, is the spatially averaged true dip taken from the surface of a clinoform. Clinoform dips magnitudes from the model simulations were calculated from the clinoform at the last timestep by extracting the bed slope at each 25 m x 25 m grid point within the foreset region. The foreset is defined as the region between the topset and bottomset (Gilbert 1885). The extent of the foreset was defined as all elevations below -0.1 m MSL down to the clinoform toe where the dip magnitude became less than 0.008°. It should be noted that Delft3D does not simulate foreset slumping or turbidity currents. Therefore the dip magnitude in the model is expected to be higher on average than would be found in nature. For the Goose River Delta, the average clinoform dip magnitude was taken from a multibeam bathymetry survey of the southern active delta lobe. The multibeam bathymetry point data were interpolated into a raster in ArcGIS. Slopes were calculated from the raster using Arc Toolbox. The foreset region was extracted and averaged in the same fashion as for the Delft3D simulations. Clinoform dips were gathered from the Panther Tongue using a laser ranger to measure two trends and plunges of foresets on two faces with differing bearings. The attitude of the resulting bed was then corrected for tectonic dip. Locations of these measurements are shown in Figure 5. These data were gathered throughout the extent of the Panther Tongue Mbr. outcrop belt, but these stratigraphic data are inherently less representative of the ancient system than the model and modern delta data. Clinoform dip magnitudes are easily measurable in the field and in seismic line and could be inverted to help determine the basin depth and rate of BLF that were influencing a delta's formation.

Topset roughness, X, is defined as the standard deviation of topset elevations that are greater than 0 m above MSL. Edmonds and Slingerland (2010) conjectured that this variable should be correlated with the avulsion period because high channel levees that should suppress avulsions also increase the topset roughness. Topset roughness was extracted from the Delft3D deltas by calculating the standard deviation of elevations taken every 25 m that were greater than the final base level. Topset roughness was measured on the Goose River Delta from dGPS points taken at random intervals along a strike line across the delta. The topset of Panther Tongue Delta has been removed by subsequent erosion and was not measured. Topset roughness is a good indicator of the degree of down-stepping that has occurred.

Proximal to distal trends in delta grain size for the Delft3D simulations were measured as a rate of fining, G. The average grain size of each delta lobe in a simulation was approximated using the D50 of 100 representative cells of each lobe each 0.1 m thick x 25 x 25 m. The D50 of each lobe was then regressed against distance from the delta apex to the toe of the delta lobe. The slope of the regression line corresponds to G. A large value of G indicates a large rate of fining in delta lobes from proximal to distal across the whole delta. This variable was not measured for the Goose River Delta. Grain sizes were measured in outcrops of the Panther Tongue, although not enough data regarding the number, position, and age of lobes were available to perform a meaningful correlation. Mean grain size could be inverted to determine the basin depth and rate of BLF conditions in which a delta formed.

Average delta lobe area, A, in the Delft3D simulations is defined as the areal extent of the topset for each lobe at the time of abandonment. The shoreline was defined as the 0 m MSL contour separating the subaerial and subaqueous portions of the delta. The 0 m MSL contour was not traced into distributary channels. Delta lobes in the Goose River Delta were delineated and measured using a digital elevation model and aerial photographs. This variable was not measured for the Panther Tongue Delta. Average lobe size would be useful for hydrocarbon exploration.

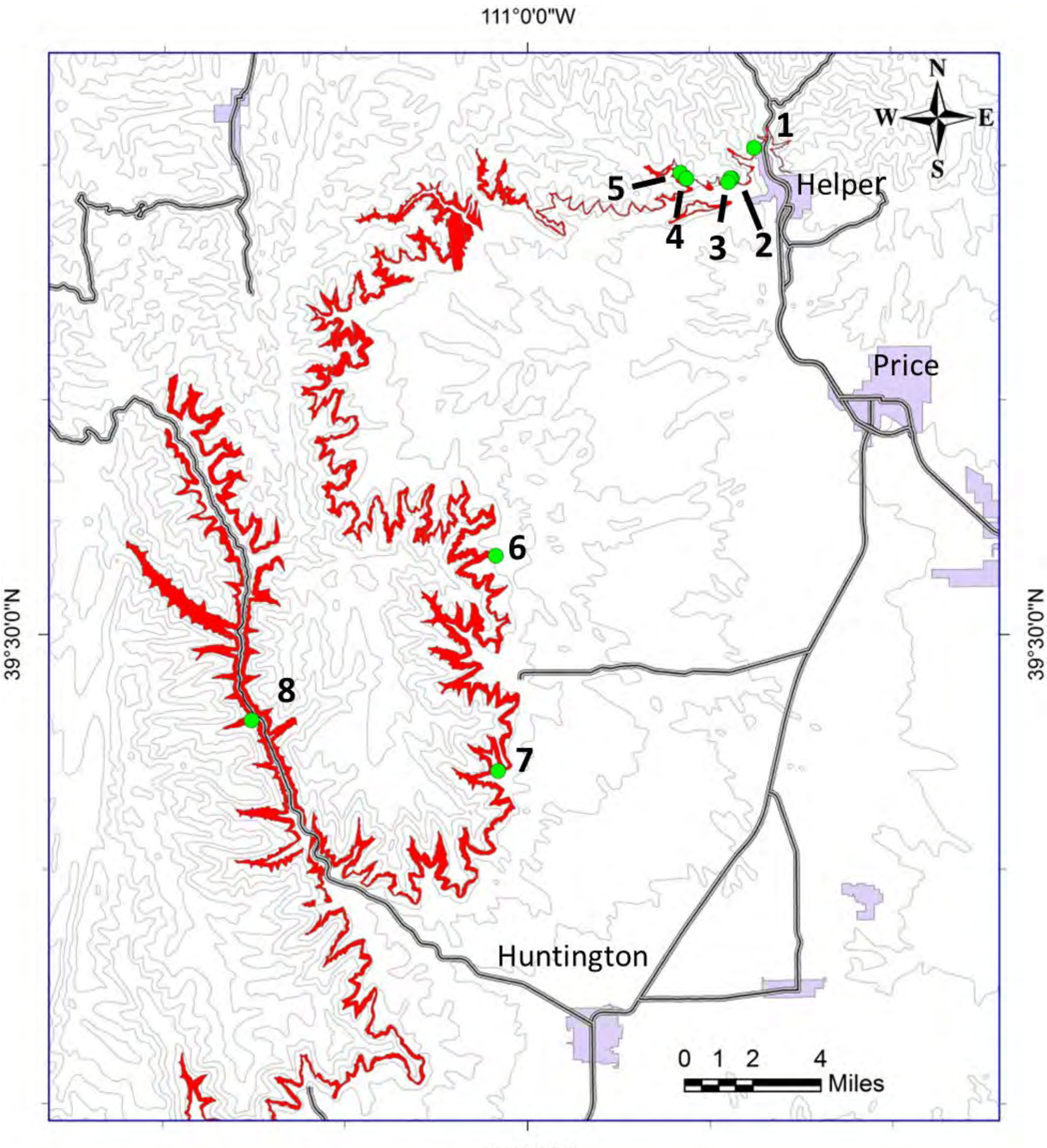

Figure 5. Clinoforms in the Panther Tongue Mbr. of the Starr Point Fm. were measured using a laser ranger at the locations indicated above. The red outlines the Panther Tongue Mbr. outcrop belt.

Numerical Experiments

Model Description

We simulated 12 river deltas using Delft3D, a physics-based, fluid flow and sediment transport model for modeling morphodynamic systems at time scales of minutes to hundreds of years (e.g., Storms et al.,2007; Edmonds and Slingerland, 2010; Canestrelli et al., 2013; Caldwell and Edmonds, 2014; van der Vegt et al., 2014). The software solves the Navier-Stokes equations for an incompressible fluid and makes use of the shallow water and Boussinesq assumptions.

Hydrodynamics

We used Delft 3D in its 2-D depth-averaged mode in which u_x and u_y, the x- and y-directed flow velocities (m s^{-1}), are obtained from the depth-averaged conservation of momentum equations for a homogeneous fluid,

$$\frac{\partial u_x}{\partial t} + u_x\frac{\partial u_x}{\partial x} + u_y\frac{\partial u_x}{\partial y} + f u_y = -\frac{1}{\rho}\frac{\partial P}{\partial x} + \frac{\tau_{sx} - \tau_{bx}}{\rho(d+\zeta)} + F_{u_x} \tag{6}$$

$$\frac{\partial u_y}{\partial t} + u_x\frac{\partial u_y}{\partial x} + u_y\frac{\partial u_y}{\partial y} - f u_x = -\frac{1}{\rho}\frac{\partial P}{\partial y} + \frac{\tau_{sy} - \tau_{by}}{\rho(d+\zeta)} + F_{u_y} \tag{7}$$

where P, f, ρ, ζ and d are the fluid pressure (N m^{-2}), Coriolis parameter (s^{-1}), fluid density (kg m^{-3}), water level above a reference plane (m), and the water depth below the reference plane (m), respectively. Fu_x and Fu_y are the x- and y- directed horizontal Reynold's stresses (m s^{-2}), τ_{sx} and τ_{sy} are the x- and y-directed shear stresses (N m^{-2}) at the water surface (set to zero in these experiments), while τ_{bx} and τ_{by} are the x- and y-directed shear stresses (N m^{-2}) at the bed. The bed shear stresses are calculated as,

$$\frac{\tau_{bx}}{\rho} = c_f u_x\sqrt{u_x^2 + u_y^2} \tag{8}$$

$$\frac{\tau_{by}}{\rho} = c_f u_y\sqrt{u_x^2 + u_y^2} \tag{9}$$

where c_f is the dimensionless Chezy friction factor.

The continuity equation for water is computed as,

$$\frac{\partial \zeta}{\partial t} + \frac{\partial[(d+\zeta)u_x]}{\partial x} + \frac{\partial[(d+\zeta)u_y]}{\partial y} = Q \tag{10}$$

where Q (m s^{-1}) is the contribution per unit area due to the discharge or withdrawal of water, precipitation, and evaporation.

The x- and y-directed horizontal Reynold's stresses, F_U and F_V , are computed using a horizontal large eddy simulator in which the horizontal eddy viscosity is defined as:

$$\nu_H = \upsilon_{SGS} + \upsilon_H^{back} \tag{11}$$

where υ_H is the horizontal eddy viscosity (m^2 s^{-1}), $\upsilon_{SGS}$is the contribution from the sub-grid scale horizontal eddy viscosity modeled with the HLES (m^2 s^{-1}), and υ_H^{back} is the user-defined background horizontal eddy viscosity (m^2 s^{-1}). Similarly, the horizontal eddy diffusivity is calculated as:

$$D_H = D_{SGS} + D_H^{back} \tag{12}$$

where D_H is the total horiztonal eddy diffusivity coefficient (m^2 s^{-1}), D_{SGS} the contribution from the sub-grid scale horizontal eddy viscosity modeled with the horizontal large eddy simulation technique (HLES), and D_H^{back} is the user-defined background horizontal eddy viscosity (m^2 s^{-1}). The effect of sub-grid scale turbulence on the horizontal viscosity coefficient is computed using Uittenbogaard and van Vossen's (2004) HLES technique in which ν_{SGS}, the sub-grid eddy viscosity (m^2 s^{-1}), is given by:

$$\nu_{SGS} = \frac{1}{k_s^2}\left(\sqrt{(\gamma\sigma_T S^*)^2 + B^2} - B\right) \tag{13}$$

with:

$$B = \frac{3g|\underline{u_x}|}{4HC^2} \tag{14}$$

where k_s is the truncation wave number (m^{-1}), γ is a dimensionless coefficient relating the spectral energy density to the wave number, σ_T is the dimensionless Prandtl-Schmidt number, and S^* (s^{-1}) is the strain rate tensor based upon the low, then high pass filtered, computationally resolved, horizontal velocity vector $\underline{U}$ (m s^{-1}), B is a damping bed friction term (s^{-1}), C is the Chezy friction coefficient (m$^{1/2}$s^{-1}), and H is the total water depth (m).

The sub-grid scale eddy diffusivity for the mixing of mud is:

$$D_{SGS} = \frac{\nu_{SGS}}{\sigma_T} \tag{15}$$

Sediment Transport

After the hydrodynamic equations are solved, sediment transport is computed. In Delft3D silt- and clay-sized particles are called cohesive. Both cohesive and non-cohesive suspended sediment transport are computed using the depth-averaged 3D advection-diffusion equation:

$$\frac{\partial c_i}{\partial t}+\frac{\partial u_x c_i}{\partial x}+\frac{\partial u_y c_i}{\partial y}+\frac{\partial (u_z - w_{s,i})c_i}{\partial z}=\frac{\partial}{\partial x}\left(\varepsilon_{s,x,i}\frac{\partial c_i}{\partial x}\right)+\frac{\partial}{\partial y}\left(\varepsilon_{s,y,i}\frac{\partial c_i}{\partial y}\right)+\frac{\partial}{\partial z}\left(\varepsilon_{s,z,i}\frac{\partial c_i}{\partial z}\right) \tag{16}$$

where c_i is the mass concentration of the ith sediment fraction (kg m^{-3}), u, v, and w are flow velocity components (m s^{-1}), and $\varepsilon_{s,x,i}$, $\varepsilon_{s,y,i}$, and $\varepsilon_{s,z,i}$ are the eddy diffusivities of the ith sediment fraction (m^2 s^{-1}).

Non-cohesive settling velocities are computed using a Van Rijn (1993) formulation,

$$w_{s,i} = \begin{cases} \dfrac{RgD_i^2}{18\nu}, & 65\mu m < D_i < 100\mu m \\ \dfrac{10\nu}{D_i}\left(\sqrt{1+\dfrac{0.01RgD_i^3}{\nu^2}}-1\right), & 100\mu m < D_i < 1000\mu m \\ 1.1\sqrt{RgD_i}\ , & 1000\mu m < D_i \end{cases} \tag{17}$$

where $w_{s,i}$ is the settling velocity of the ith sediment fraction, $R=\rho_s/\rho_w - 1$ is the submerged specific gravity, ρ_s is the specific density of sediment (kg m^{-3}), ρ_w is the specific density of water (kg m^{-3}), g is the acceleration due to gravity (m s^{-2}), D_i is the grain size of the ith sediment fraction (m), and ν is the kinematic viscosity coefficient of water (m^2 s^{-1}) (*cf.*, Caldwell and Edmonds, 2014).

The exchange of sediment from suspension to the bed, and vice versa, is modeled by calculating,

$$-w_{s,i}c_i - \varepsilon_{s,z,i}\frac{\partial c_i}{\partial z} = D_i - E_i = T_{d,i}, at\ z = z_b \tag{18}$$

where D_i is the sediment deposition rate of the i^{th} sediment fraction (m s^{-1}), $E_i$is the sediment erosion rate of the i^{th} sediment fraction (m s^{-1}), $T_{d,i}$ is the net deposition or erosion rate of the i^{th} sediment fraction (m s^{-1}), and z_b is the elevation of the bed (m).

Delft3D computes erosion and deposition of cohesive sediment using the Partheniades-Krone formulation (Partheniades, 1965),

$$S_{e,i} = \begin{cases} \left(\dfrac{\tau_0}{\tau_{ce(C)}} - 1\right), & when\ \tau_0 > \tau_{ce(C)} \\ 0, & when\ \tau_0 \leq \tau_{ce(C)} \end{cases}$$
$$S_{d,i} = w_{s,i}c_{b,i}\begin{cases} \left(\dfrac{\tau_0}{\tau_{cd(C)}} - 1\right), & when\ \tau_0 < \tau_{cd(C)} \\ 0, & when\ \tau_0 \geq \tau_{cd(C)} \end{cases} \tag{19}$$

where $S_{e,i}$ is the erosion function for the i^{th} sediment fraction (kg m^{-2} s^{-1}) , $S_{d,i}$ is the deposition function for the i^{th} sediment fraction (kg m^{-2} s^{-1}), τ_0 is the bed shear stress (N m^{-2}), $\tau_{ce(C)}$ is the user-defined critical shear stress for erosion (N m^{-2}), $\tau_{cd(C)}$ is the user-defined critical shear stress for deposition (N m^{-2}), and $c_{b,i}$ is the average sediment concentration of the i^{th} sediment fraction in the near bottom computational layer (kg m^{-3}).

Bedload transport is computed using a Van Rijn (1993) formulation,

$$q_{b,i} = 0.006 w_{s,i} D_i \left(\frac{u\left(u - u_{c,i}\right)^{1.4}}{\left(RgD_i\right)^{1.2}} \right) \tag{20}$$

where $q_{b,i}$ is the bedload sediment discharge per unit width of the i^{th} sediment fraction (m^2 s^{-1}), u is the depth-averaged flow velocity (m s^{-1}), and $u_{c,i}$ is the critical depth-averaged flow velocity for entrainment of the i^{th} sediment fraction based upon the Shields curve (m s^{-1}).

Bed elevation changes are calculated using a modified Exner equation with a user-defined morphological acceleration factor

$$\left(1-\varepsilon_{por}\right)\frac{\partial z_b}{\partial t} = -f_{MORFAC}\frac{\partial S_x}{\partial x} - \frac{\partial S_y}{\partial y} + T_d \qquad (21)$$

where ε_{por} is the bed porosity, z_b is the bed elevation (m), S_x, S_y are the total sediment transport components per unit width in the x- and y-directions (m^2 s^{-1}), and T_d is the deposition or erosion rate of suspended sediment (m s^{-1}).

Experimental Design

Twelve deltas were simulated prograding into isothermal, freshwater basins of varying initial water depths that experienced varying rates of base level fall (Fig. 4). Basin depths were set to 4, 8, 12, and 20 m deep and at each basin depth the rates of base level fall varied among 0, 5, and 10 mm yr^{-1}. Delta growth was terminated when the ratios of initial basin volume to the volume of sediment that had entered the basin were identical. For example, the deltas were allowed to prograde into the 8 m deep basin for twice as long, and therefore received twice the sediment as in the 4 m deep basin. Base level fall was simulated by prescribing a constant rate of decrease in water level at the open boundaries of the model. The trunk stream discharged 1000 m^3s^{-1} of water into the basin along with 450 kg s^{-1} of sediment. This sediment load is roughly 8 times larger than that of the Goose River, but equal in size to many medium-size river systems. The higher sediment load was necessary to complete the simulations in a computable time. Five size fractions were weighted to form an approximate lognormal distribution around a D_{50} of 170 µm (45 kg s^{-1} of 25 µm, 112.5 kg s^{-1} of 50 µm, 135 kg s^{-1} of 150 µm, 112.5 kg s^{-1} of 250 µm, 45 kg s^{-1} of 275 µm). We make the assumption that bankfull discharge is required to effect morphologic change. In nature, bankfull discharge is limited to a small fraction of the year. We used a 14-day intermittency factor in the simulations in which 14 days of simulated bankfull discharge and subsequent morphologic change in Delft3D is equal to the amount of bankfull discharge expected in one year. In addition, each hydrologic timestep was made to equal 500 morphologic timesteps by letting $f_{MORPHFAC}$ in Eqn. 18 equal to 500.

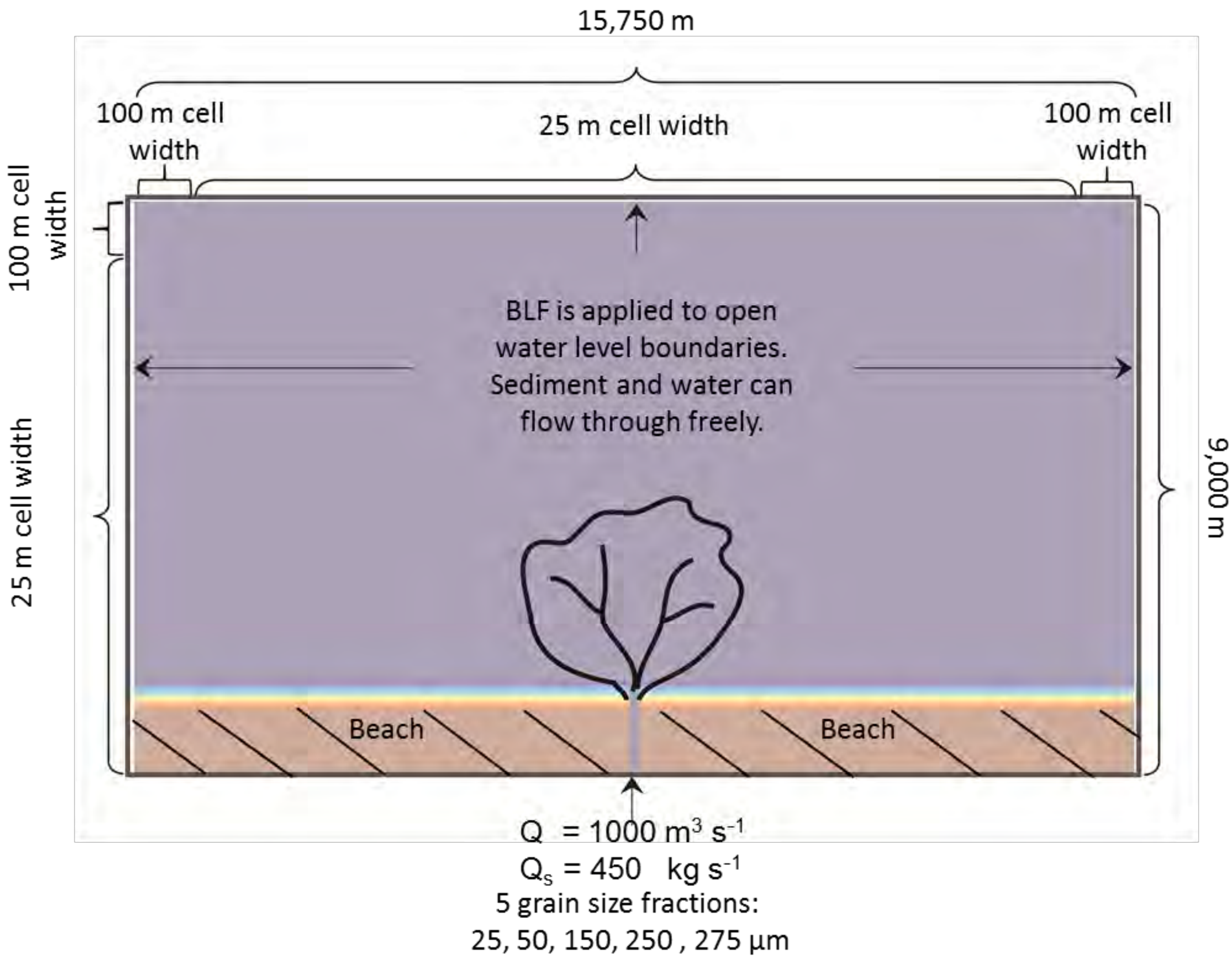

Figure 6. Schematic of the model domain.

The computational domain (Fig. 6) consisted of an open basin 15,750 m wide and 9,000 m long, along the southern edge of which sat a 1000 m wide coast of constant 3 m elevation. The beach face was 500 m wide and sloped seaward to the ultimate basin depth of a given run. Through the beach at a point equidistant from the western, northern, and eastern open boundaries flowed a trunk stream 150 m wide and 1300 m long with an initial depth sloping linearly from 4 m deep at the boundary to the ultimate basin depth of a given simulation. The western, northern, and eastern edges of the computational domain were open boundaries through which water and sediment could be transported freely. The basin was free of waves, tides, and Coriolis acceleration. The fluid density of the basin, 1000 kg m^{-3}, is constant and equal to that of the river. Near the river mouth the state variables were computed on a 25 by 25 m square grid; in the outer region the spacing was increased to 100 x 100 m. This allowed for the region of interest to be far from the boundaries without sacrificing too much computational time. To meet the Courant-Friedrichs-Lewy condition for stability and accuracy the time step was set to 6 s. All Delft3D input files to reproduce the simulated delta experiencing 10 mm yr^{-1} of BLF in a 4 m deep basin are included in Appendix A.

Model Results

Delta Planform Morphology

The deltas predicted by Delft3D for basins of varying initial depth and rates of relative base level fall are illustrated in Figure 5. The deltas are compared at the time when the ratios of basin accommodation space to cumulative volume of sediment delivered to the basin are all equal. Thus the delta formed in a 20 m deep basin with no BLF is composed of five times the volume of sediment as the 4 m basin and has taken five times as long to form. Inspection of Figure 7 shows that deltas prograding into shallower basins experiencing little or no relative base level fall possess rectangular shore-parallel planforms of low rugosity, compared to deeper water, falling base level deltas which are narrower and more birdsfoot in planform. The latter develop more rugose shorelines and down-stepping abandoned lobes. Also, they are more likely to have fewer simultaneously active distributary channels and these channels are more likely to migrate laterally, forming inset strath terraces underlain by abandoned channel fill.

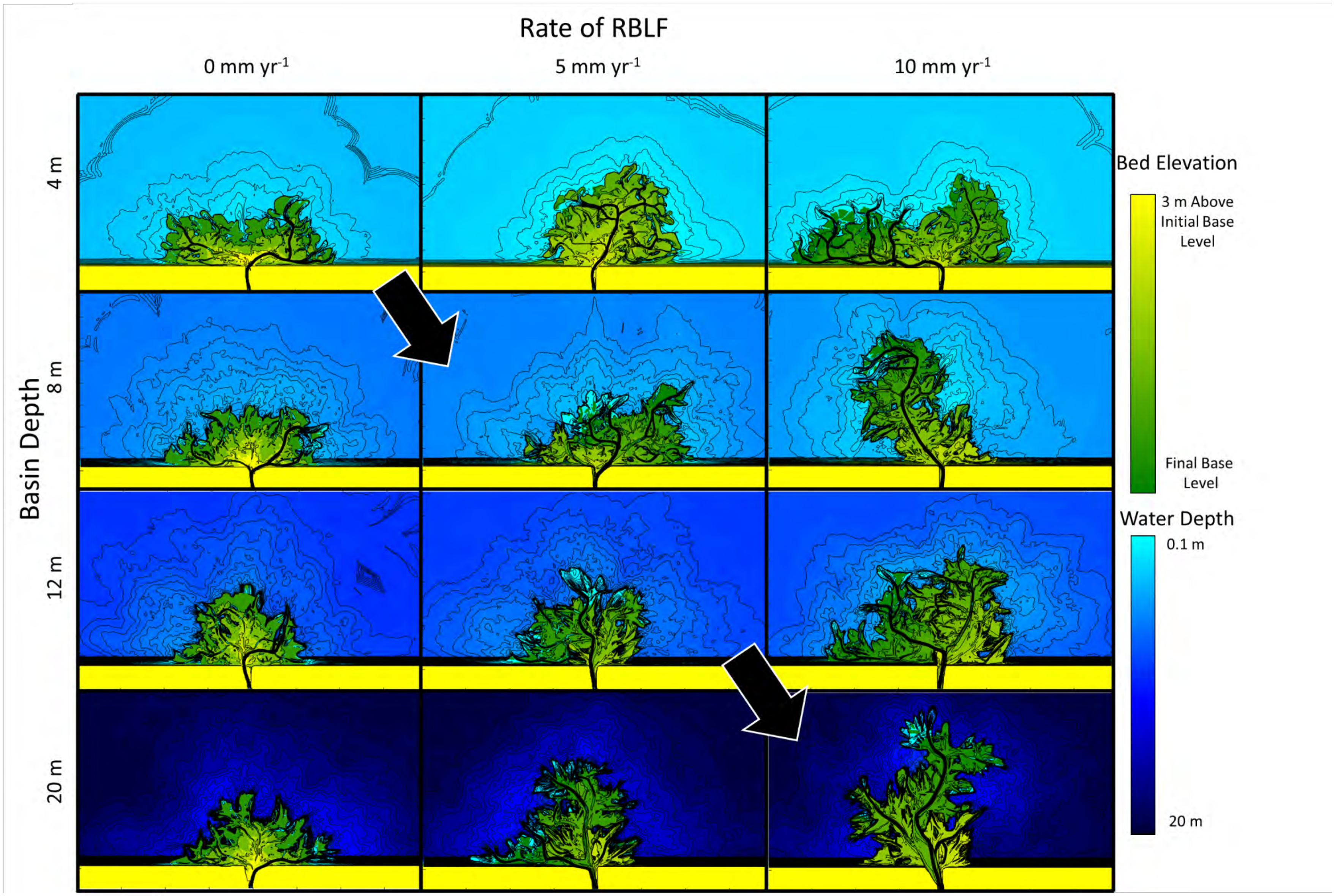

Figure 7. Bed elevation of the simulated deltas. A diagonal line from upper left to lower right represents an increase in initial accommodation space and an increase in the rate at which that accommodation is lost through time. Shoreline trajectories become steeper along this diagonal line.

A diagonal line from upper left to lower right in Figure 7 represents an increase in initial accommodation space and an increase in the rate at which that accommodation is lost through time. For a fixed sediment feed, as in these experiments, a deeper initial basin creates a slower rate of delta-front progradation. Higher rates of BLF decrease the elevation of the shoreline at a faster rate. The combination of these two vectors defines the trajectory of the delta shoreline. We measure this as a slope, S_T, as defined by Eqn. 1 (Fig. 8). Shoreline trajectory can therefore provide information about initial basin depth and rate of BLF when $S_T < 0$. This is advantageous because the shoreline trajectory is measurable in seismic lines and field outcrops (Posamentier and Morris, 2000). Thus if one measures shoreline trajectory and gains some insight into the rate of BLF and basin depth a delta was forming in, then he/she can predict the morphologies and internal geometries for that delta.

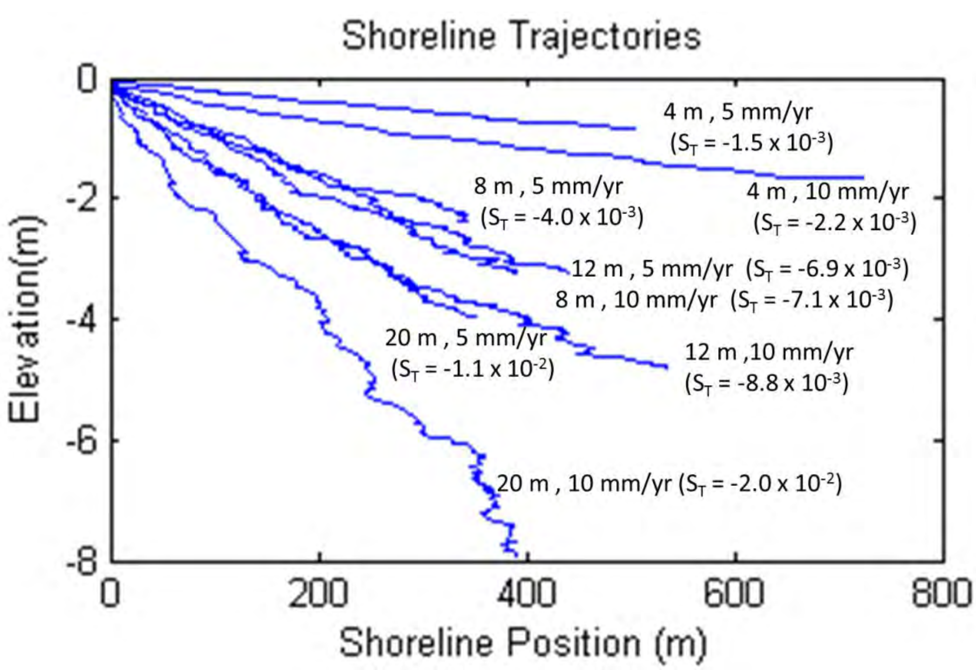

Figure 8. Shoreline trajectories produced from the Delft3D simulated deltas shown in Figure 7 experiencing base level fall. They were measured through time using Equation 1. Each run with base level fall is shown here labeled with the initial basin depth, the rate of base level fall, and time-averaged S_T.

The contributions of each variable—initial basin depth and rate of BLF—can be understood by holding one constant while varying the other. The R^2 values are coefficients of determination from linear regressions of the logarithmic-transformed data are used to make power law relationships linear. They describe what percentage of the variability in the dependent variables (y-axis) can be accounted for by the independent variables (x-axis). F-tests run on the simple linear regressions yield the statistical significance of the relationship (p-values). P-values less than 0.05 represent greater than 95% and are considered to be statistically significant. Ignoring rate of BLF and treating each simulated delta as an independent realization, reveals that increasing initial basin depth decreases the time-averaged number of active distributaries ($R^2 = 0.85$, $p = 1.7 \times 10^{-5}$) (Fig. 9), increases the avulsion period ($R^2 = 0.86$, $p = 1.4 \times 10^{-5}$) (Fig. 10), creates significantly more rugose shorelines ($R^2 = 0.62$, $p = 2.4 \times 10^{-3}$) (Fig. 11), the area of individual delta lobes decreases ($R^2 = 0.43$, $p = 0.02$) (Fig. 12), decreases topset/foreset ratios ($R^2 = 0.53$, $p = 0.0196$) (Fig.13), and increases average clinoform dip magnitudes ($R^2 = 0.91$, $p = 1.6 \times 10^{-6}$) (Fig. 14), and foreset dip azimuths become more variable ($R^2 = 0.73$, $p= 3.68 \times 10^{-4}$) (Fig.15). Initial basin depth has little effect on delta topset roughness, overall topset area, and delta aspect ratio. If initial basin depth is held constant while BLF rate increases, the model results predict that topset roughness increases ($R^2 = 0.85$, $p = 1.9 \times 10^{-5}$) (Fig. 16), total delta topset area increases ($R^2 = 0.83$, $p = 4.1 \times 10^{-5}$) (Fig. 17), and the aspect ratio decreases indicating more elongate deltas ($R^2 = 0.39$, $p= 0.029$) (Fig. 18). There is no aggradation of the topset outside of distributary channels when there BLF.

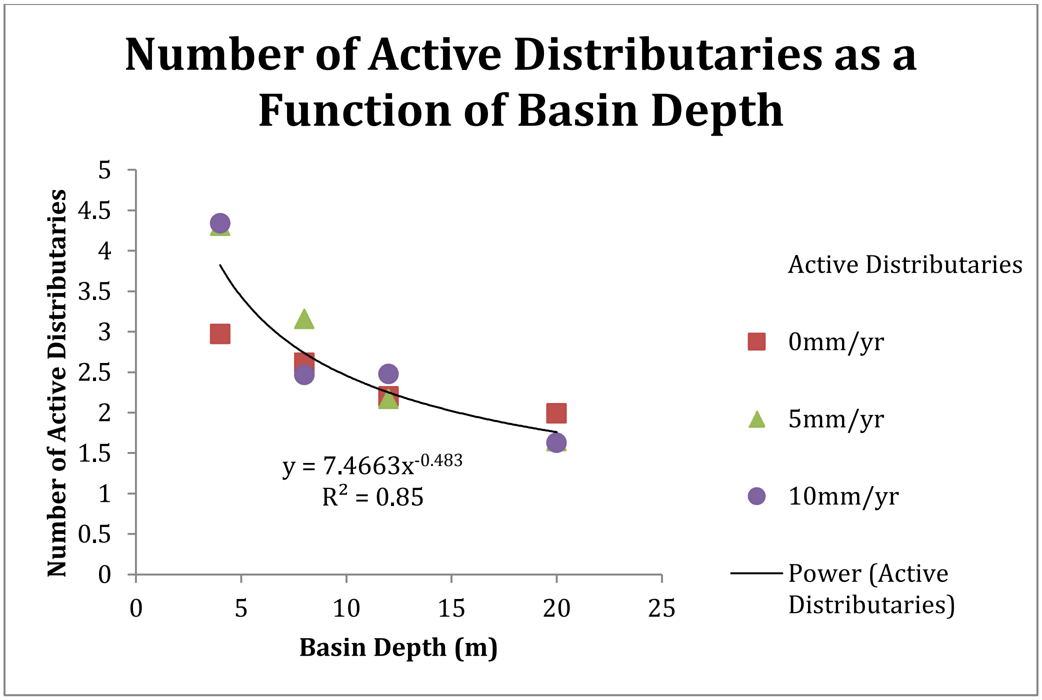

Figure 9. The time-averaged number of active distributaries decreases significantly according to a power law relationship with basin depth ($p = 1.7 \times 10^{-5}$).

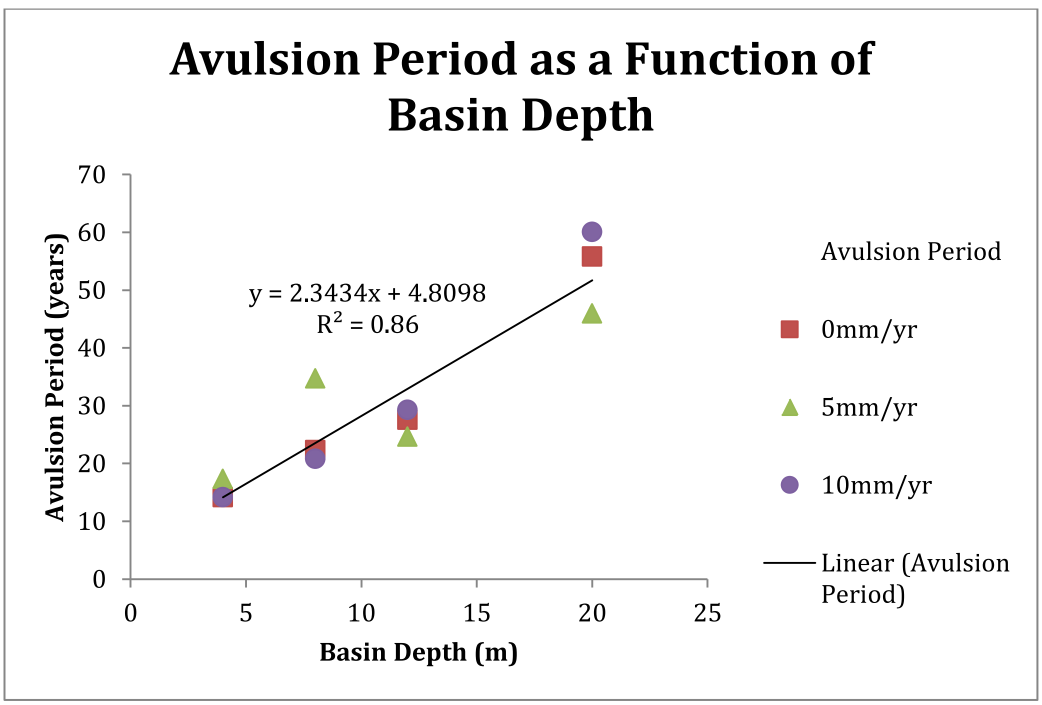

Figure 10. Avulsion period increases significantly with basin depth in a linear relationship

($p = 1.4 \times 10^{-5}$).

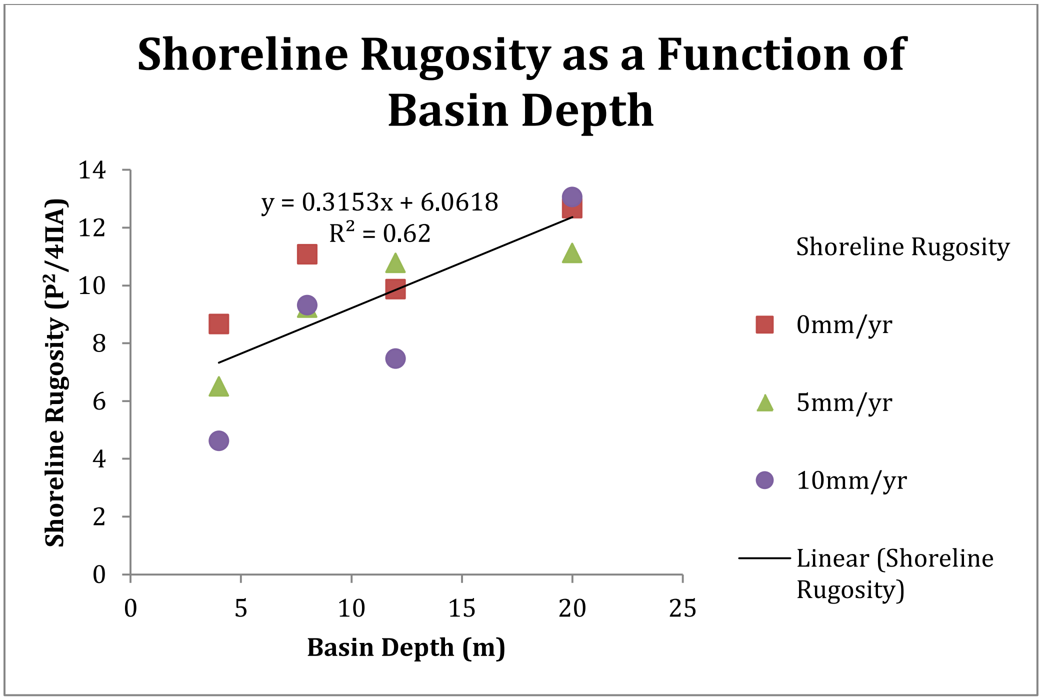

Figure 11. Shoreline rugosity increases significantly with basin depth in a linear relationship ($p = 2.4 \times 10^{-3}$).

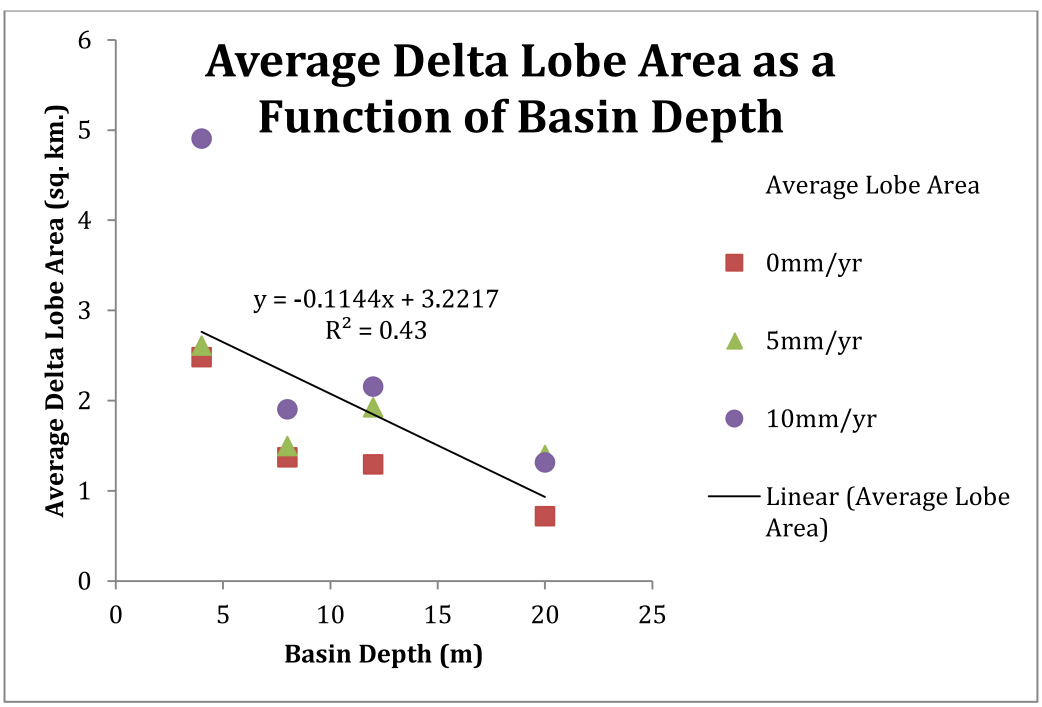

Figure 12. The average delta lobe area shows a moderate correlation with basin depth. The linear relationship is statistically significant ($p = 0.02$).

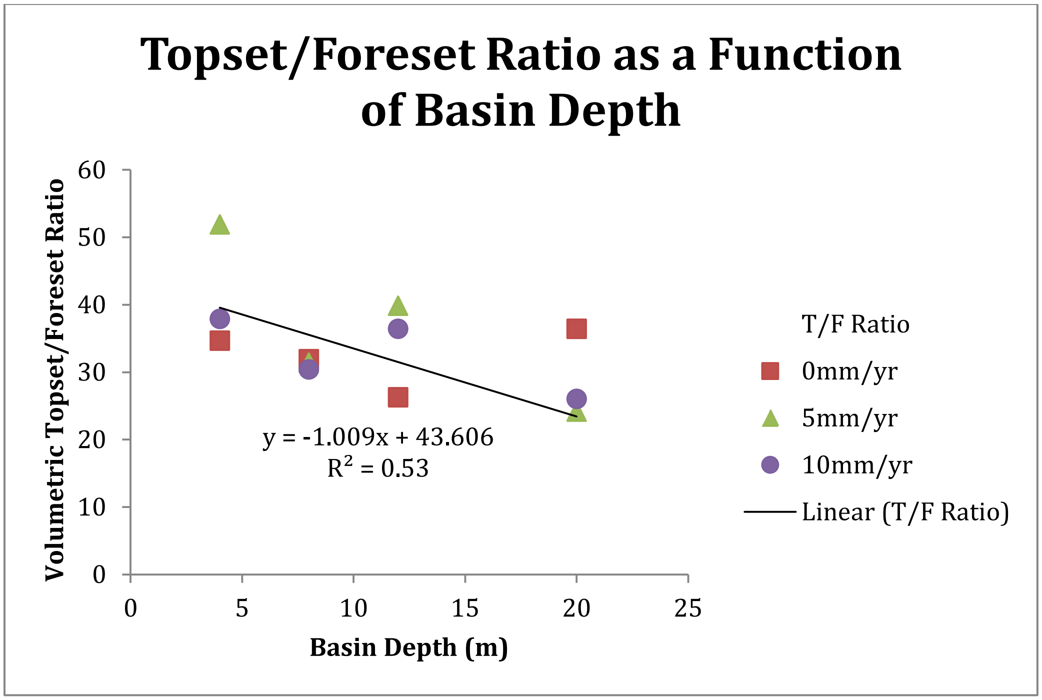

Figure 13. The topset/foreset ratio shows a moderate linear correlation with basin depth ($p = 0.0196$).

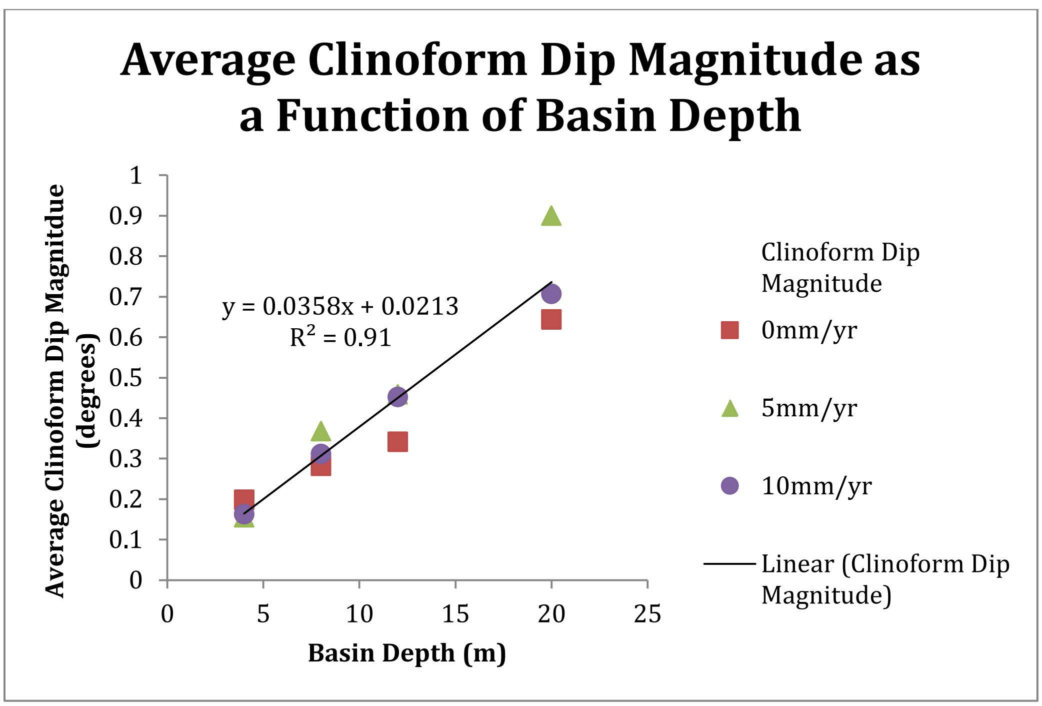

Figure 14. The average clinoform dip magnitude shows a strong linear correlation with basin depth ($p= 1.74 \times 10^{-6}$).

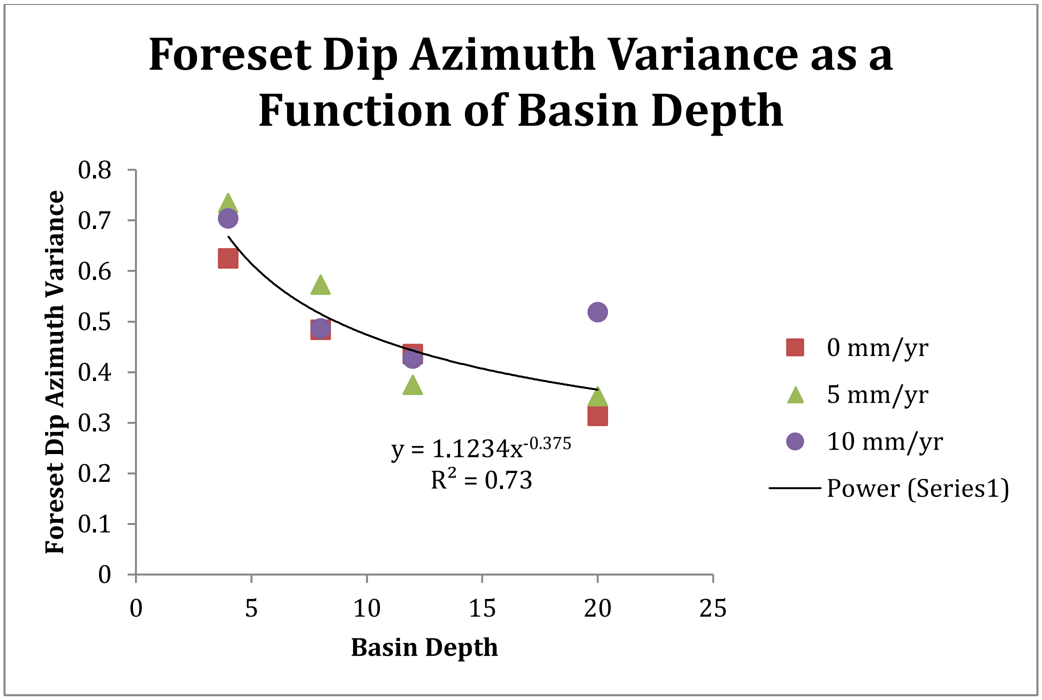

Figure 15. Foreset dip azimuths become more variable (lower values of $\bar{\boldsymbol{R}}$) as basin depth increases (p=3.68 x 10^{-4}).

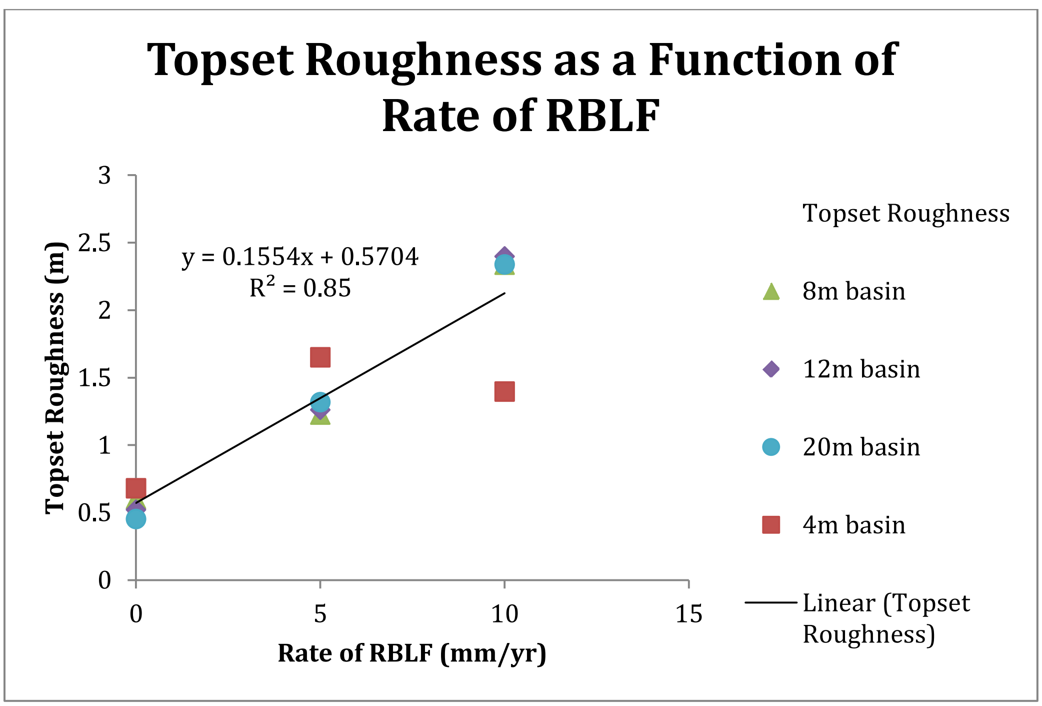

Figure 16. Topset roughness exhibits a strong linear relationship with the rate of BLF (p = 1.85 x 10^{-5}).

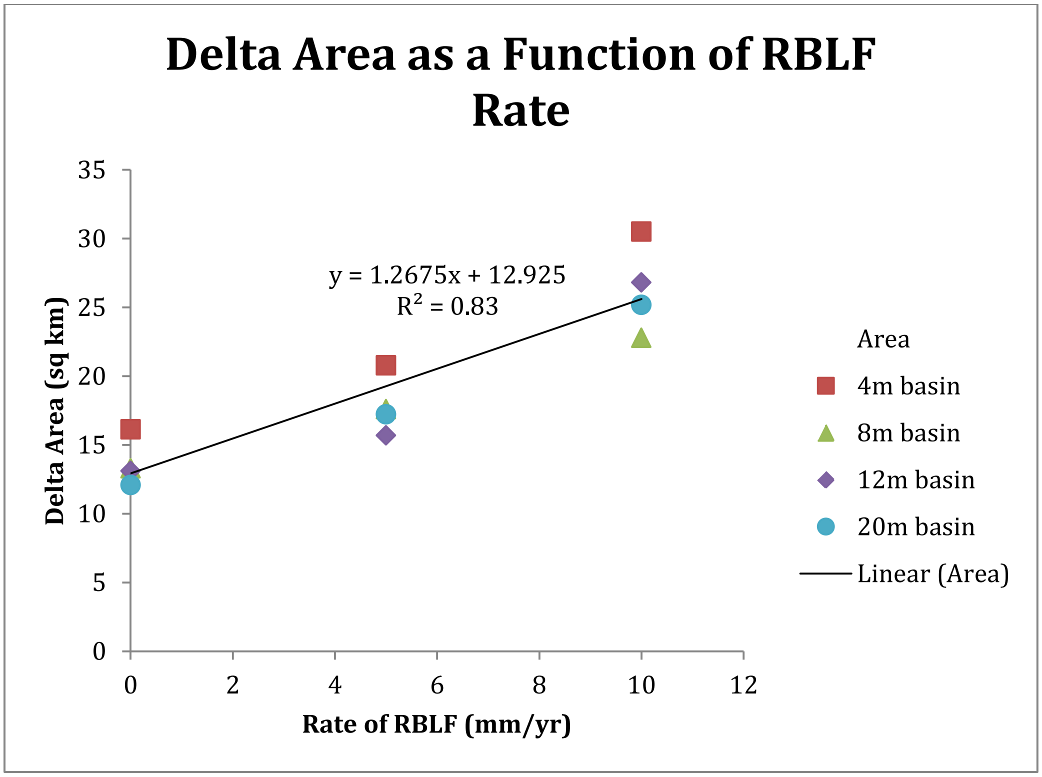

Figure 17. The total area of the delta topset increases linearly with the rate of BLF ($p = 4.06 \times 10^{-5}$).

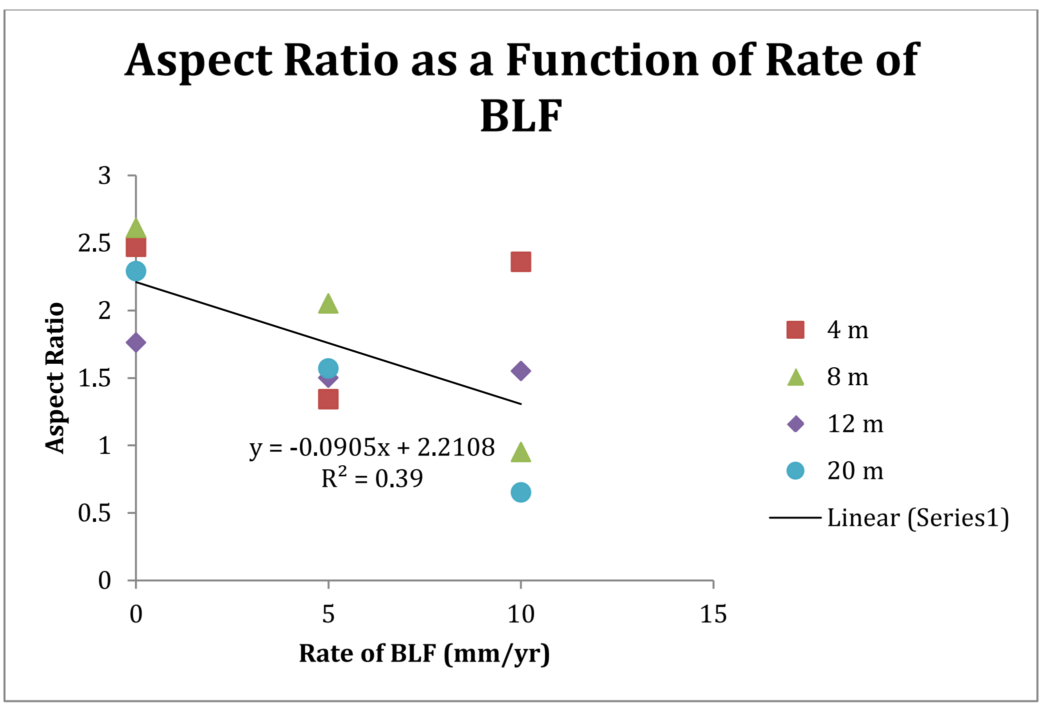

Figure 18. Aspect ratios decrease as rates of BLF increase indicating that deltas become more elongate under BLF forcing (p= 0.029).

Delta Internal Geometry

Of particular interest are the accretionary deposits that form in distributary channels. They form as discrete packages of sediment separated by chronostratigraphic, accretionary surfaces. These accretionary deposits are seen in all simulated deltas regardless of BLF or initial basin depth (Fig. 19). The distance between two accretionary surfaces along an axis perpendicular to the channel's centerline decreases as initial basin depth increases, indicating a slower rate of accretion for the deposit. Under high rates of BLF, down-stepping terraces form (Fig. 20). Inspection of bed elevations through time show that these terraces arise as the distributary channels migrate laterally within the incised distributary channel. Consequently, there is a trajectory for these accretionary surfaces that is analogous to the shoreline trajectory because it becomes steeper with deeper initial basin depths and higher rates of BLF. (Note: More Delft3D simulated internal geometry can be seen in Appendix C).

BLF and basin depth do not exhibit a strong effect on the spatial grain size distributions of simulated deltas. The coarsest grains are located in the topset and upper foreset. Mud drapes occur intermittently in both distributary channel fills and clinoforms. The lower foreset tends to be finer-grained. All deltas, regardless of initial basin depth or rate of BLF, exhibit weak lobe fining from proximal to distal, although this trend is not statistically different from no trend. As a result, we must consider mean delta lobe grain size to remain statistically constant from proximal to distal.

Clinoform heights and mean dip magnitudes decrease from proximal to distal with BLF. Clinoform heights, measured from the rollover point to the basin floor, decrease systematically as base level falls. The trajectory of the clinoform rollover defines the shoreline trajectory. No subaqueous clinoform rollovers formed in any of the simulated deltas thus precluding the existence of 'fore-shortened' stratigraphy in the model (Posamentier and Morris, 2000). As base level falls, the delta is prograding in to shallower water which results in decreasing clinoform dip magnitudes from proximal to distal. Clinoform dip magnitudes also decrease in the absence of BLF because the delta is prograding on top of previously deposited pro-delta muds which cause a reduction in water depth. Steepening clinoform dip magnitudes are not observed in any of the simulated deltas.

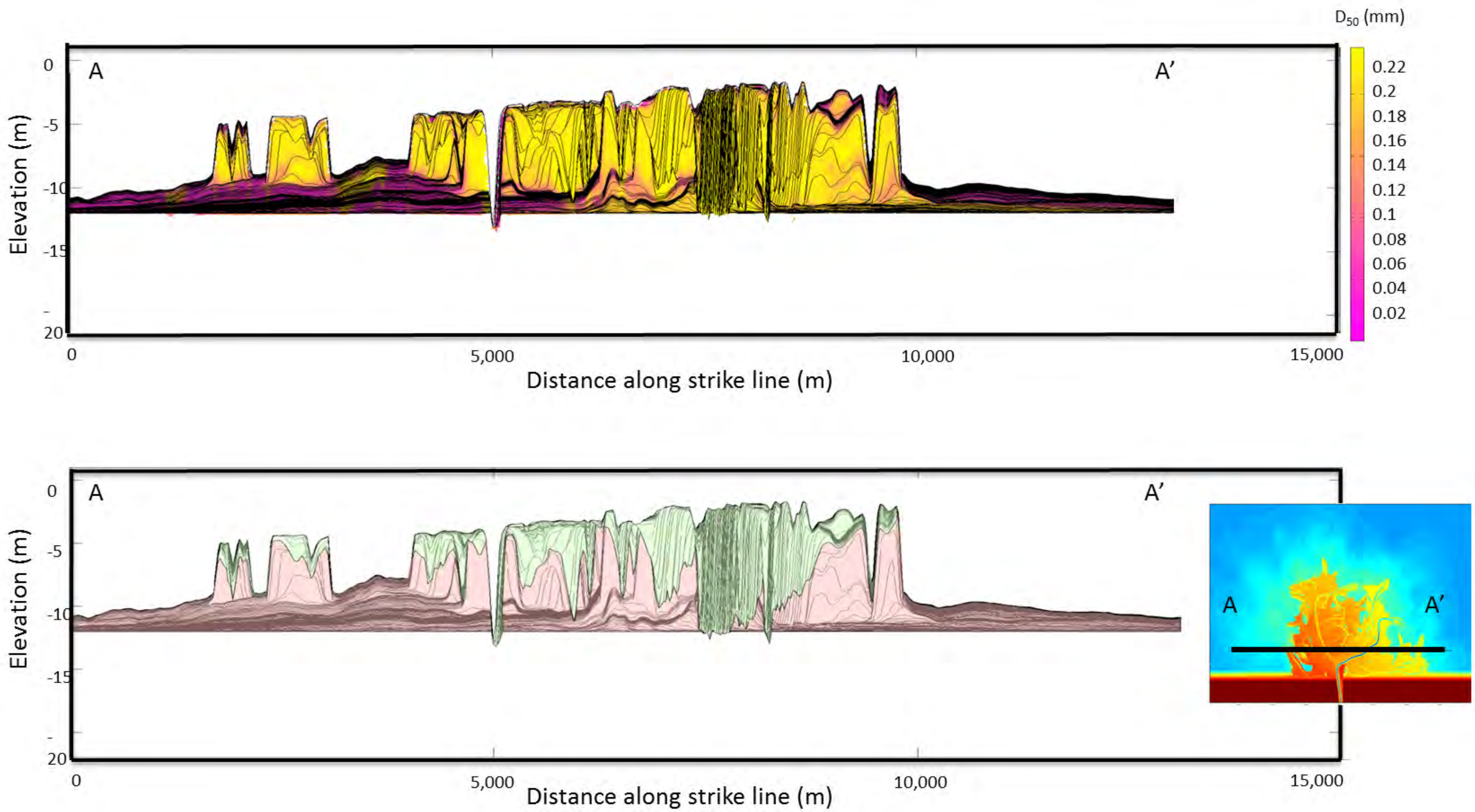

Figure 19. A Delft3D-generated, representative strike line showing grains size distributions and clinoforms in a simulated delta formed in a 12 m deep basin while experiencing 10 mm yr^{-1} of BLF (top). Below, the topset (green) and foreset (pink) facies have been defined. Black lines represent chronostratigraphic surfaces

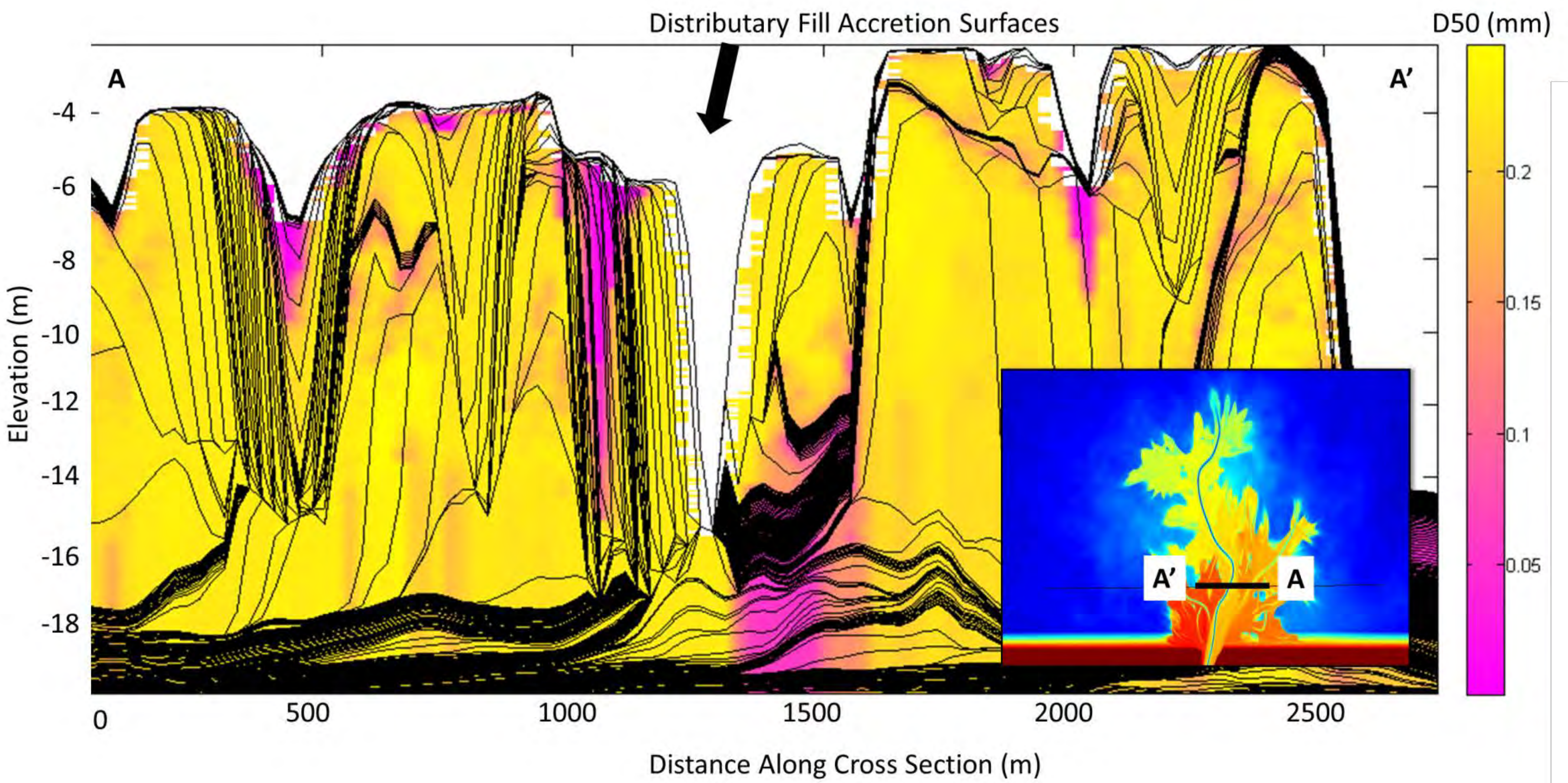

Figure 20. Model results shown are from a simulated delta prograding into 20 m water depth and experiencing 10 mm yr^{-1} BLF (S_T = - 0.02). Inset strath terraces forms regardless of rate of BLF. The down-stepping of the inset terraces is a result of the accretion rate and the rate of BLF, and can be thought of as analogous to shoreline trajectory.

Discussion

Shoreline trajectory is set by the rate of BLF and the progradation rate of the delta, and the latter is set by basin depth and BLF. By considering the effect of S_T, we are essentially weighting the relative importance of rate of BLF and basin depth on the formation of a delta. To illustrate the relationship between the rate of BLF, basin depth, and shoreline trajectory we propose a 2D model of delta progradation. It can be extended to account for radial growth of a delta, but this effect is excluded here for simplicity.

2D Model Derivation

Using a material balance law we assume that the amount of sediment fed to the delta front, q_s (m^2 s^{-1}), must fill the accommodation space to base level, or:

$$q_s = H\frac{dx}{dt} \tag{22}$$

where H (m) is the water depth at time , t (seconds), x is the position of the shoreline (m), and $\frac{\partial x}{\partial t}$ is the rate of progradation (m s^{-1}). H varies with time in proportion to the rate of BLF, $\dot{r}$(m s^{-1}). This relationship can be defined for a constant rate of BLF as,

$$H = H_0 - \dot{r}t \tag{23}$$

where H_0 is the initial basin depth (m). Therefore Eqn. 21 becomes,

$$q_s = (H_0 - \dot{r}t)\frac{dx}{dt} \tag{24}$$

To account for possible incision of the topset, we consider that the sediment flux delivered to the shoreline varies as a function of the sediment flux of the trunk stream, q_{so} (m^2 s^{-1}), the rate of BLF, and position of the shoreline such that,

$$q_s = q_{so} + \dot{r}x \tag{25}$$

A scenario could arise in which all of the previously deposited material down to the new base level is re-excavated during BLF, thus requiring a steepening of slope. We, however, ignore changes in bed slope. Substituting Eqn. 24 into Eqn. 23:

$$q_{so} + \dot{r}x = (H_0 - \dot{r}t)\frac{dx}{dt} \tag{26}$$

which can be rearranged as,

$$\frac{dx}{q_{s0} + \dot{r}x} = \frac{dt}{H_0 - \dot{r}t} \tag{27}$$

Each side is of the form ,

$$\int \frac{dx}{a + bx} = \frac{1}{b}\ln(a + bx) \tag{28}$$

Therefore we can integrate the ordinary differential equation to get,

$$\frac{1}{\dot{r}}\ln(q_{s0} + \dot{r}x)\Big|_0^x = -\frac{1}{\dot{r}}\ln(H_0 - \dot{r}t)\Big|_0^t \tag{29}$$

which can be rewritten as,

$$\ln(q_{s0} + \dot{r}x) - \ln(q_{s0}) = -[\ln(H_0 - \dot{r}t) - \ln(H_0)] \tag{30}$$

or,

$$\ln\left(\frac{q_{s0} - \dot{r}x}{q_{s0}}\right) = -\ln\left(\frac{H_0 - \dot{r}t}{H_0}\right) \tag{31}$$

This can be further simplified to,

$$\frac{q_{s0} - r\dot{x}}{q_{s0}} = \frac{H_0}{H_0 - \dot{r}t} \tag{32}$$

Solving for x yields,

$$x = \frac{q_{s0}}{\dot{r}} - \frac{q_{s0}H_0}{\dot{r}(H_0 - \dot{r}t)} \tag{33}$$

Taking the derivative of x yields the rate of horizontal progradation, $\frac{dx}{dt}$ (m s^{-1}),

$$\frac{dx}{dt} = \frac{q_{s0}H_0}{(H_0 - \dot{r}t)^2} \tag{34}$$

Therefore the horizontal progradation rate is proportional to both the sediment flux, q_{s0}, and $\frac{H_0}{(H_0-\dot{r}t)^2}$. The latter is a scaled ratio such that at t=0, and for very large H_0 the term is approximately $\frac{1}{H_0}$ and the rate of progradation is essentially independent of $\dot{r}$. For t approaching $\frac{H_0}{\dot{r}}$, the term becomes infinitely large as base level approaches the basin floor. In this case the rate of BLF sets the progradation rate. Thus for constant q_{s0}, H_0 sets the scale, while the rate of BLF, sets the progradation rate. Furthermore the shoreline trajectory can be defined as,

$$S_T = -\arctan\left(\frac{H_0 - \dot{r}t}{\frac{q_{s0}}{\dot{r}} - \frac{q_{s0}H_0}{\dot{r}(H_0 - \dot{r}t)}}\right) \tag{35}$$

This case is strictly 2D which may be appropriate for the simulated deltas that incise their topset, and become elongate, thereby inhibiting radial growth.

Analysis

As the above analysis indicates, both basin depth and the rate or BLF control S_T but one dominates the other under selected conditions. The relative influence of basin depth and rate of BLF on each variable can be gleaned from a multiple linear regression (MLR) of the variable as a function of basin depth and rate of BLF. P-values associated with F-tests assess the fit of the MLR to the data; p-values less than 0.05 provide greater than 95% confidence that the model possesses a statistically good fit. Student's t-tests of MLR correlation coefficients yield p-values indicating the individual statistical significance of basin depth and rate of BLF. Basin depth and rate of BLF are deemed statistically significant if their respective t-test p-values are less than 0.05 (greater than 95% confidence).

Examination of the MLR results in Table 1 indicates that basin depth plays a stronger role than rate of BLF in setting the number of active distributaries, shoreline rugosity, average area of delta lobes, and avulsion period. Conversely, rate of BLF influences topset roughness, total area of the delta topset, foreset dip azimuth statistic, and the coefficient of determination for progressive lobe fining more than basin depth.

Variable Name	*F*-test *p*-value	Basin Depth *t*-test *p*-value	Rates of BLF *t*-value *p*-value	Stronger Predictor
Number of Active Distributaries	2.67E-03	8.50E-04	0.46	Depth
Avulsion Period	1.38E-04	3.81E-05	0.81	Depth
Shoreline Rugosity	2.63E-03	1.34E-03	0.083	Depth
Average Delta Lobe Area	0.012	0.01042	0.060	Depth
Foreset Dip Azimuth Variance	4.15E-03	7.88E-04	0.17	Depth
Aspect Ratio	0.038	0.17	0.024	BLF
Topset Roughness	1.68E-04	0.69	1.68E-04	BLF
Total Delta Area	8.87E-05	0.10	3.01E-05	BLF

Table 1. The results from the multiple linear regression (MLR) indicate how strongly basin depth and rate of BLF influence each variable. F-tests determine the quality of the MLR model fit to the data. The p-values associated with the F-tests indicate the statistical confidence we have that the MLR model is a good fit. Student's t-test assess the relative contribution of basin depth and rate of BLF to the MLR model. The resulting p-values indicate whether basin depth or rate of BLF are a strong predictor for each variable. P-values less than 0.05 are considered statistically significant.

Shoreline rugosity correlates with basin depth and steeper shoreline trajectories because basin depth reduces the number of active distributaries and increases the avulsion period. There are fewer active distributaries in deeper basins because it takes a longer period of time for river mouth bars to aggrade to a bed elevation at which they can bifurcate distributaries, therefore deeper basins have fewer bifurcations and thus fewer active distributary channels. Fewer active distributaries create a less equitable distribution of sediment around the delta's perimeter. Avulsions occur when the distributaries aggrade and test their levees in order to attain a steeper water surface slope (Slingerland and Smith 2004). Distributaries forming in deeper basins require more time to aggrade to the bed elevation where they can test their levees, therefore, avulsion period increases with deeper initial basin depths. Less frequent changes in the position of active distributaries due to longer avulsion periods, focuses deposition around the perimeter to only a few locations for a long time. Fewer active distributaries and longer avulsion periods result less equitable distribution of sediment to around the delta's perimeter which in turn causes highly rugose shorelines (Figs. 21 and 22) and highly variable foreset dip azimuths. MLR results show that shoreline rugosity is effected by rate of BLF as well as basin depth, likely through BLF inhibiting mouth bar formation and channel bifurcation, therefore it may also be appropriate to conceptualize shoreline rugosity as a function of shoreline trajectory when $S_T < 0$. Shoreline rugosity can be predicted using the following MLR equation:

$$\log Shoreline\ Rugosity = 0.32 * \log Basin\ Depth - 0.2 * \log Rate\ of\ BLF \tag{35}$$

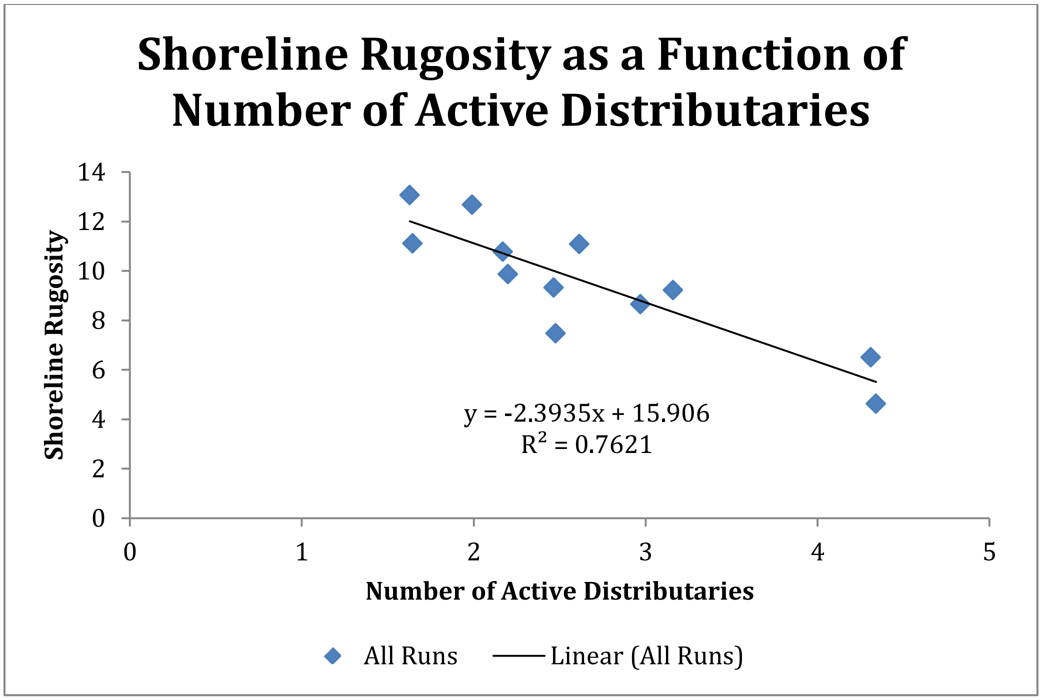

Figure 21. Shoreline rugosity decreases significantly as the number of active distributaries increases ($p = 2.1 \times 10^{-4}$). High numbers of active distributaries are able to deliver sediment to the shoreline more equitably resulting in fan deltas with smooth shorelines.

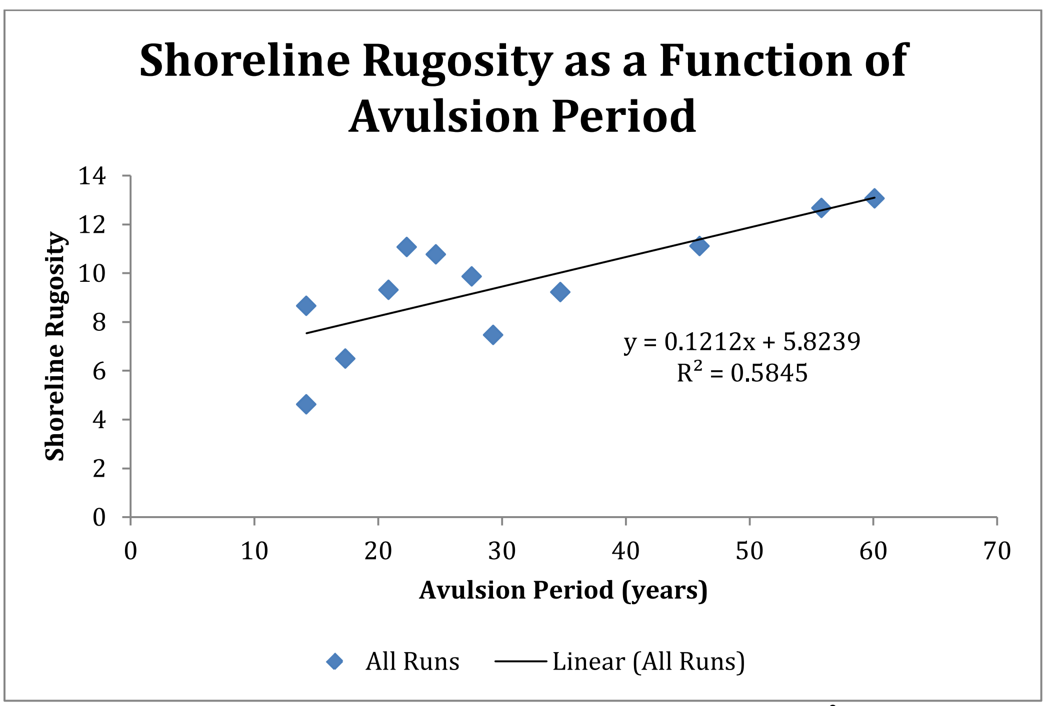

Figure 22. Shoreline rugosity increases as the avulsion period ($p=3.78 \times 10^{-3}$). Long avulsion periods focus sediment deposition at one locality for a longer period of time, thereby causing irregularly-shaped, rugose shorelines.

The shoreline trajectory is a good predictor of a delta's internal geometry and vice versa. As the shoreline trajectory steepens, clinoform heights decrease from proximal to distal. Accurate clinoform heights may be difficult to measure in the rock record though, due to subsequent erosion. Clinoform dip magnitudes, on the other hand, have a high preservation potential and could provide a useful metric for identifying basin depth and BLF in ancient deltas. The average clinoform dip magnitude is strongly dependent upon the basin depth (Fig. 13) because deeper basin depths result in tractional sediment transport occurring over a smaller portion of the delta front than in shallower basins. Tractional sediment transport creates shallower clinoform slopes than suspended transport, therefore we expect deeper initial basin depths to result in tractional transport accounting for less of the total sediment transport along the delta front and thus larger clinoform dip magnitudes. Clinoform dip magnitudes decrease from proximal to distal under BLF if the basin floor bathymetry is flat because of the delta is prograding into increasingly shallow water. It should be noted, however, that Delft3D lacks an algorithm to account for slumps or other gravity-driven flows of sediment down the delta foreset, thereby overestimating clinoform dip magnitudes. The effects of clinoform height and dip magnitude can be conceptualized for deltas of varying shoreline trajectories prograding into basins with varying slopes. In Figure 23 it can be seen that when the shoreline trajectory is steeper than the basin slope, which is the case in the simulated deltas, that BLF results in shorter clinoform heights and shallower clinoform dips magnitudes. When the shoreline trajectory and basin slope are equal clinoform heights and dip magnitudes should remain constant. In the scenario where the shoreline trajectory is shallower (or zero) than the basin slope, increasing clinoform heights and dip magnitudes should increase. Note that BLF is not a necessary condition for increased clinoform dip magnitudes.

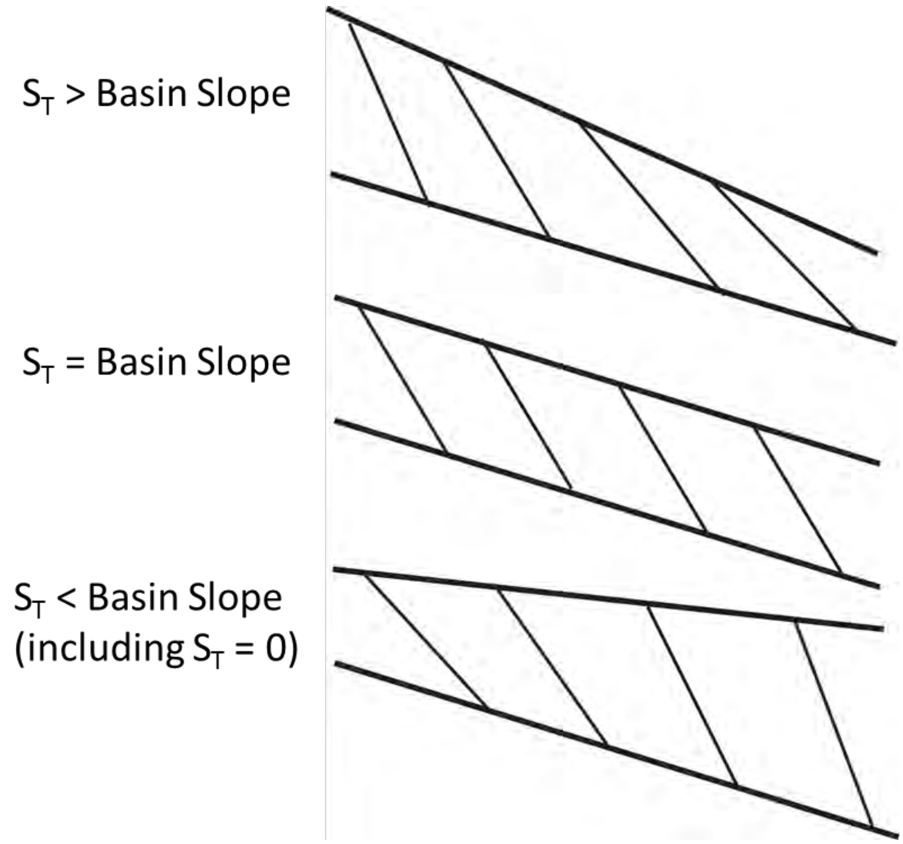

Figure 23. Conceptual diagram of clinoform height and dip varying based upon relationship between shoreline trajectory and basin slope. When S_T > basin slope, clinoform heights and dip magnitudes decrease from proximal to distal. When S_T =basin slope, clinoform heights and dip magnitudes remain constant. When S_T< basin slope, or S_T=0, clinoform heights and dip magnitudes increase from proximal to distal.

Foreset facies increase in thickness more with increasing basin depth than their corresponding topset because the topset thickness is set by the relatively constant height of levees and point bars in distributary channels. This in turn causes topset/foreset ratios to decrease with increasing basin depth. The statistically constant average grain size of delta lobes from proximal to distal indicates that neither basin depth nor rate of BLF have any significant impact on grain size. This stands in contrast to the predictions made by Posamentier and Morris (2000), but it must be noted that the modelling presented here does not account for rejuvenation of the fluvial catchment which could feasibly cause an increase in average grain size over time.

In summary, basin depth and rate of BLF are good predictors of a simulated delta's planform and internal geometry. If all other factors except basin depth and rate of BLF are held constant, increasing basin depth decreases the number of active distributaries, increases shoreline rugosity, decreases average area of delta lobes, increases avulsion period, and increases foreset azimuth dip variance. Increasing rates of BLF lead to greater topset roughness, a larger total area of the delta topset, and a more elongate aspect ratio. Shoreline trajectory, for cases where there is BLF and $S_T < 0$, may better predict the effects of initial basin depth and BLF on the number of active distributaries and the shoreline rugsoity than either basin depth or BLF could alone. Physical processes including greater time periods required for aggradation within distributary channels can be linked to a deeper basin depths and lead to longer avulsion periods and fewer active distributaries. Consequently, deposition is focused in one or two locations for a long time before the locus of deposition shifts, thereby causing highly rugose shorelines and complex delta front geometries.

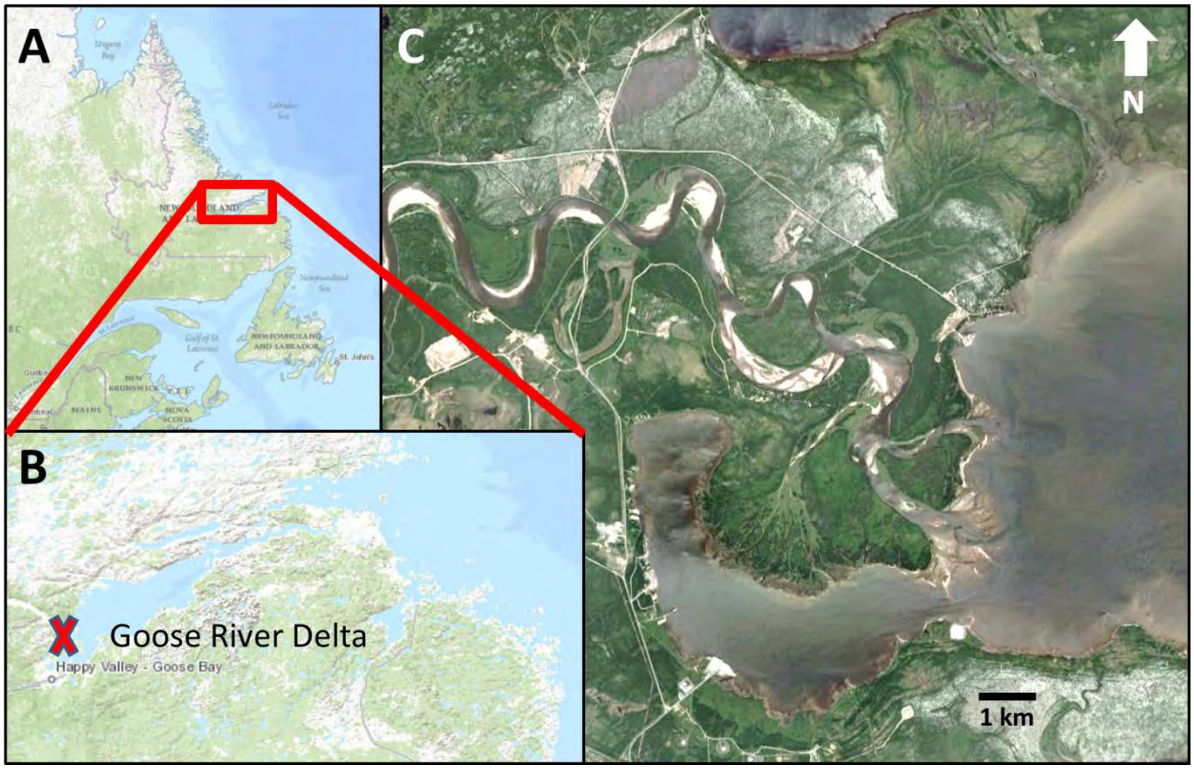

Figure 24. The Goose River Delta is located in Goose Bay, Labrador, Canada (A) where is prograding into the tip of the Lake Melville fjord (B). (C) is located at the X marked in (B).

Testing Model Predictions

Goose River Delta

To test the predictions of the Delft3D modelling we compare the model results to morphological and stratigraphic data collected from the Goose River Delta located in Goose Bay, Labrador, Canada. Here the Goose River drains a 3436 km^2 catchment (Anonymous, 2001) into the western tip of Lake Melville (Fig. 24). The Goose River Delta was chosen for this study because post-glacial rebound in the region has resulted in 5 mm yr^{-1} of BLF over the last 8,000 years (Clark and Fitzhugh 1992; Liverman 1997). Radiocarbon and OSL dates in combination with the elevation of abandoned delta lobes corroborate a BLF rate of 5 mm yr^{-1}. The delta consists of two active lobes with at least three inactive lobes upstream. The river is ungauged; sporadic measurements taken from 1948 to 1952 (Coachman, 1953) indicate highly variable discharges ranging from 5 $m^3 s^{-1}$ in March to 532 $m^3 s^{-1}$ during the spring freshet in May.

The sediment load of the Goose River is unknown. Laser particle size analysis of sediment samples collected from topset and foreset facies, including bottom grabs from the modern delta front, were weighted by measuring the vertical distance between samples and interpolating to approximate the change in grain size moving down the delta front. Interpolated values were then averaged to obtain an average grain size in the Goose River Delta of 150 μm, with grains ranging from ~10 cm diameter cobbles to < 20 μm clays. The Goose River Delta probably prograded over an irregular fjord bathymetry; at present it is prograding into 30 m water depth. The shoreline trajectory of the Goose River Delta over the last 5350 years was estimated by calculating the slope of a straight line from a large distibutary (perhaps the paleo-trunk stream) identified in the upper-most abandoned lobe to the present day shoreline of the southern active lobe. It is -0.15° (S_T = -2.6 x 10^{-3}). Given the Goose River Delta's average grain size and relatively shallow shoreline trajectory, its morphometry should be most closely predicted by the simulated delta which prograded into 20 m water depth under a 5 mm yr^{-1} BLF forcing.

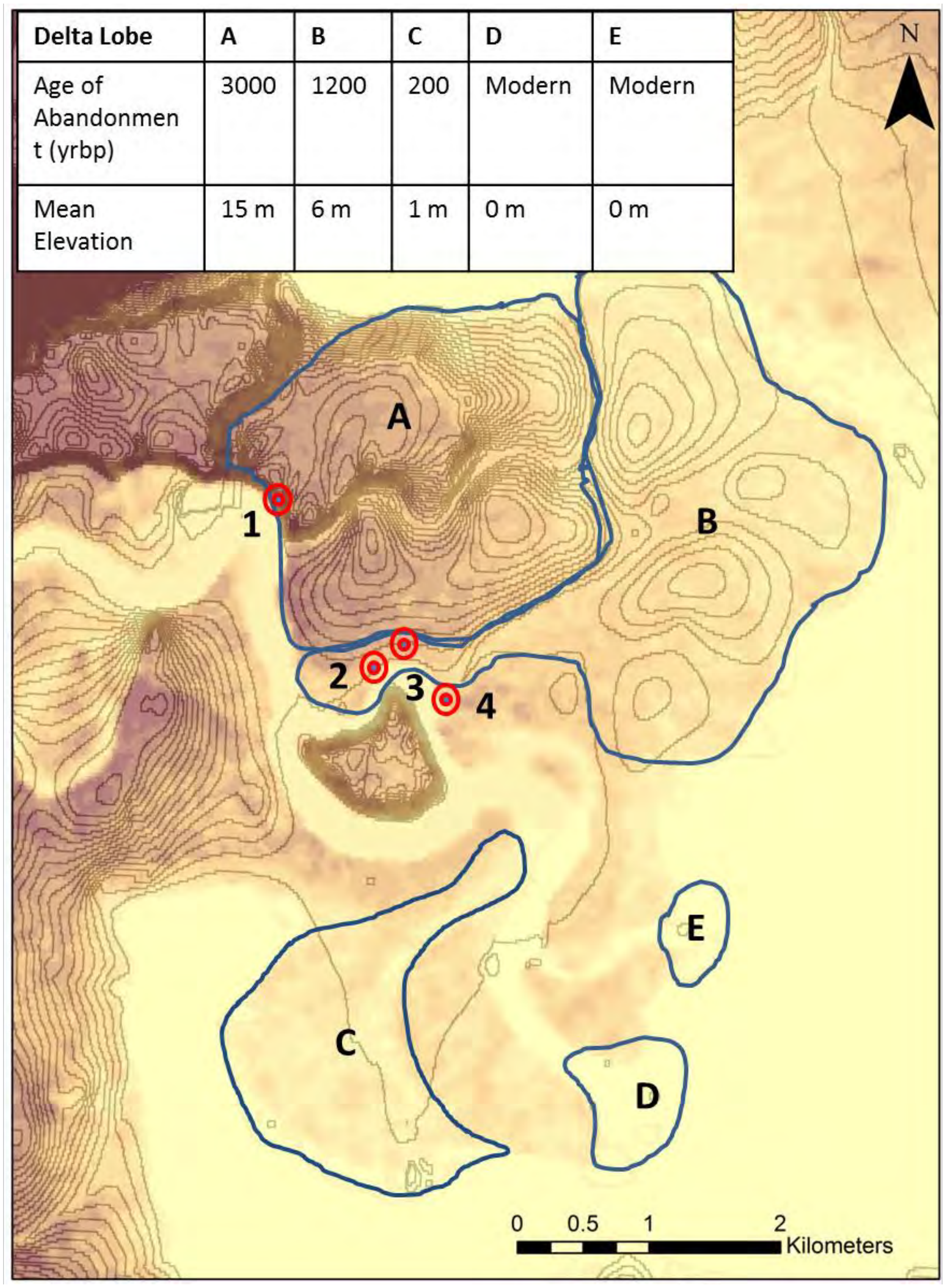

Delta Lobe	A	B	C	D	E
Age of Abandonment (yrbp)	3000	1200	200	Modern	Modern
Mean Elevation	15 m	6 m	1 m	0 m	0 m

Figure 25. Locations of the stratigraphic sections indicated on a digital elevation map of the Goose River Delta. Delta lobes are outlined in black corresponding to the yellow outline, P, enclosing the area, A, in Figure 2. Darker colors represent higher elevations while lighter colors are lower elevations. The contours are elevations with a contour interval of 2 m.

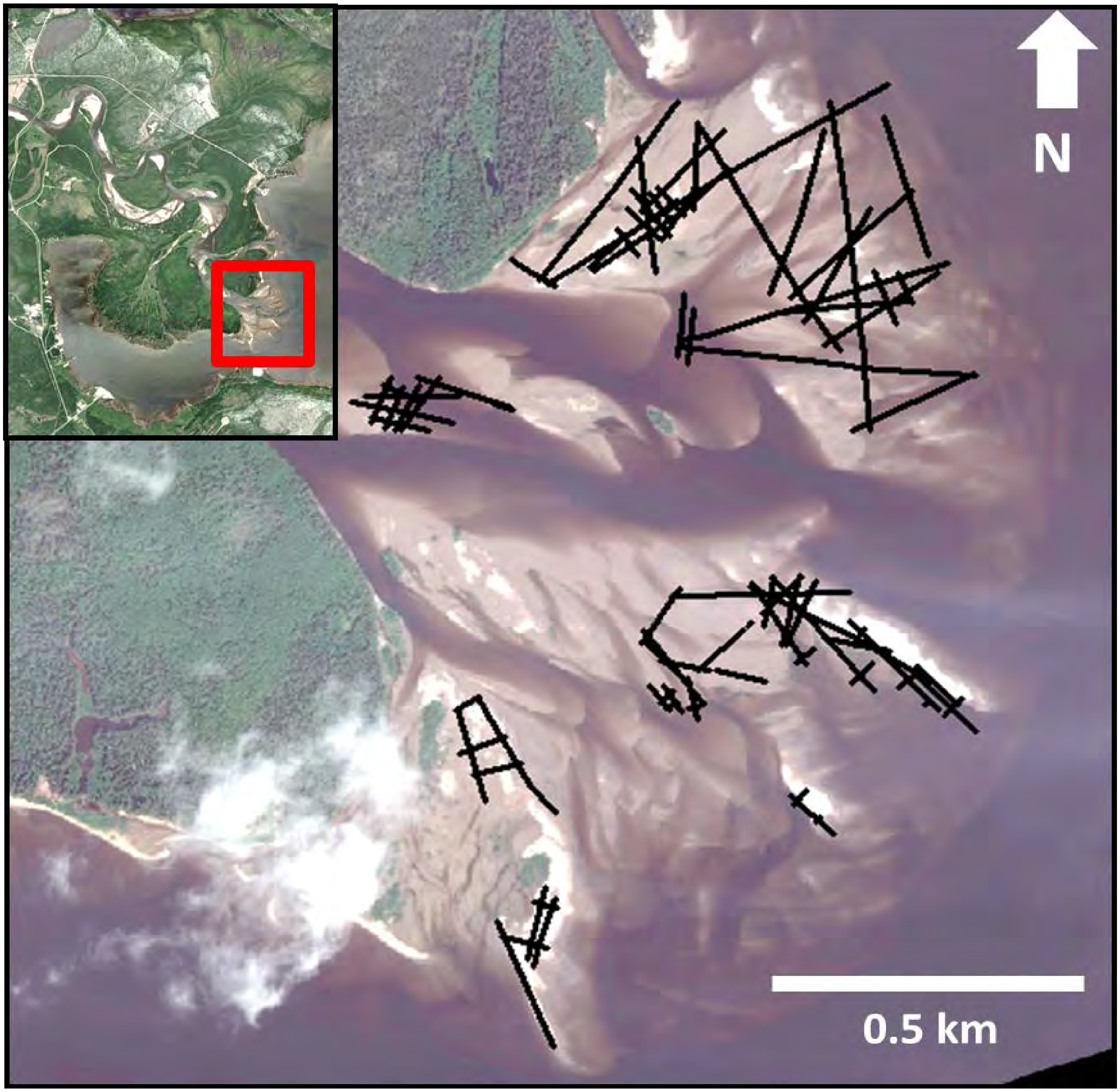

Figure 26. Locations of GPR lines collected along the southern active lobe of the Goose River Delta are indicated here in black.

Methods

Stratigraphic sections were logged at four locations (Figs. 27-31, see Fig. 25 for locations) in the Goose River's cut banks where sediments of abandoned delta lobes are exposed. The section at locality 3 (Location 3, Fig. 25) was extended downward by sinking a 3.6 m vibracore from 0.5 m above river level. Ground penetrating radar data were collected along the lines shown in Figure 26 with a Software and Sensors pulseEKKO PRO GPR using 100 MHz antennae. GPR data were processed by dewowing the data, applying a bandpass filter, and migrating the data using an F-K Stolt migration with a 1-layered velocity model with halfspace velocity of 0.6m ns^{-1}. 0.6m ns^{-1} is the velocity of electromagnetic waves through water-saturated clay and sand. The GPR data were then converted from the time to depth domain. Clinoforms were identified in the lines and their slope was measured using a linear line fitted using MATLAB. Rapid attenuation of high frequency energy resulted in poor data quality with spurious low frequency signals at depth. As a result, only lines with clear clinoforms were retained for use in the dataset. (Processed and interpreted GPR lines can be examined in Appendix D).

The morphometry of the Goose River Delta was defined from an aerial photo, single beam and multibeam bathymetric data, parabolic echosounder data, and dGPS measurements. A composite aerial photo was taken from a helicopter in August 2012. At the time, the tide and flow discharge were low providing maximum subaerial exposure. Bathymetry data were collected using a single-beam fish finder as well as a RESON 7125SV2 200/400kHz multibeam echo sounder (MBES). The MBES was used in conjunction with an Applanix POS-MV motion reference unit to correct for movement of the boat. This combination allowed for bed elevations to be mapped accurately to within 0.05 m. We defined the shoreline as the -1m contour because that is the shallowest reliable depth from the MBES. The sub-bottom stratigraphy was imaged using an Innomar Parametric Echo Sounder (PES) operating at 6 kHz and 100kHz. Real-time kinematic GPS was used to provide horizontal positional accuracy of 0.02 m.

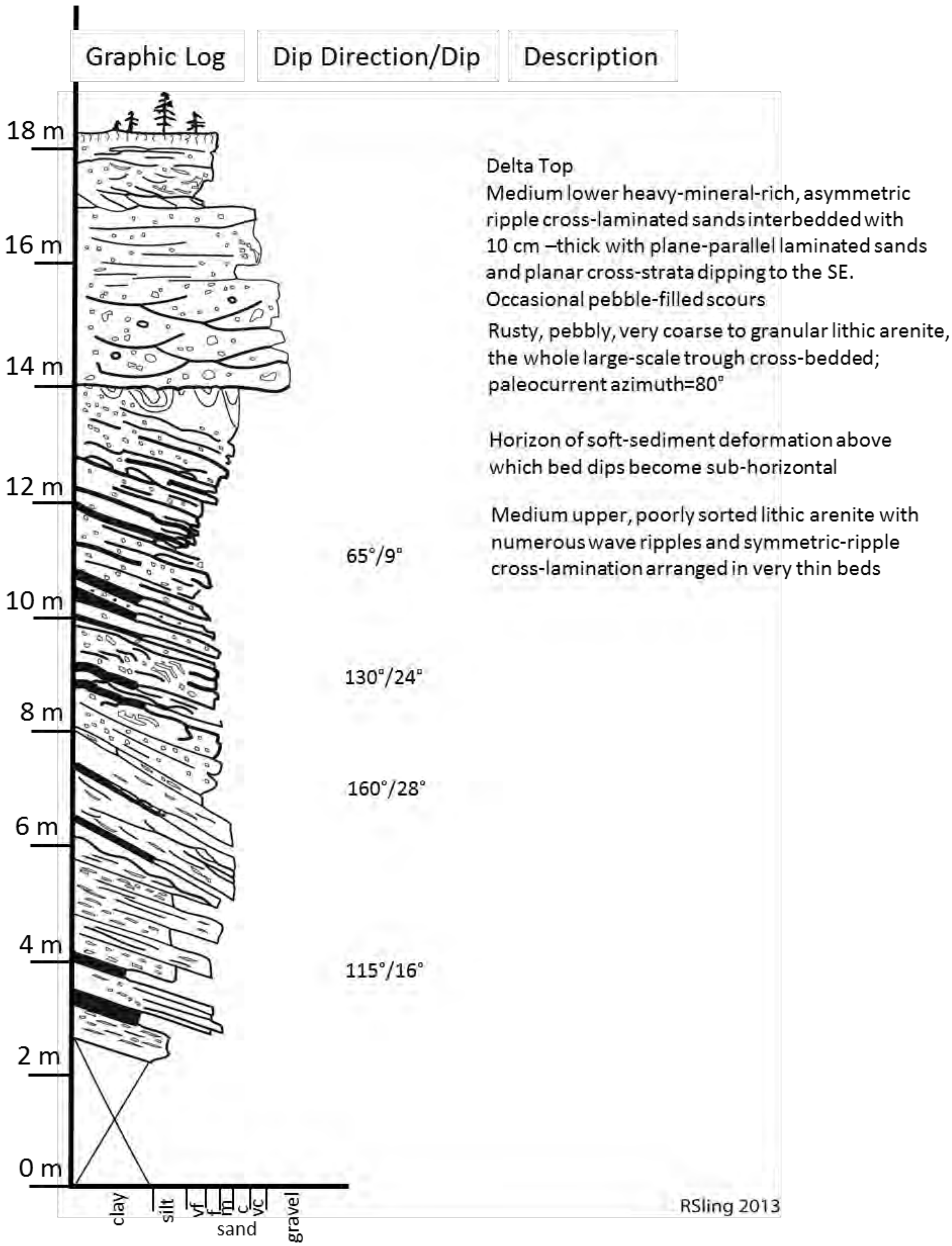

Figure 27. Stratigraphic section from location 1 in Fig.28. (N 53.39694°, W 60.40011°) (Slingerland,2013).

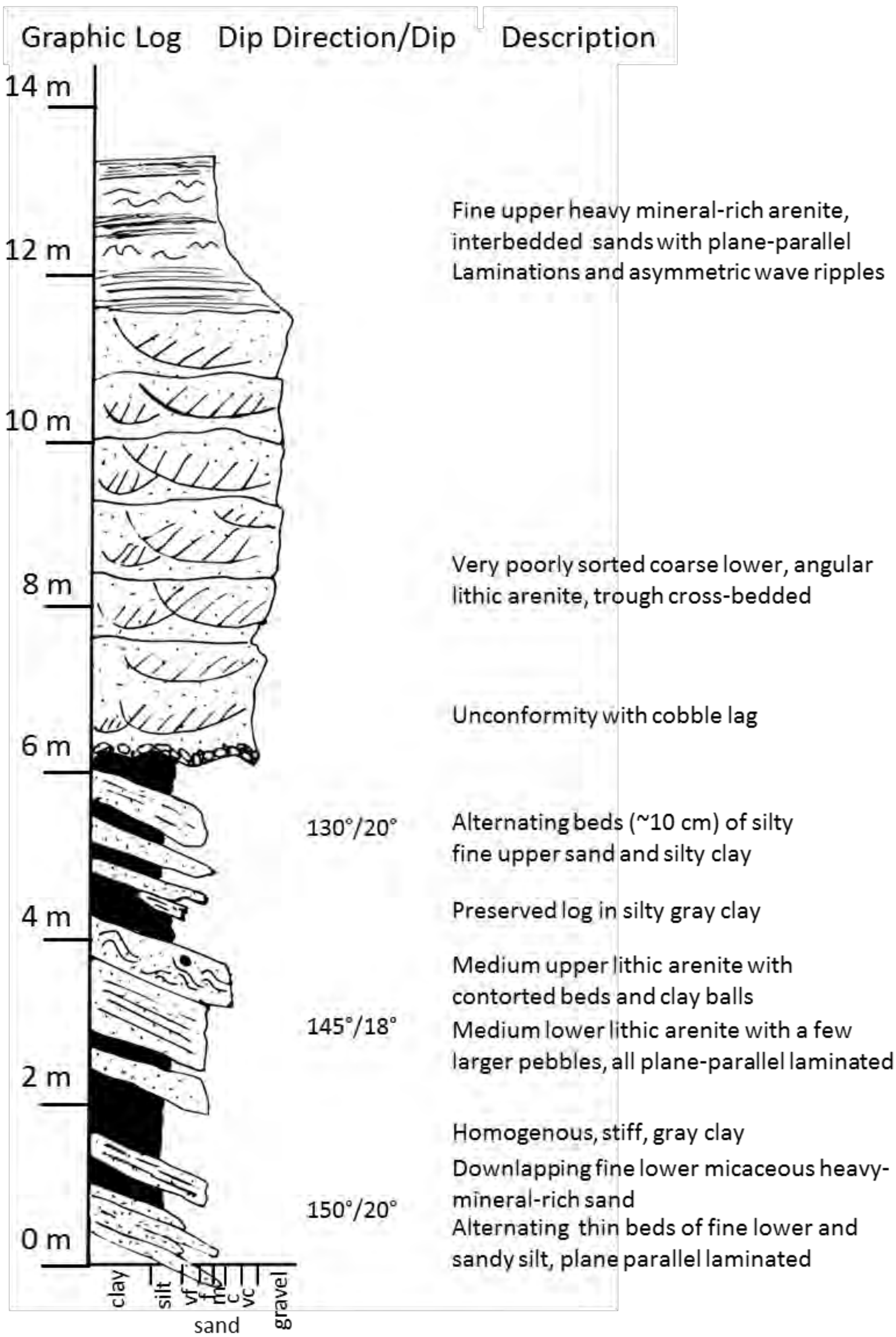

Figure 28. Stratigraphic section from location 2 in Fig.28 (N 53.3874139°, W 60.38614°)

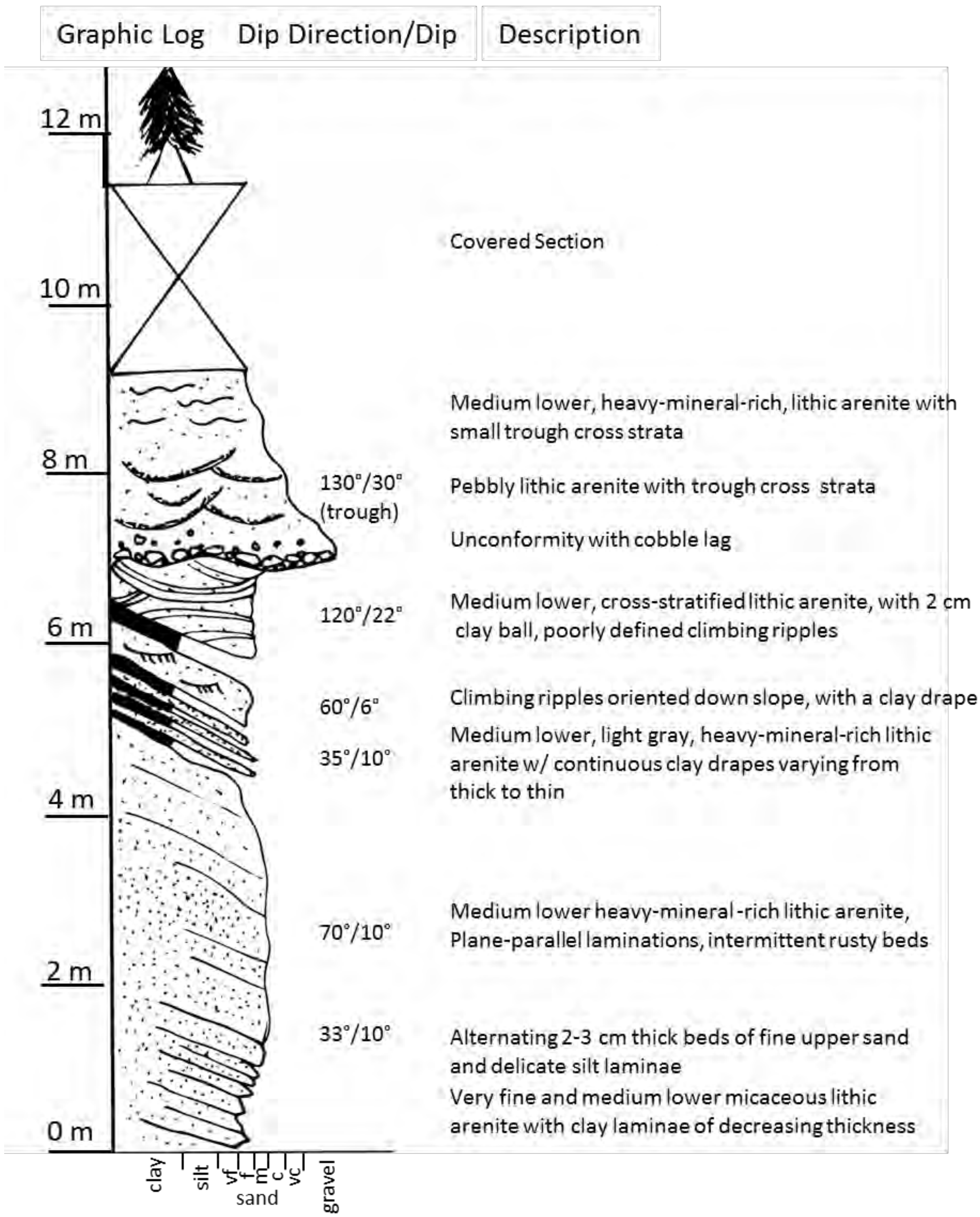

Figure 29. Stratigraphic section from location 3 in Fig. 28. (N 53.38744°, W 6038478°).

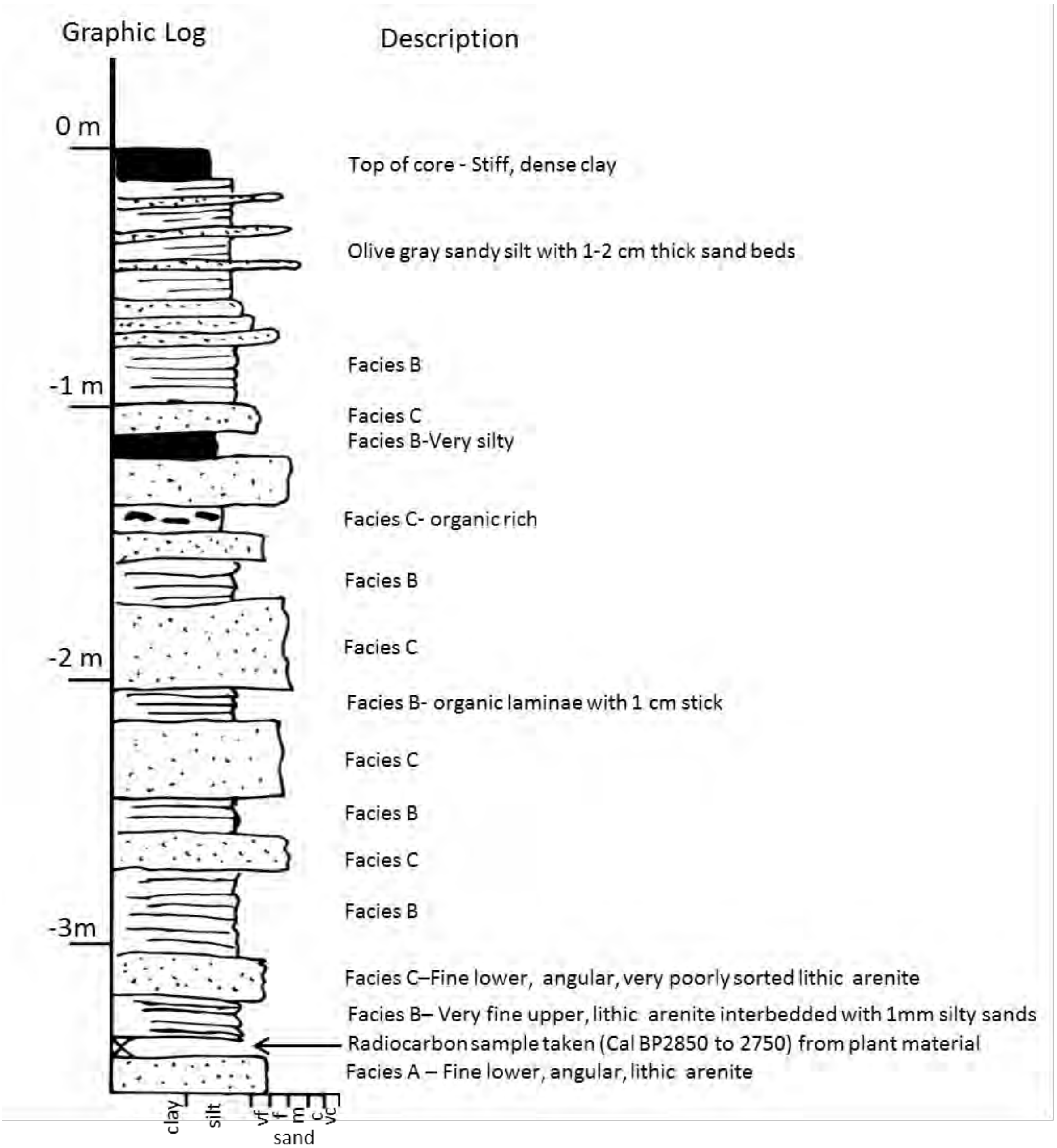

Figure 30. Graphic log of vibracore sunk 0.5m above river level at location 3 in Fig. 28. (N 53.38744°, W 6038478°). Depositional dips of beds are not shown due to uncertainty in dip magnitudes.

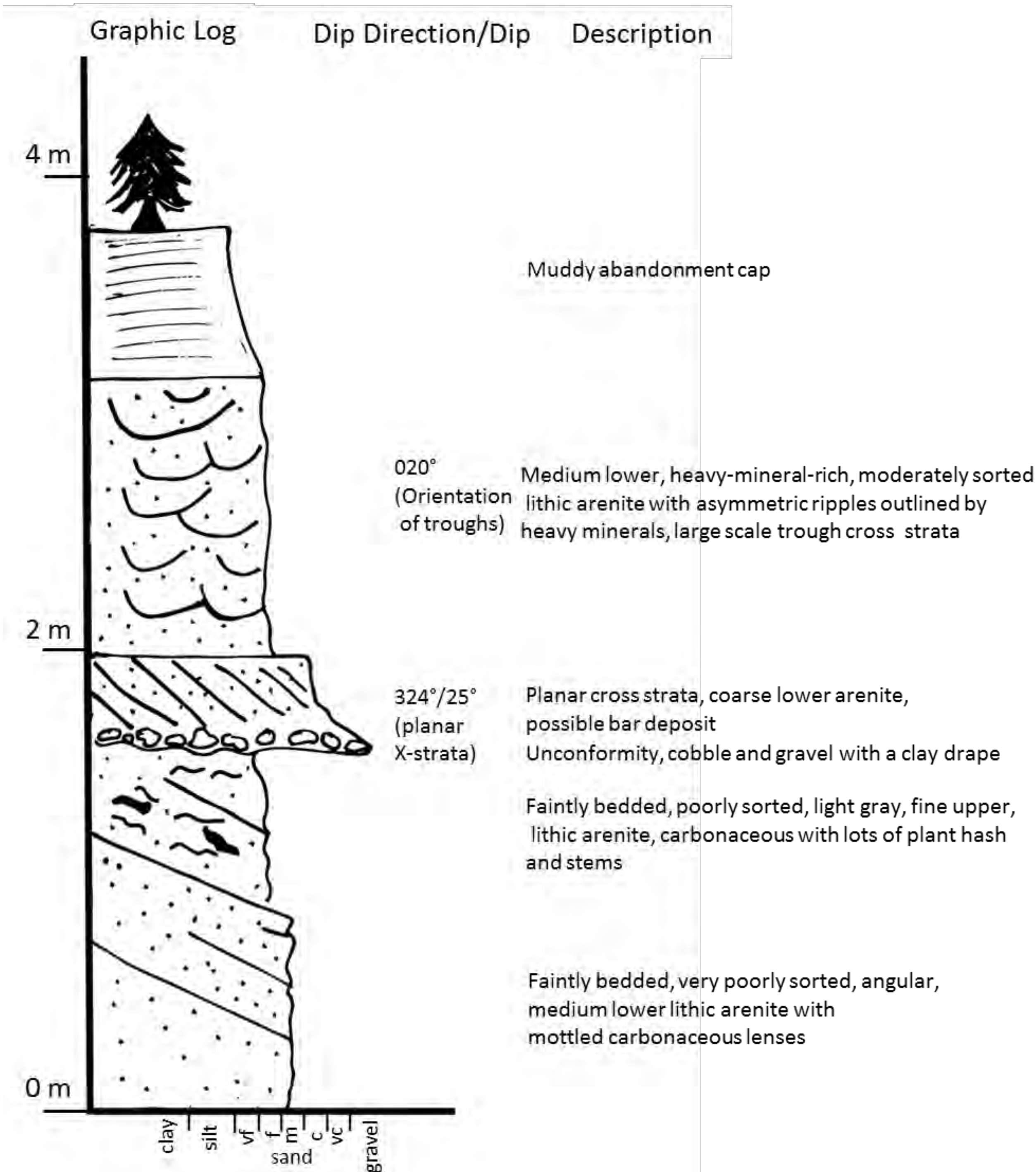

Figure 31. Stratigraphic section from location 4 in Fig.28. (N 53.38733°, W 60.38397°).

Results

The Goose River Delta's shoreline trajectory is -0.15° (S_T = -2.6 x 10^{-3}). Combined, the northern and southern active lobes of the Goose River Delta possess four to five (mean =4.333) distributaries time-averaged from 1952 to 2012 with a maximum width of at least 50 m (Fig. 32). Five delta lobes created via lobe switching events (avulsions) over the last 5350 years were identified by careful study of the digital elevation model (DEM). (Fig. 25 and 33), Thus the avulsion period is 1070 years. The Goose River receives only an eighth of the sediment of the simulated deltas, therefore the scaled avulsion period is $1070 \div 8 = 134$ years. A rough estimation of the sediment flux was made to normalize the avulsion period by estimating the volume of sediment in the Goose River Delta and dividing that by the oldest measured radiocarbon date (5350 years). We assumed the previous bathymetry sloped from roughly 15 m water depth to the present day 30 m water depth in order to make this sediment flux estimate. Multibeam bathymetry data indicate a mean clinoform dip magnitude of 4° with a standard deviation of 4.4°. Similarly, GPR data indicate a mean clinoform dip magnitude of 3.9° with a standard deviation of 2.5°. The modern clinoform (foreset) is steepest at the top with dips averaging between 10-12°, decreasing to horizontal at the base. Interpretation of the DEM and orthophotos yield a shoreline rugosity of 2.3 for the Goose River Delta complex (including the abandoned lobes). dGPS points along a random strike line estimate the Goose River Delta's topset roughness to be 0.11 m.

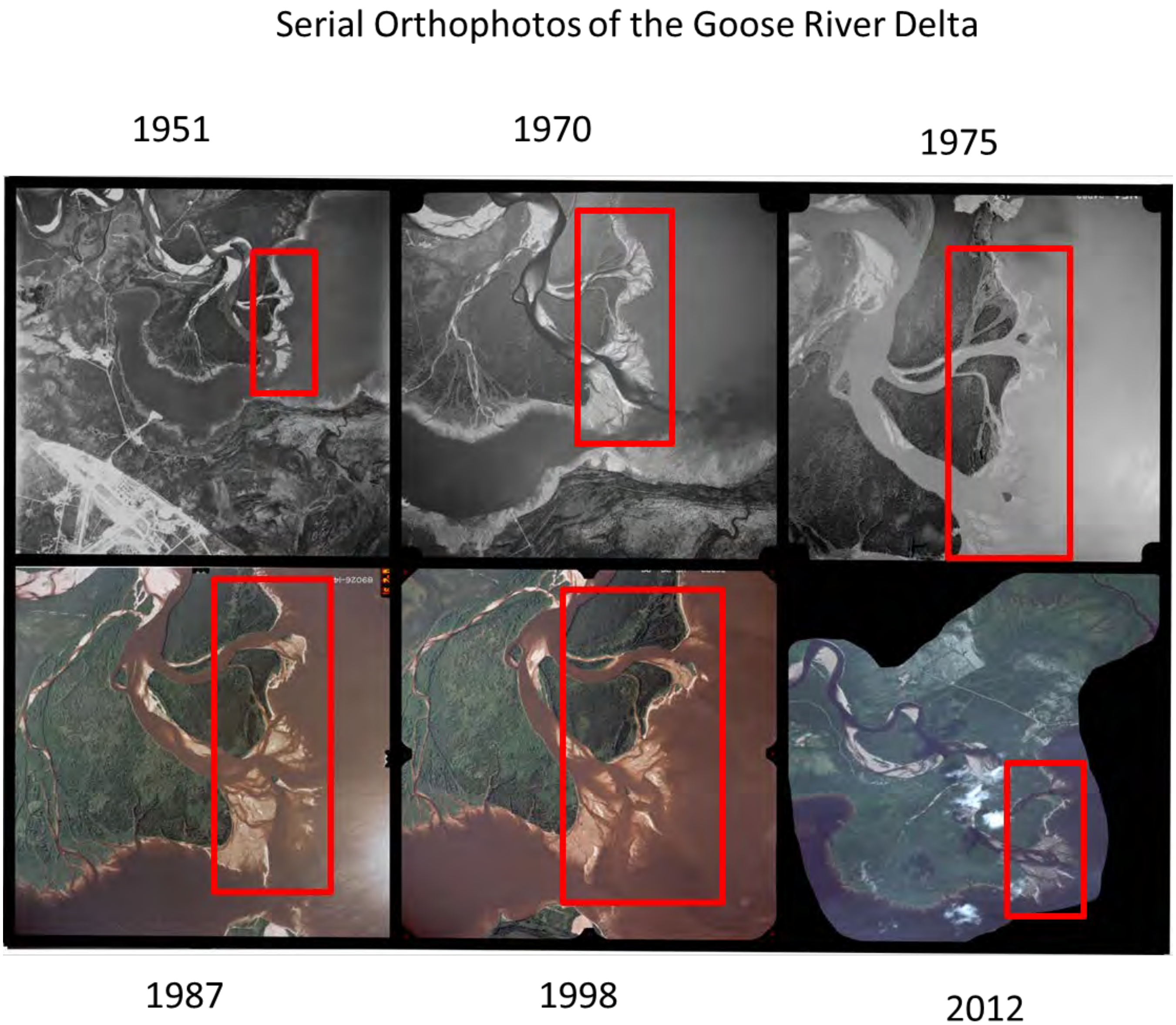

Figure 32. Serial orthophotos of the Goose River Delta used to measure the time-averaged number of active distributaries through time. Red boxes indicate the area in which distributaries were counted. We identified five active distributaries greater than 50 m wide in 1951, five in 1970, 7 in 1975, three in 1987, three in 1998, and three in 2012. Each orthophoto was given equal weight in the average. (Images from 1951 – 1998 from Newfoundland and Labrador Department of Conservation; 2012 satellite image was purchased from MapMart).

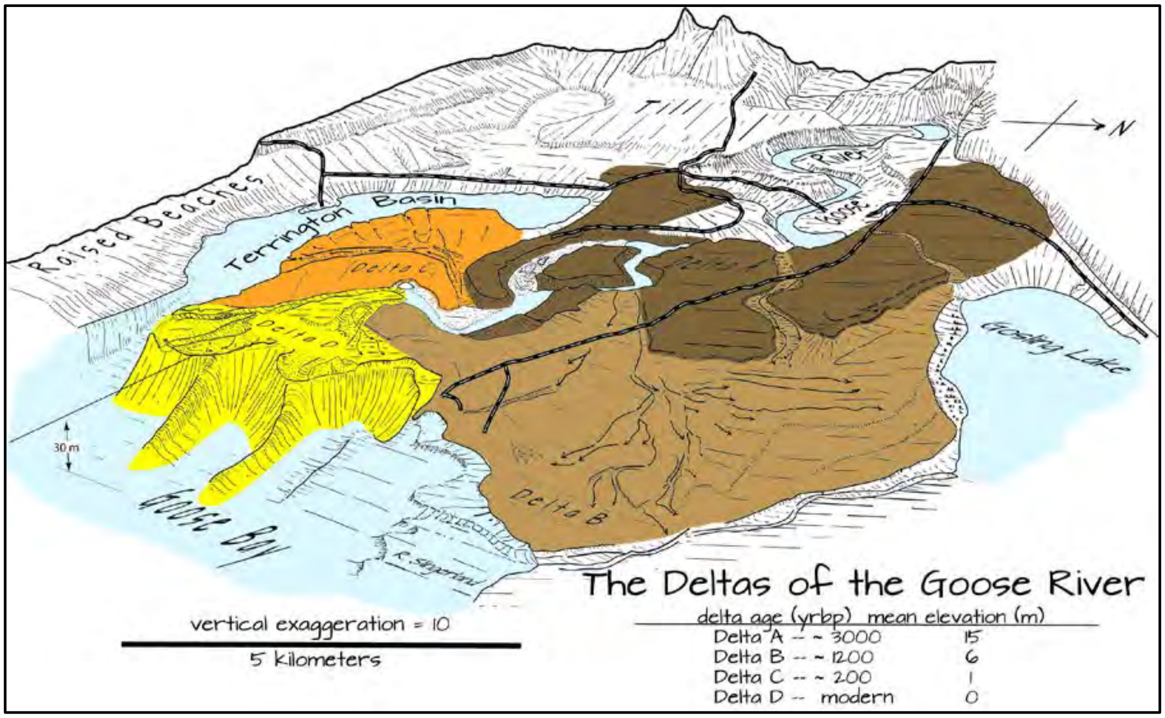

Figure 33. The location, radiocarbon age, and elevation of each lobe of the Goose River Delta are defined in this sketch (Slingerland, 2013).

Discussion

The simulated deltas can be used to predict the morphology and internal geometry of the Goose River Delta. It is important to recognize that while grain size and shoreline trajectories may be similar in the simulated deltas and the Goose River Delta, there are differences in basin depth, water discharge, and sediment discharge between the simulated deltas and the Goose River Delta. Recognizing these differences and testing the model against the Goose River Delta allows us to determine how applicable the model is to deltas with different boundary and initial conditions.

The regression equations derived from the Delft3D modeling predict one to two active distributaries on average for a delta with a similar basin depth to the Goose River Delta. Six aerial photos taken at random ice-free times document an average of four to five distributaries, fairly similar to the predicted, even though the serial orthophotos cover a short interval in relation to the age of the delta (~5350 years). The disparity that exists is likely due to the fact that we are comparing simulated deltas forming in flat basins to a delta forming in a fjord with irregular pre-existing bathymetry. The predicted avulsion period based upon basin depth for a delta like the Goose River Delta is 75 years. The observed, flux-corrected avulsion period is 134 years. One possible explanation for this disparity is that the Goose River Delta's sediment flux may be less than our estimate. A second explanation may be that the irregular, and possibly confining, fjord bathymetry limited the possibility of a steeper water surface slope being through avulsions and lateral lobe switching thereby increasing the avulsion period. The predicted clinoform dip magnitude for a delta with basin depth like the Goose River Delta is 1.1°. It is important to note that the largest simulated clinoform dips (~0.9°) are observed in the 20m deep basin, while the Goose River Delta is prograding into 30 m water depth which is deeper than any simulated delta. Goose River Delta clinoform dips are steeper than expected (4°). This disparity may reflect the role of slumping (Fig.34) and other gravity driven grain flows on the delta front which is not accounted for in the Delft3D simulations. Using MLR Equation 35, we predict that the shoreline rugosity for a delta with a shoreline trajectory like the Goose River Delta should be five to six while the actual value is two to three. Wave and tide energy acting upon the Goose River Delta may be the cause of the smoother than expected shoreline. The less rugose shoreline is consistent, however, with the Goose River Delta possessing more active distributaries that deliver sediment to the perimeter of the delta more evenly.

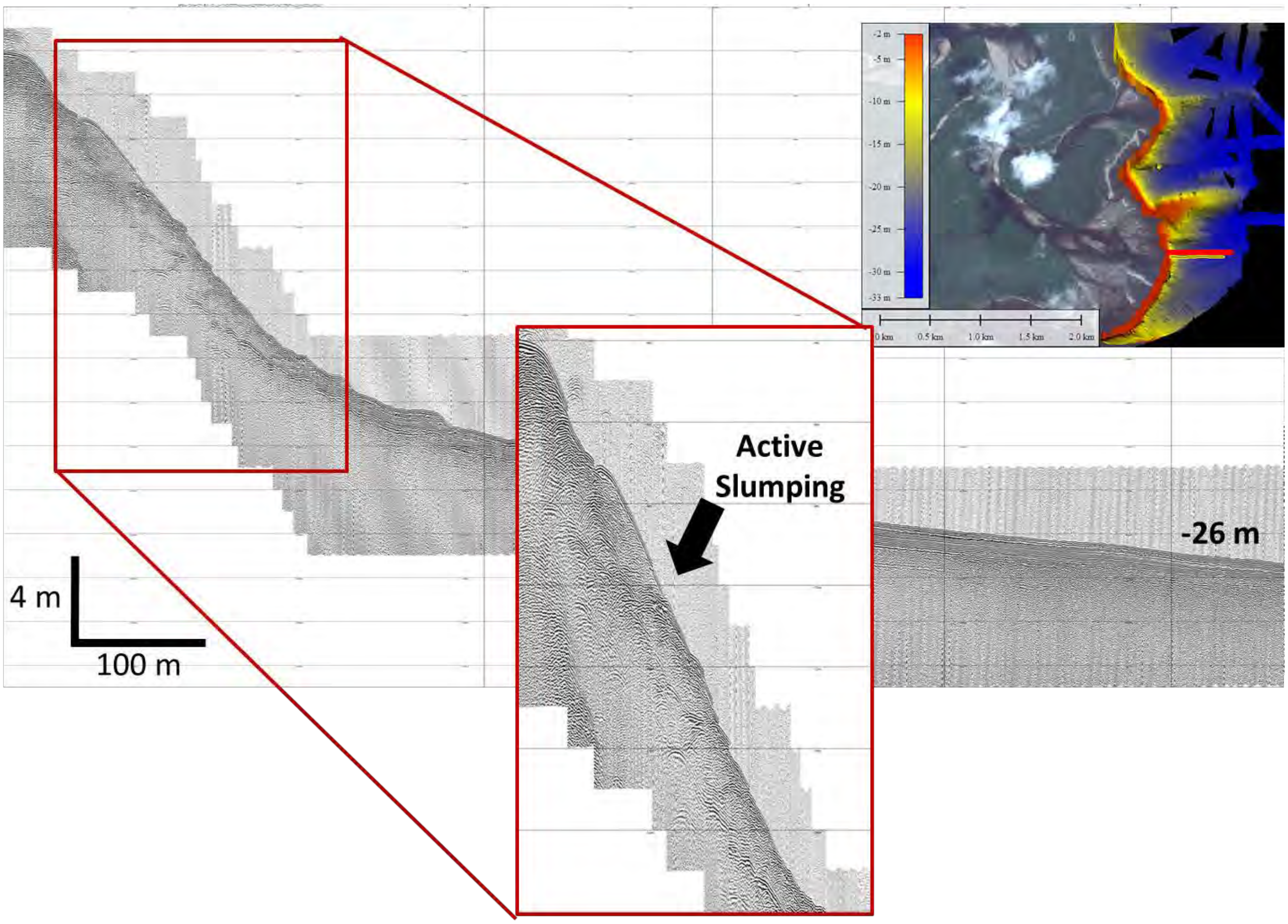

Figure 34. Slumping down the delta front can be seen in this image produced from Parabolic Echo Sounder data (J. Best pers. com., 2012). It is important to note that Delft3D does not account for slumping.

Application to the Ancient

The Panther Tongue Member of the Starr Point Formation near Helper, Utah is reported to be a forced-regressive delta, but there is some level of doubt in the evidence to support this interpretation. Here we apply the relationships predicted by the Delft3D modeling to test the idea that the Panther Tongue Delta experienced BLF.

Panther Tongue Delta

The Panther Tongue Member of the Starr Point Formation was deposited during the Late Cretaceous (Campanian; 83.6-72.1 Ma) as a deltaic succession prograding north-northeast to south-southwest into the Western Interior Cretaceous Seaway (Newman and Chan, 1991; Hwang and Heller, 2002; Edwards et al., 2005; Olariu and Bhattacharya, 2005; Howell, Skorstad et al., 2008, Howell, Vassel et al., 2008; Enge, Howell et al., 2010a; Enge, Howell et al., 2010b; Enge, Howell et al., 2010c; Hampson, Gani et al., 2011) (Fig. 35 and Fig. 36). The Panther Tongue Mbr. was first described as a deltaic "parasequence deposited at eustatic lowstand" (Newman and Chan 1991), and later re-characterized as a falling stage systems tract (FSST) (Posamentier, Morris et al. 1995) . As evidence that the Panther Tongue was deposited during a fall in relative sea level, Posamentier and Morris (2000) cited: 1) a basinward decreasing clinoform height, due to a shallowing of water depth; 2) an absence of preserved delta topset deposits; 3) a sharp-based contact between the FSST and the underlying highstand systems tract (HST), in this case the Mancos Shale; 4) a shift from proximal, inertia-dominated suspension-type deposition to distal bed-load dominated deposition; and, 5) fore-shortened stratigraphy, where clinoform heights are less than would be expected for a given water depth (i.e., a 20 m high clinoform forming in 75 m of water). In a later paper, Posamentier and Morris (2000) cited the Panther Tongue as an example of a classic forced regressive delta, even though their criterion 1 cannot be applied to the PT because of poor outcrops and subsequent ravinement at the beginning of the transgressive systems tract. Criterion 5 cannot reasonably be used as evidence of a forced-regressive origin for the Panther Tongue Mbr. because subaquoeous clinoform rollovers can exist even in deltas experiencing relative base level rise like the Fly River Delta of Papua New Guinea (Slingerland et al., 2008). They acknowledged that each of their lines of evidence alone was circumstantial, but proposed that when observed together the converging lines of evidence strongly indicated a forced regression. Hwang and Heller (2002), make a significant contribution by recognizing what they called lowstand, healing phase deposits onlapping clinoforms of the Panther Tongue Mbr. on the east side of Price River Canyon. Furthermore, they recognized the ravinement surface at the top of the Panther Tongue as a transgressive lag deposit, further corroborating the notion that the Panther Tongue belongs to the FSST.

The shoreline trajectory of the Panther Tongue Mbr. is debated. Howell, Skorstad, et al. (2008) assigned the Panther Tongue a positive shoreline trajectory of 0.07 degrees which, if accurate, would be inconsistent with a forced-regressive origin. In conflict with this shoreline trajectory, they also cited Posamentier and Morris (2000), and stated that the Panther Tongue Delta was deposited during a forced regression. We assume then, that they did not follow the convention of other workers who defined the trajectory as negative downwards. Even so, it is unclear how they determined this value, because the clinoform rollovers from which one would measure a shoreline trajectory have been removed by the subsequent ravinement surface. Hampson, Gani et al. (2011) interpreted the Panther Tongue as a single parasequence containing multiple delta lobes experiencing BLF. They ascribed a shoreline trajectory of -0.02° to the Panther Tongue Mbr. by using a novel approach in which they measured the down-dip pinchout of proximal delta front deposits in a dip-oriented outcrop perpendicular to the subregional shoreline orientation. This requires accurately removing the local tectonic dip which is large (~7°) compared to the S_T.

The reported rates and magnitudes of BLF for the Panther Tongue Delta vary considerably, with limited evidence provided to support one value over another. Hampson, Gani et al. (2011) conjecture that low-amplitude (< 30m), high-frequency (< 400 kyr) glacio-eustatic, relative sea level cycles controlled the deposition of the Panther Tongue. They cited a lack of topset facies and offlapping delta lobes as evidence of BLF during Panther Tongue times. However, the authors claim there is little evidence to suggest BLF during deposition of a time-equivalent wave-dominated shoreline to the south of the Panther Tongue Mbr. To reconcile this conflict, the authors proposed that the un-named wave-dominated shoreline to the south was deposited during a period of relative base level rise and that subsequent BLF resulted in the rapid progradation of the Panther Tongue Delta. In Sowbelly Gulch, near Standardville, UT, Newman and Chan (1991) observed single-story sand bodies that they interpreted to be distributary channel deposits. Olariu and Bhattacharya (2005) called these channel facies "terminal" distributaries, cutting river mouth bars. The bars then aggraded upstream and laterally filled them. The resulting sand bodies were preserved in a delta-front environment free of subaerial erosion. Both aggradational mouth bars and a lack of subaerial erosion seemingly conflict with BLF occurring during deposition of this proximal area of the Panther Tongue Mbr. A contrasting interpretation suggests that these channels were submarine channels formed in an estuarine environment during subsequent relative base level rise (Hwang and Heller 2002).

The water depth into which the Panther Tongue Delta prograded has received limited attention from previous researchers, and depth estimates that do exist are not well justified. Posamentier and Morris (2000) cite unpublished biostratigraphical data from a personal communication, arguing that the Panther Tongue Delta prograded into water depths deeper than 75 m. They use this water depth estimate in relation to the typical, preserved clinoform height (~25 m) as evidence of fore-shortened stratigraphy and a forced-regressive origin of the Panther Tongue Mbr. However, a more reliable estimate of paleo-water depth can be obtained by assuming that wave-rippled strata were deposited at or above fair weather wave base (typically 5-20 m). In the proximal portions of the Panther Tongue Mbr., both Newman and Chan (1991) and Olariu et al. (2010) document wave ripples in lower delta front sands positioned less than 2 meters above the basal, prodelta muds. The presence of wave ripples in a lower delta front depositional environment indicates that the delta was prograding into water very close to fair weather wave base. Based on this reasoning and truncated clinoform heights of up to 25 m, we propose that the Panther Tongue Delta prograded into a paleo-water depths of 20-30 m. This is similar to the 10-30 m water depths conjectured for the Turonian Ferron Sandstone Mbr. in a similar tectonic setting 50 km to the south (Ahmed et al., 2014).

Measurements of clinoform dip magnitudes are more consistent across previous studies, although limited in spatial distribution to the northern proximal portion of the Panther Tongue Mbr. near Helper, UT. In a series of papers (Enge and Howell 2010a, Enge, Howell et al. 2010b, Enge, Howell et al. 2010c), the authors reported clinoform dips ranging from 0.4° to 2.65° as measured by LIDAR in the proximal portion of the Panther Tongue. Olariu et al. (2010) use LIDAR to measure clinoform dip magnitudes near the study areas of Enge and Howell's (2010a, 2010b) and Enge, Howell et al. (2010) and reported values ranging from fractions of a degree to 3°. Hwang and Heller (2002) reported clinoform dip magnitudes of 7° in the proximal portion of the Panther Tongue Mbr. with clinoform dip magnitudes increasing to > 20 ° in the distal, southern portion of the Panther Tongue Mbr. near Huntington Canyon. Newman and Chan (1991) also reported steep clinoform dips ranging from 15° to 30° in the southern portion of the Panther Tongue Mbr. We interpret the published clinoform dip magnitudes of the Panther Tongue Mbr. to indicate a systematic increase in dip magnitude from north to south.

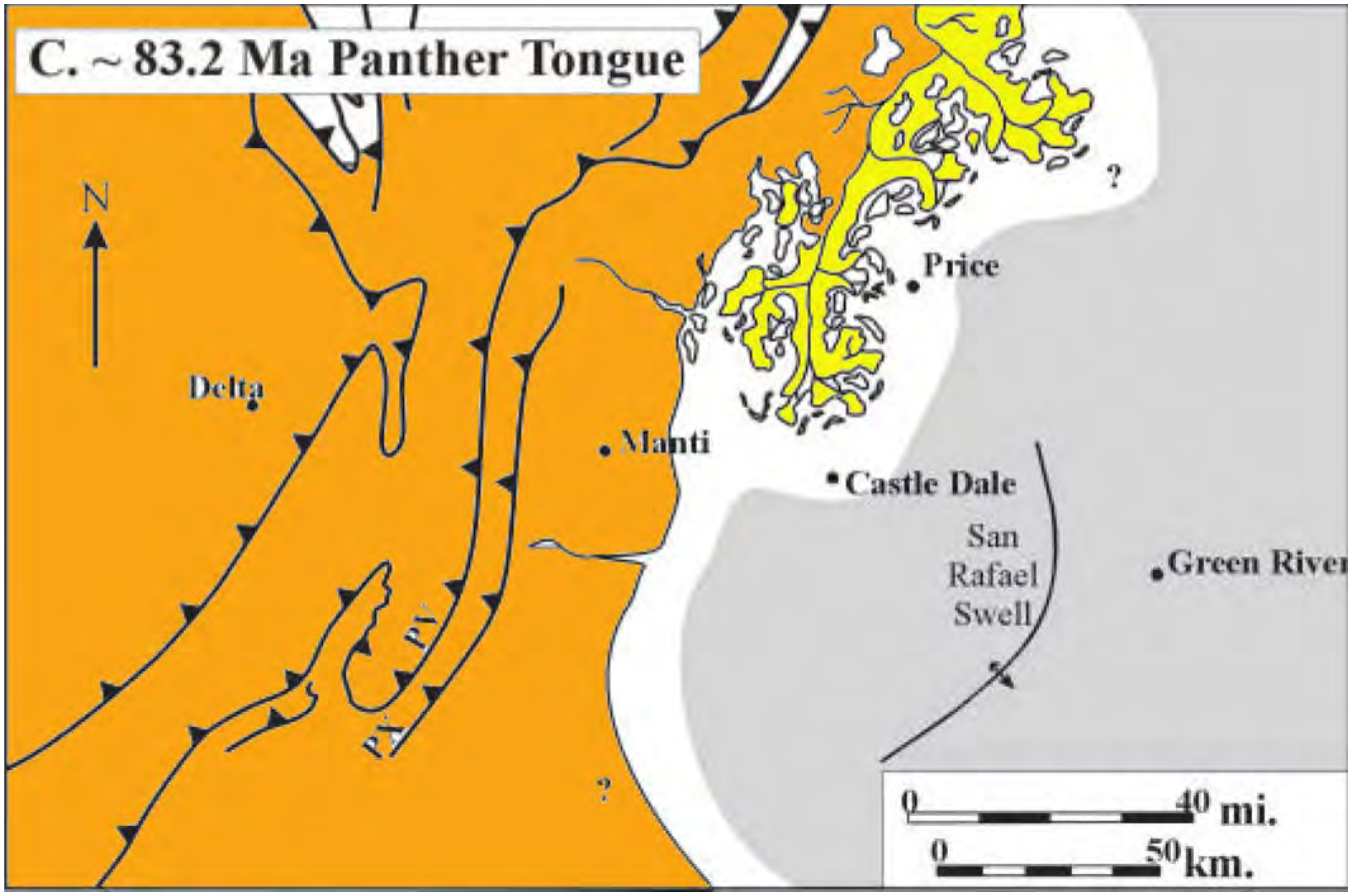

Figure 35. A paleo-reconstruction of the Panther Tongue Delta (after Edwards et al. 2005). Here there are two main delta lobes, a northern lobe prograding south east and a southern lobe prograding south-south west. Edwards et al. (2005) depict a highly rugose shoreline for the Panther Tongue Delta.

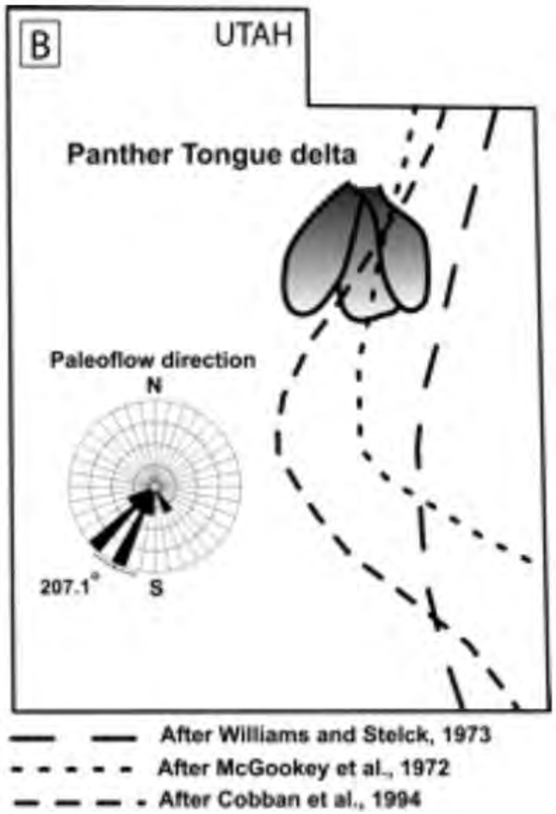

Figure 36. An interpretation of the Panther Tongue Delta from Olariu et al. (2010). They also depict three delta lobes and show the paleo-shoreline of the Western Interior Cretaceous Seaway during the Campanian. Their reconstruction of the Panther Tongue Delta indicate a lobate morphology.

Methods

To supplement the data collected by others we measured clinoform dips and dip directions in the Panther Tongue Mbr. using a laser ranger. Data were collected from locations that had two opposing cliff faces containing easily identifiable clinoform beds on either side of a canyon (Fig. 5). Points in x, y, z space were shot along individual clinoform beds with the laser ranger and a trend and plunge were calculated relative to true north. Shooting the same or adjacent bed on the other side of the canyon provided a second trend and plunge. Using the two trends and plunges, we calculated a true dip and dip direction for the clinoform tops just below the truncation surface. Depositional dips were then corrected for the tectonic dip obtained from the ravinement surface at each data collection location. A structure-contour map of coal measures overlying the Panther Tongue Mbr. (USGS Coal Resource Occurrence Map of the

Standardville Quandrangle, Carbon County, Utah) was used to corroborate the tectonic dip near Price River Canyon. Guttercasts and flutes were also measured to determine the local paleoflow direction.

Results

Clinoform dip, dip direction, and paleoflow directions are presented in Tables 2 and 3, respectively. The average clinoform dip over all exposures is 4.4°. The variability in dip direction, measured by the foreset dip azimuth statistic is 0.19 (N = 11). The mean grain size of the Panther Tongue Mbr. increases from fine sand in the proximal, northern portion of the Panther Tongue Mbr. to medium sand in the distal, southern portion of the Panther Tongue Mbr. Hampson, Gani, et al.'s (2011) measurement of -0.02° ($S_T = -3.5 \times 10^{-4}$) and Howell, Skorstad, et al.'s (2008) measurement of -0.07° ($S_T = -1.2 \times 10^{-3}$) will be considered the maximum and minimum estimates of shoreline trajectory for the Panther Tongue Mbr., respectively.

Location	Dip Azimuth (°)	Dip Magnitude (°)
1	169	1.5
2	169	2.5
2	274	6
4	164	2
4	239	7
4	254	11
6	180	4
6	128	12
7	253	6
8	290	11
8	328	12

Table 2. Clinoform dips and dip directions collected from the Panther Tongue Mbr. of the Starr Point Fm. Locations correspond to points in Figure 3. Note that the clinoform dip magnitudes increase to the south.

Location	Paleocurrent Indicator	Azimuth
1	Gutter Cast	200
1	Gutter Cast	215
1	Gutter Cast	221
2	Flute	204
2	Gutter Cast	204
2	Gutter Cast	210
3	Gutter Cast	220
5	Gutter Cast	210
5	Gutter Cast	224
5	Gutter Cast	230
5	Flute	234
5	Flute	235
5	Gutter Cast	244
5	Gutter Cast	245
5	Gutter Cast	248
5	Gutter Cast	248
5	Gutter Cast	252
5	Gutter Cast	252

Table 3. Paleocurrent indicators documented in the Panther Tongue Mbr. of the Starr Point Fm. Locations correspond to points in Figure 3.

Discussion

The grain size, basin depth, and shoreline trajectory of the Panther Tongue Mbr. fall within, or just outside, the parameter space of the model results presented earlier. Mean grain size estimates for the Panther Tongue Mbr. range from fine to medium sand. The mean grain size of the Delft3D simulations is 170 μm diameter fine sand. The Panther Tongue Delta likely prograded into 20-30 m water depth. Simulation basin depths range from 4 to 20 m deep. Therefore, the Panther Tongue Delta probably prograded at a slower rate than the simulated deltas. Shallow shoreline trajectory estimates therefore indicate a slow rate of BLF. It is difficult to compare discharges (Q), sediment fluxes (Q_s), and Q/Q_s ratios between the Delft3D model and the Panther Tongue Delta because the trunk stream of the Panther Tongue Delta is not exposed in outcrop, but the model results are scalable. By testing the model predictions against the Goose River Delta, which itself has different water depths, discharges, sediment fluxes, and Q/Q_s ratios, we validated that the model results are scalable to some extent, and can therefore reasonably be applied to the Panther Tongue Delta.

For basin depths between 20 m and 30 m, Delft3D modelling predicts average clinoform dip magnitudes ranging from 0.74° and 1.1°, and foreset dip azimuth variability ranging from 0.37 to 0.31, respectively. The observed clinoform dip magnitude (4.4°) is within a factor of four of the predicted value while the observed foreset dip azimuth variability (0.53) is within a factor of two (Table 2). It is worth noting that the basin depth of the Panther Tongue Mbr. is similar to that of the Goose River Delta (~30 m) and both deltas possess average of clinoform dip magnitudes between 4° and 5°. This consistency suggests that basin depth may be a reasonable predictor of clinoform dip magnitude in the field, and that the Delft3D simulations tend to underestimate clinoform dip magnitudes. Increasing clinoform dip magnitudes from proximal to distal are consistent within an increase in water depth from proximal to distal. The discrepancy between the predicted and observed foreset dip azimuth variability may be due to the Panther Tongue Delta prograding into slightly shallower water across the whole basin, regardless of any difference between proximal and distal water depths. The disparity could also be due to the small sample size (N=11) of the observed foreset dip azimuth data. Limited exposures are inherently a problem in outcrop studies, and the observed data may not have provided a representative value of the foreset dip azimuth variability for the Panther Tongue Mbr.

The similarity of the average clinoform dip magnitude in the Panther Tongue Mbr. and Goose River Delta suggests that the estimates of basin depth are reasonable estimates for portions of the Panther Tongue Delta. Earlier workers speculated that the higher magnitude clinoform dips in the southern part of the Panther Tongue are part of a different lobe than the clinoforms located near Helper, UT (Hwang and Heller, 2002; Hampson, Gani et al., 2011). We agree with the interpretation that this is a separate delta lobe. The increased mean grain size and clinoform dips are inconsistent with the delta-front facies observed in the proximal, northern portion of the Panther Tongue Mbr., and indicate a change in the forcings experienced by the delta as one might expect in a separate lobe formed at a different time. Hwang and Heller (2002) have suggested that an increased wave climate caused the higher clinoform dips in the southern lobe. We propose an alternative hypothesis: the change in clinoform dip could also be due to the Panther Tongue Delta prograding into progressively deeper water, and that BLF is not a necessary condition for this change in clinoform dip magnitude to arise. Our hypothesis is consistent with Delft3D modelling results indicating that basin depth is more highly correlated with steeper clinoform dip magnitudes than BLF. If true, then the southern lobe of the Panther Tongue Delta should possess fewer active distributaries, a longer avulsion period, smaller average lobe areas, lower initial topset/foreset ratios (not considering the subsequent ravinement), and a more rugose shoreline than would be present in the proximal portions of the Panther Tongue Mbr. where water depths were shallower.

The Delft3D modelling presented here assumes there is no wave or tide influence on the simulated deltas, so it is important to consider the effects of waves and tides might have had on the Panther Tongue Delta. Waves would cause littoral drift along the delta front and inhibit river mouth bar formation, causing fewer active distributaries. Littoral drift would smooth the shoreline as well and decrease the shoreline rugosity. Wave winnowing could result in removal of fine grain sediments leaving only coarser grains in the delta foreset. These coarser grains may then result in a steeper clinoform dip magnitude. This lends credibility to the hypothesis of Hwang and Heller (2002) that the southern lobe of the Panther Tongue is coarser with steeper clinoforms due to increased wave influence, but it does not rule out our own hypothesis that the Panther Tongue Delta was prograding into deeper water. Tide action would also inhibit mouth bar formation and therefore result in fewer active distributaries. Tides could potentially create more rugose shorelines complex delta fronts. There is little evidence for tide influence on the Panther Tongue, however.

In summary, Delft3D predictions of average clinoform dip magnitude and foreset dip azimuth variability are a reasonable fit with observed values. The Goose River Delta and Panther Tongue Mbr. probably prograded into similar water depths, and consequently, contain clinoforms of similar dip magnitudes. We interpret the southern region of the Panther Tongue Mbr. with steep clinoform dips to be a separate delta lobe. We propose that the steeper clinoform dips in the southern exposures are the result of the Panther Tongue Delta prograding into deeper water, and not necessarily experiencing BLF. We conjecture that the southern lobe of the Panther Tongue Delta possessed fewer active distributaries, a longer avulsion period, smaller average lobe areas, lower initial topset/foreset ratios, and a more rugose shoreline than the more proximal, northern lobe of the Panther Tongue Delta where the water depth was shallower.

Conclusions

Delft3D simulations predict a range of morphometries for medium-sized, coarse-grained deltas prograding on shelves of very shallow to medium depths and under various rates of BLF. Deep basins experiencing high rates of BLF produce deltas with steep, negative shoreline trajectories, fewer active distributaries and longer avulsion periods. The result is a more rugose shoreline. Deeper initial basin depths are also associated with smaller average lobe areas, smaller topset/foreset ratios, less variability in foreset dip azimuths, and steeper clinoforms. We found that BLF alone is a good predictor of topset roughness and a delta's aspect ratio. Within our modelled parameter space, we saw no topset aggradation in any simulated delta with BLF. Additionally, we found that there is no change in mean grain size from proximal to distal. Model predictions of a delta's planform and internal geometry are consistent with the Goose River Delta in Labrador, Canada which is known to be experiencing 5 mm yr^{-1} of BLF. We applied our model to the Cretaceous Panther Tongue Mbr. in the Book Cliffs of Utah to re-evaluate the role of BLF in the formation of the Panther Tongue Delta. We have reinterpreted the Panther Tongue Delta's southern lobe be to prograding into deeper water resulting in a steeper clinoform dip magnitudes, and that BLF was not a necessary condition for to cause this change in clinoform dip.

References

Ahmed, Sumiyyah, et al. "Facies Architecture and Stratigraphic Evolution of A River-Dominated Delta Front, Turonian Ferron Sandstone, Utah, USA." *Journal of Sedimentary Research* 84.2 (2014): 97-121.

Anonymous, 2001. Aquatic environment in the Goose Bay estuary: AMEC Earth & Environmental Ltd.

Burpee et al. (In Review). Grain Size Controls on Planform Morphology and Stratigraphy of River-Dominated Deltas.

Caldwell, Rebecca L., and Douglas A. Edmonds. "The effects of sediment properties on deltaic processes and morphologies: A numerical modeling study." *Journal of Geophysical Research: Earth Surface* (2014).

Canestrelli, Alberto, et al. "Importance of frictional effects and jet instability on the morphodynamics of river mouth bars and levees." *Journal of Geophysical Research: Oceans* 119.1 (2014): 509-522

Clark, P.U. and W.W. Fitzhugh, 1992, Postglacial relative sea level history of the Labrador coast and interpretation of the archaeological record *in* L.L. Johnson and M. Stright, eds., Paleoshorelines and prehistory: An investigation of method. Boca Raton, USA, CRC Press: 189 p.

Coachman, L.K., 1953 River flow and winter hydrograph structure of the Hamilton Inlet – Lake Melville estuary of Labrador: Blue Dolphin Labrador Expedition, unpubplished manuscript. 19 p.

Howell, J., and Flint, S., “Sequences and systems tracts in the Book Cliffs.” In Coe, Angela L.; Bosence, Dam W.J.; Church, Kevin D.; Flint, Stephen S.; Howell, John A. and Wilson, R. Chris L. (2003). *The Sedimentary record of sea-level change.* Cambridge, UK: Cambridge University Press and the Open University.

Edmonds, Douglas A., and Rudy L. Slingerland. "Significant effect of sediment cohesion on delta morphology." *Nature Geoscience* 3.2 (2009): 105-109.

Edmonds, Douglas A., John B. Shaw, and David Mohrig. "Topset-dominated deltas: A new model for river delta stratigraphy." *Geology* 39.12 (2011): 1175-1178.

Edwards, Chris M., John A. Howell, and Stephen S. Flint. "Depositional and stratigraphic architecture of the Santonian Emery Sandstone of the Mancos Shale: implications for late Cretaceous evolution of the Western Interior Foreland Basin of central Utah, USA." *Journal of Sedimentary Research* 75.2 (2005): 280-299.

Enge, A. D. and J. A. Howell (2010). "Impact of deltaic clinothems on reservoir performance: Dynamic studies of reservoir analogs from the Ferron Sandstone Member and Panther Tongue, Utah." AAPG Bulletin **94**(2): 139-161.

Enge, A. D., et al. (2010). "The geometry and internal architecture of stream mouth bars in the Panther Tongue and Ferron Sandstone Members, Utah, U.S.A." Journal of Sedimentary Research **80**: 1018-1031.

Enge, A. D., et al. (2010). "Quantifying clinothem geometry in a forced-regressive river-dominated delta, Panther Tongue Member, Utah, USA." Sedimentology **57**: 1750-1770.

Gilbert, G.K. (1885). The topographic features of lake shores; U.S. Geolological Survey. Fifth Annual Report., p.69-123.

Hampson, G. J., et al. (2011). "Along-strike and down-dip variations in shallow-marine sequence stratigraphic architecture: Upper Cretaceous Star Point Sandstone, Wasatch Plateau, Central Utah, USA." Journal of Sedimentary Research **81**(3): 159-184.

Hart, B. S., and B. F. Long. "Forced regressions and lowstand deltas: Holocene Canadian examples." *Journal of Sedimentary Research* 66.4 (1996).

Howell, J., Vassel, A., et al. (2008). "Modelling of dipping clinoform barriers within deltaic outcrop analogues from the Cretaceous Western Interior Basin, USA." Geological Society, London, Special Publications **309**(1): 99-121.

Howell, J. A., Skorstad, A., et al. (2008). "Sedimentological parameterization of shallow-marine reservoirs." Petroleum Geoscience **14**(1): 17-34.

Hwang, I. G. and P. L. Heller (2002). "Anatomy of a transgressive lag: Panther Tongue Sandstone, Star Point Formation, central Utah." Sedimentology **49**: 977-999.

Lorenzo-Trueba, Jorge, Vaughan R. Voller, and Chris Paola. "A geometric model for the dynamics of a fluvially dominated deltaic system under base-level change." *Computers & Geosciences* 53 (2013): 39-47.

Kolla, V., et al. "Sequence stratigraphy and architecture of the late Pleistocene Lagniappe delta complex, northeast Gulf of Mexico." *Geological Society, London, Special Publications* 172.1 (2000): 291-327.

Liverman, David GE. "Quaternary Geology of the Goose Bay area." *Current Research. Newfoundland and Labrador Department of Mines and Energy, Geological Survey, Report* (1997): 97-1.

Muto, Tetsuji, and Ron J. Steel. "Autogenic response of fluvial deltas to steady sea-level fall: implications from flume-tank experiments." *Geology* 32.5 (2004): 401-404.

Muto, Tetsuji, and John B. Swenson. "Large-scale fluvial grade as a nonequilibrium state in linked depositional systems: Theory and experiment." *Journal of Geophysical Research: Earth Surface (2003–2012)* 110.F3 (2005).

Muto, Tetsuji, and John B. Swenson. "Autogenic attainment of large-scale alluvial grade with steady sea-level fall: An analog tank-flume experiment." *Geology* 34.3 (2006): 161-164.

Newman, K. F. and M. A. Chan (1991). Depositional facies and sequences in the Upper Cretaceous Panther Tongue Member of the Star Point Formation, Wasatch Plateau, Utah. Geology of East-central Utah. T. C. Chidsey, Jr. Salt Lake City, Utah Geological Association. **18:** 65-75.

Olariu, C., et al. "Integrated study of ancient delta-front deposits using outcrop, ground-penetrating radar, and 3-D photo-realistic data, Cretaceous Panther Tongue Sandstone, Utah." *River Deltas—Concepts, Models, and Examples: SEPM, Special Publication* 83 (2005): 393-411.

Olariu, Cornel, and Janok P. Bhattacharya. "Terminal distributary channels and delta front architecture of river-dominated delta systems." *Journal of Sedimentary Research* 76.2 (2006): 212-233.

Olariu, Cornel, Ronald J. Steel, and Andrew L. Petter. "Delta-front hyperpycnal bed geometry and implications for reservoir modeling: Cretaceous Panther Tongue delta, Book Cliffs, Utah." *AAPG bulletin* 94.6 (2010): 819-845.

Petter, Andrew L., and Tetsuji Muto. "Sustained alluvial aggradation and autogenic detachment of the alluvial river from the shoreline in response to steady fall of relative sea level." *Journal of Sedimentary Research* 78.2 (2008): 98-111.

Porębski, Szczepan J., and Ronald J. Steel. "Shelf-margin deltas: their stratigraphic significance and relation to deepwater sands." *Earth-Science Reviews* 62.3 (2003): 283-326.

Porebski, Szczepan J., and Ronald J. Steel. "Deltas and sea-level change." *Journal of Sedimentary Research* 76.3 (2006): 390-403.

Posamentier, Henry W., et al. "Forced regressions in a sequence stratigraphic framework: concepts, examples, and exploration significance (1)." *AAPG bulletin* 76.11 (1992): 1687-1709.

Posamentier, Henry W., George P. Allen, and David P. James. "High Resolution Sequence Stratigraphy--The East Coulee Delta, Alberta." *Journal of Sedimentary Research* 62.2 (1992).

Posamentier, H. W., et al. (1995). "The Panther Tongue Sandstone, Utah - an Example of a Forced Regressive Deposit." <u>Tongues, Ridges, and Wedges</u>.

Posamentier, H. W. and W. R. Morris (2000). "Aspects of the stratal architecture of forced regressive deposits." <u>Geological Society, London, Special Publications</u> **172**(1): 19-46.

Prince, Guy D., and Peter M. Burgess. "Numerical Modeling of Falling-Stage Topset Aggradation: Implications for Distinguishing Between Forced and Unforced Regressions In the Geological Record." *Journal of Sedimentary Research* 83.9 (2013): 767-781.

Reading, H. G., and J. D. Collinson. "The mouths of rivers: estuaries, deltas and fans at the sea shore." *Sedimentary Environments: Processes, Facies and Stratigraphy* (1996).

Sala, Monique, and Bernard Long. "Évolution des structures deltaïques du delta de la rivière Natashquan, Québec." *Géographie physique et Quaternaire* 43.3 (1989): 311-323.

Suter, John R., and Henry L. Berryhill Jr. "Late Quaternary shelf-margin deltas, northwest Gulf of Mexico." *AAPG Bulletin* 69.1 (1985): 77-91.

Slingerland, Rudy, and Norman D. Smith. "River avulsions and their deposits." *Annu. Rev. Earth Planet. Sci.* 32 (2004): 257-285.

Storms, Joep EA, et al. "Initial morphologic and stratigraphic delta evolution related to buoyant river plumes." *Coastal Sediments' 07*. ASCE, 2007.

Swenson, John B., and Tetsuji Muto. "Response of coastal plain rivers to falling relative sea-level: allogenic controls on the aggradational phase." *Sedimentology* 54.1 (2007): 207-221.

Tzanis, A., 2010. matGPR Release 2: A freeware MATLAB® package for the analysis & interpretation of common and single offset GPR data, FastTimes, 15 (1), 17 – 43

van der Vegt, H., J. E. A. Storms, and D. J. R. Walstra. "Establishing 3D Numerical Reservoir Analogues-Modelling the Formation of Sand Bodies in Deltaic Environments." *76th EAGE Conference and Exhibition 2014*. 2014.

Walker, Roger G, and Noel P. James. *Facies Models: Response to Sea Level Change*. St. John's, Nfld: Geological Association of Canada = Association géologique du Canada, 1992. Print.

Appendix A

Delft3D Setup Files for Simulated Delta in 4 m Water Depth and 10 mm yr^{-1} BLF

MDF-File

```
4m_10mm_final.mdf
Ident = #Delft3D-FLOW .03.02 3.42.00.17790#
Commnt =
Runtxt = #JAC 5/16/2014#
#5grains D50 170um#
#4m flat depth#
#10mm/yr with 14 day#
#intermittency factor#
#erosion factor 0.33#
#sloping channel#
Filcco = #..\5_16Grid.grd#
Anglat = 0.0000000e+000
Grdang = 0.0000000e+000
Filgrd = #..\5_16Grid.enc#
MNKmax = 584 338 1
Thick = 1.0000000e+002
Commnt =
Fildep = #..\4m.dep#
Commnt =
Commnt = no. dry points: 0
Commnt = no. thin dams: 0
Commnt =
Itdate = #2014-01-02#
Tunit = #M#
Tstart = 0.0000000e+000
Tstop = 1.5782400e+006
Dt = 0.1
Tzone = 0
Commnt =
Sub1 = # #
Sub2 = # C #
Namc1 = #SedimentNC275 #
Namc2 = #SedimentNC250 #
Namc3 = #SedimentNC150 #
Namc4 = #SedimentCOH0.21931 #
Namc5 = #SedimentCOH0.05651 #
Commnt =
Wnsvwp = #N#
Wndint = #Y#
Commnt =
Zeta0 = 0.0000000e+000
C01 = 0.0000000e+000
C02 = 0.0000000e+000
C03 = 0.0000000e+000
C04 = 0.0000000e+000
C05 = 0.0000000e+000
Commnt =
Commnt = no. open boundaries: 4
Filbnd = #4m_10mm_final.bnd#
FilbcT = #4m_10mm_final.bct#
FilbcC = #4m_10mm_final.bcc#
Rettis = 0.0000000e+000
```

```
0.0000000e+000
0.0000000e+000
0.0000000e+000
Rettib = 0.0000000e+000
0.0000000e+000
0.0000000e+000
0.0000000e+000
Commnt =
Ag = 9.8100000e+000
Rhow = 1.0000000e+003
Tempw = 1.5000000e+001
Salw = 3.1000000e+001
Wstres = 6.3000000e-004 0.0000000e+000 7.2300000e-003 1.0000000e+002
7.2300000e-003 1.0000000e+002
Rhoa = 1.0000000e+000
Betac = 5.0000000e-001
Equili = #N#
Ktemp = 0
Fclou = 0.0000000e+000
Sarea = 0.0000000e+000
Temint = #Y#
Commnt =
Roumet = #C#
Ccofu = 6.5000000e+001
Ccofv = 6.5000000e+001
Xlo = 0.0000000e+000
Vicouv = 1.0000000e-003
Dicouv = 1.0000000e-003
Htur2d = #Y#
Page 1
4m_10mm_final.mdf
Htural = 1.6666660e+000
Hturnd = 2
Hturst = 7.0000000e-001
Hturlp = 3.3333330e-001
Hturrt = 1.0000000e+000
Hturdm = 0.0000000e+000
Hturel = #Y#
Irov = 0
Filsed = #4m_10mm_final.sed#
Filmor = #4m_10mm_final.mor#
Commnt =
Iter = 2
Dryflp = #YES#
Dpsopt = #MAX#
Dpuopt = #MOR#
Dryflc = 1.0000000e-001
Dco = 0.0000000e+000
Tlfsmo = 6.0000000e+001
ThetQH = 0.0000000e+000
Forfuv = #Y#
Forfww = #N#
Sigcor = #N#
Trasol = #Cyclic-method#
```

```
Momsol = #Cyclic#
Commnt =
Commnt = no. discharges: 0
Commnt = no. observation points: 1
Filsta = #4m_10mm_final.obs#
Commnt = no. drogues: 0
Commnt =
Commnt =
Commnt = no. cross sections: 1
Filcrs = #4m_10mm_final.crs#
Commnt =
SMhydr = #YYYYY#
SMderv = #YYYYYY#
SMproc = #YYYYYYYYYY#
PMhydr = #YYYYYY#
PMderv = #YYY#
PMproc = #YYYYYYYYYY#
SHhydr = #YYYY#
SHderv = #YYYYY#
SHproc = #YYYYYYYYYY#
SHflux = #YYYY#
PHhydr = #YYYYYY#
PHderv = #YYY#
PHproc = #YYYYYYYYYY#
PHflux = #YYYY#
Online = #N#
Flmap = 0.0000000e+000 60 1.5782400e+006
Flhis = 0.0000000e+000 0 1.5782400e+006
Flpp = 0.0000000e+000 0 0.0000000e+000
Flrst = 1440
Commnt =
Commnt =
```

BND-file

```
4m_10mm_final.bnd
east Z T 584 337 584 2 0.0000000e+000
north Z T 2 338 583 338 0.0000000e+000
west Z T 1 2 1 337 0.0000000e+000
feeder T T 291 1 295 1 0.0000000e+000 Uniform
Page 1
```

BCC-file

```
4m_10mm_final.mdf
Ident = #Delft3D-FLOW .03.02 3.42.00.17790#
Commnt =
Runtxt = #JAC 5/16/2014#
#5grains D50 170um#
#4m flat depth#
#10mm/yr with 14 day#
#intermittency factor#
#erosion factor 0.33#
#sloping channel#
Filcco = #..\5_16Grid.grd#
Anglat = 0.0000000e+000
Grdang = 0.0000000e+000
Filgrd = #..\5_16Grid.enc#
MNKmax = 584 338 1
Thick = 1.0000000e+002
Commnt =
Fildep = #..\4m.dep#
Commnt =
Commnt = no. dry points: 0
Commnt = no. thin dams: 0
Commnt =
Itdate = #2014-01-02#
Tunit = #M#
Tstart = 0.0000000e+000
Tstop = 1.5782400e+006
Dt = 0.1
Tzone = 0
Commnt =
Sub1 = # #
Sub2 = # C #
Namc1 = #SedimentNC275 #
Namc2 = #SedimentNC250 #
Namc3 = #SedimentNC150 #
Namc4 = #SedimentCOH0.21931 #
Namc5 = #SedimentCOH0.05651 #
Commnt =
Wnsvwp = #N#
Wndint = #Y#
Commnt =
Zeta0 = 0.0000000e+000
C01 = 0.0000000e+000
C02 = 0.0000000e+000
C03 = 0.0000000e+000
C04 = 0.0000000e+000
C05 = 0.0000000e+000
Commnt =
Commnt = no. open boundaries: 4
Filbnd = #4m_10mm_final.bnd#
FilbcT = #4m_10mm_final.bct#
FilbcC = #4m_10mm_final.bcc#
Rettis = 0.0000000e+000
```

```
0.0000000e+000
0.0000000e+000
0.0000000e+000
Rettib = 0.0000000e+000
0.0000000e+000
0.0000000e+000
0.0000000e+000
Commnt =
Ag = 9.8100000e+000
Rhow = 1.0000000e+003
Tempw = 1.5000000e+001
Salw = 3.1000000e+001
Wstres = 6.3000000e-004 0.0000000e+000 7.2300000e-003 1.0000000e+002
7.2300000e-003 1.0000000e+002
Rhoa = 1.0000000e+000
Betac = 5.0000000e-001
Equili = #N#
Ktemp = 0
Fclou = 0.0000000e+000
Sarea = 0.0000000e+000
Temint = #Y#
Commnt =
Roumet = #C#
Ccofu = 6.5000000e+001
Ccofv = 6.5000000e+001
Xlo = 0.0000000e+000
Vicouv = 1.0000000e-003
Dicouv = 1.0000000e-003
Htur2d = #Y#
Page 1
4m_10mm_final.mdf
Htural = 1.6666660e+000
Hturnd = 2
Hturst = 7.0000000e-001
Hturlp = 3.3333330e-001
Hturrt = 1.0000000e+000
Hturdm = 0.0000000e+000
Hturel = #Y#
Irov = 0
Filsed = #4m_10mm_final.sed#
Filmor = #4m_10mm_final.mor#
Commnt =
Iter = 2
Dryflp = #YES#
Dpsopt = #MAX#
Dpuopt = #MOR#
Dryflc = 1.0000000e-001
Dco = 0.0000000e+000
Tlfsmo = 6.0000000e+001
ThetQH = 0.0000000e+000
Forfuv = #Y#
Forfww = #N#
Sigcor = #N#
Trasol = #Cyclic-method#
```

```
Momsol = #Cyclic#
Commnt =
Commnt = no. discharges: 0
Commnt = no. observation points: 1
Filsta = #4m_10mm_final.obs#
Commnt = no. drogues: 0
Commnt =
Commnt =
Commnt = no. cross sections: 1
Filcrs = #4m_10mm_final.crs#
Commnt =
SMhydr = #YYYYY#
Smderv = #YYYYYY#
Smproc = #YYYYYYYYYY#
Pmhydr = #YYYYYY#
Pmderv = #YYY#
Pmproc = #YYYYYYYYYY#
Shhydr = #YYYY#
Shderv = #YYYYY#
Shproc = #YYYYYYYYYY#
Shflux = #YYYY#
Phhydr = #YYYYYY#
Phderv = #YYY#
Phproc = #YYYYYYYYYY#
Phflux = #YYYY#
Online = #N#
Flmap = 0.0000000e+000 60 1.5782400e+006
Flhis = 0.0000000e+000 0 1.5782400e+006
Flpp = 0.0000000e+000 0 0.0000000e+000
Flrst = 1440
Commnt =
Commnt =
```

BCT-file

```
4m_10mm_final.bct
table-name ‘Boundary Section : 1’
contents ‘Uniform ‘
location ‘east ‘
time-function ‘non-equidistant’
reference-time 20140102
time-unit ‘minutes’
interpolation ‘linear’
parameter ‘time ‘ unit ‘[min]’
parameter ‘water elevation (z) end A’ unit ‘[m]’
parameter ‘water elevation (z) end B’ unit ‘[m]’
records-in-table 2
0.0000000e+000 0.0000000e+000 0.0000000e+000
1.5782400e+006 -3.9107140e+002 -3.9107140e+002
table-name ‘Boundary Section : 2’
contents ‘Uniform ‘
location ‘north ‘
time-function ‘non-equidistant’
reference-time 20140102
time-unit ‘minutes’
interpolation ‘linear’
parameter ‘time ‘ unit ‘[min]’
parameter ‘water elevation (z) end A’ unit ‘[m]’
parameter ‘water elevation (z) end B’ unit ‘[m]’
records-in-table 2
0.0000000e+000 0.0000000e+000 0.0000000e+000
1.5782400e+006 -3.9107140e+002 -3.9107140e+002
table-name ‘Boundary Section : 3’
contents ‘Uniform ‘
location ‘west ‘
time-function ‘non-equidistant’
reference-time 20140102
time-unit ‘minutes’
interpolation ‘linear’
parameter ‘time ‘ unit ‘[min]’
parameter ‘water elevation (z) end A’ unit ‘[m]’
parameter ‘water elevation (z) end B’ unit ‘[m]’
records-in-table 2
0.0000000e+000 0.0000000e+000 0.0000000e+000
1.5782400e+006 -3.9107140e+002 -3.9107140e+002
table-name ‘Boundary Section : 4’
contents ‘Uniform ‘
location ‘feeder ‘
time-function ‘non-equidistant’
reference-time 20140102
time-unit ‘minutes’
interpolation ‘linear’
parameter ‘time ‘ unit ‘[min]’
parameter ‘total discharge (t) end A’ unit ‘[m3/s]’
parameter ‘total discharge (t) end B’ unit ‘[m3/s]’
records-in-table 2
0.0000000e+000 1.0000000e+003 9.9999900e+002
```

1.5782400e+006 1.0000000e+003 9.9999900e+002

MOR-file

```
4m_10mm_final.mor
[MorphologyFileInformation]
FileCreatedBy = Delft3D FLOW-GUI, Version: 3.42.00.17790
FileCreationDate = Fri May 16 2014, 17:09:58
FileVersion = 02.00
[Morphology]
EpsPar = false Vertical mixing distribution according to van Rijn
(overrules k-epsilon model)
IopKCW = 1 Flag for determining Rc and Rw
RDC = 0.01 [m] Current related roughness height (only used if IopKCW
<> 1)
RDW = 0.02 [m] Wave related roughness height (only used if IopKCW <>
1)
MorFac = 5.0000000e+002 [-] Morphological scale factor
MorStt = 3.6000000e+002 [min] Spin-up interval from TStart till start
of
morphological changes
Thresh = 5.0000001e-002 [m] Threshold sediment thickness for
transport and
erosion reduction
MorUpd = true Update bathymetry during FLOW simulation
EqmBc = false Equilibrium sand concentration profile at inflow
boundaries
DensIn = false Include effect of sediment concentration on fluid
density
AksFac = 1.0000000e+000 [-] van Rijn's reference height = AKSFAC * KS
RWave = 2.0000000e+000 [-] Wave related roughness = RWAVE * estimated
ripple
height. Van Rijn Recommends range 1-3
AlfaBs = 1.0000000e+000 [-] Streamwise bed gradient factor for bed
load transport
AlfaBn = 1.5000000e+000 [-] Transverse bed gradient factor for bed
load transport
Sus = 1.0000000e+000 [-] Multiplication factor for suspended sediment
reference concentration
Bed = 1.0000000e+000 [-] Multiplication factor for bed-load transport
vector
magnitude
SusW = 1.0000000e+000 [-] Wave-related suspended sed. transport
factor
BedW = 1.0000000e+000 [-] Wave-related bed-load sed. transport factor
SedThr = 1.0000000e-001 [m] Minimum water depth for sediment
computations
ThetSD = 3.3000000e-001 [-] Factor for erosion of adjacent dry cells
HMaxTH = 1.5000000e+000 [m] Max depth for variable THETSD. Set <
SEDTHR to use
global value only
FWFac = 1.0000000e+000 [-] Vertical mixing distribution according to
van Rijn
(overrules k-epsilon model)
[Output]
SourceSinkTerms = True
```

```
Bedslope = True
Frac = True
MudFrac = True
Percentiles = True
HidExp = True
Bedforms = True
Dm = True
Dg = True
[UnderLayer]
IUnderLyr = 2
MxNuLyr = 100
TTLForm = 1
ThTrLyr = 0.2
ThUnlyr = 0.1
UpdBaseLyr = 1
```

SED-file

```
4m_10mm_final.sed
[SedimentFileInformation]
FileCreatedBy = Delft3D FLOW-GUI, Version: 3.42.00.17790
FileCreationDate = Fri May 16 2014, 17:09:57
FileVersion = 02.00
[SedimentOverall]
Cref = 1.6000000e+003 [kg/m3] CSoil Reference density for hindered
settling
calculations
IopSus = 0 If Iopsus = 1: susp. sediment size depends on local
flow and wave conditions
[Sediment]
Name = #SedimentNC275# Name of sediment fraction
SedTyp = sand Must be "sand", "mud" or "bedload"
RhoSol = 2.6500000e+003 [kg/m3] Specific density
SedDia = 2.7500000e-004 [m] Median sediment diameter (D50)
CDryB = 1.6000000e+003 [kg/m3] Dry bed density
IniSedThick = 1.0000000e+001 [m] Initial sediment layer thickness at
bed (uniform
value or filename)
FacDSS = 1.0000000e+000 [-] FacDss * SedDia = Initial suspended
sediment
diameter. Range [0.6 - 1.0]
[Sediment]
Name = #SedimentNC250# Name of sediment fraction
SedTyp = sand Must be "sand", "mud" or "bedload"
RhoSol = 2.6500000e+003 [kg/m3] Specific density
SedDia = 2.5000000e-004 [m] Median sediment diameter (D50)
CDryB = 1.6000000e+003 [kg/m3] Dry bed density
IniSedThick = 2.5000000e+001 [m] Initial sediment layer thickness at
bed (uniform
value or filename)
FacDSS = 1.0000000e+000 [-] FacDss * SedDia = Initial suspended
sediment
diameter. Range [0.6 - 1.0]
[Sediment]
Name = #SedimentNC150# Name of sediment fraction
SedTyp = sand Must be "sand", "mud" or "bedload"
RhoSol = 2.6500000e+003 [kg/m3] Specific density
SedDia = 1.5000000e-004 [m] Median sediment diameter (D50)
CDryB = 1.6000000e+003 [kg/m3] Dry bed density
IniSedThick = 3.0000000e+001 [m] Initial sediment layer thickness at
bed (uniform
value or filename)
FacDSS = 1.0000000e+000 [-] FacDss * SedDia = Initial suspended
sediment
diameter. Range [0.6 - 1.0]
[Sediment]
Name = #SedimentCOH0.21931# Name of sediment fraction
SedTyp = mud Must be "sand", "mud" or "bedload"
RhoSol = 2.6500000e+003 [kg/m3] Specific density
SalMax = 0.0000000e+000 [ppt] Salinity for saline settling velocity
```

WS0 = 2.1931000e-004 [m/s] Settling velocity fresh water
WSM = 2.1931000e-004 [m/s] Settling velocity saline water
TcrSed = 1.0000000e+003 [N/m2] Critical bed shear stress for
sedimentation (uniform
value or filename)
TcrEro = 5.0000000e-001 [N/m2] Critical bed shear stress for erosion
(uniform
value or filename)
EroPar = 1.0000000e-004 [kg/m2/s] Erosion parameter (uniform
value or filename)
CDryB = 5.0000000e+002 [kg/m3] Dry bed density
IniSedThick = 1.0000000e+001 [m] Initial sediment layer thickness at
bed (uniform
value or filename)
FacDSS = 1.0000000e+000 [-] FacDss * SedDia = Initial suspended
sediment
diameter. Range [0.6 - 1.0]
[Sediment]
Name = #SedimentCOH0.05651# Name of sediment fraction
SedTyp = mud Must be "sand", "mud" or "bedload"
RhoSol = 2.6500000e+003 [kg/m3] Specific density
SalMax = 0.0000000e+000 [ppt] Salinity for saline settling velocity
WS0 = 5.6510000e-005 [m/s] Settling velocity fresh water
WSM = 5.6510000e-005 [m/s] Settling velocity saline water
TcrSed = 1.0000000e+003 [N/m2] Critical bed shear stress for
sedimentation (uniform
value or filename)
TcrEro = 5.0000000e-001 [N/m2] Critical bed shear stress for erosion
(uniform
value or filename)
EroPar = 1.0000000e-004 [kg/m2/s] Erosion parameter (uniform
value or filename)
CDryB = 5.0000000e+002 [kg/m3] Dry bed density
IniSedThick = 1.0000000e+001 [m] Initial sediment layer thickness at
bed (uniform
value or filename)
FacDSS = 1.0000000e+000 [-] FacDss * SedDia = Initial suspended
sediment
diameter. Range [0.6 - 1.0]

FIL-file

```
4m_10mm_final.fil
Domain, Checked : No
Grid : ..\5_16Grid.grd
Grid enclosure : ..\5_16Grid.enc
Bathymetry : ..\4m.dep
Dry points : none
Thin dams : none
Time frame, Checked : No
Processes, Checked : No
Initial conditions, Checked : No
Boundaries, Checked : Yes
Boundary definitions : 4m_10mm_final.bnd
Astronomical flow conditions : none
Astronomical corrections : none
Harmonic flow conditions : none
QH-relation flow conditions : none
Time series flow conditions : 4m_10mm_final.bct
Transport conditions : 4m_10mm_final.bcc
Physical parameters, Checked : No
Roughness coefficients : none
Hor. viscosity/diffusivity : none
Heat flux model data : none
Sediment data : 4m_10mm_final.sed
Morphology data : 4m_10mm_final.mor
Uniform wind data : none
Space varying wind data : none
Numerical parameters, Checked : No
Operations, Checked : No
Discharge definitions : none
Discharge data : none
Dredging and dumping data : none
Monitoring, Checked : No
Observation points : 4m_10mm_final.obs
Drogues : none
Cross-sections : 4m_10mm_final.crs
Additional parameters, Checked : No
Output, Checked : No
Fourier analysis data : none
```

Appendix B

MATLAB Scripts for Analyzing Delft3d Simulations

Clinoform Dip Magnitude and Dip Direction Code

```
%  Clinoform Dip Magnitudes for Delft3D Deltas
%
%  Code modified from "clinodipsver07062011" created by RLS and APB
%  APB April 17, 2012
%  Modified by ABM to account for base level change November 10, 2012
%  Modified by JAC 2014
% NOTE:  BE SURE TO CHANGE ALL VALUES IN CODE WHICH ARE RUN AND/OR TIME
% SPECIFIC BEFORE RUNNING!
%%
clear all; close all; clc
%%  USER ACTION REQUIRED
cd Y:\Cederberg\FinalDeltas_data\4m5mm
% 1. Load bed elevation data stored in bedlevel.mat written from Quickplot:
load bedlevel.mat
% 2. Define timestep of interest for clinoform measurment:
TStep = 112;
%dts = 0; %Amount of base level change, in meters, in a single timestep(factoring
in the MSF)Positive values relate to RBL Fall, negative to RBL Rise
dts=0.007440475646880;%5mm
%dts=0.014880951293760;%10mm%%  NO ACTION REQUIRED
% 3. Extract the bed elevation for a timestep (the timetep is the first
% number in the array counters)
Z=data.Val(TStep,:,:);
ZZ=squeeze(Z);
[row,col]=size(ZZ);
% We rotate the delta to prograde to the north because it makes the
% extraction of the clinoform slopes easier.  But note that this reverses
% the counters in the matrix.  The "flipdim" line corrects the error that
% results from bringing the Delft image from Delft to MatLab.  The image
% will come into MatLab as the mirror image of the Delft image.
ZZ=flipdim(ZZ,1);
ZZ=rot90(ZZ,3);
dem=ZZ;
dim = size(ZZ);
N=dim(2);
contour(ZZ,30)
caxis([-20 3])
hold on
% 4. Contour the shoreline (actually the -0.1 m contour)as thick black line
v=[-0.1-(dts*(TStep-1))];
contour(ZZ,v,'k','LineWidth', 2)
caxis([-20 3])
% 5. Now define the region of the delta from which you want bed (clinoform
% surface) slopes.  Generally we want to exclude the top- and bottom-set
% region. Extract the bed elevations and bed slopes of interest by setting
% all bed elevations and slopes landward of the region of interest to 0:
for j = 1:320
    for i = 1:220
    if ZZ(i,j) >= -0.10 %Eliminates the topset, except for channels
        ZZ(i,j) = NaN;
    elseif i < 30
        ZZ(i,j) = NaN;  %Eliminates the feeder channel and non-deltaic
                        %shoreline; This line number (30) may change with
                        %different deltas
    end
```

```
    end
end
%%  USER ACTION REQUIRED
% 6. Define the toes of the delta clinoform. Hit enter when done.  Be sure
% your line extends from x=0 to x=xmax and all x values are unique.
[X,Y]=ginput;
X=round(X);
Y=round(Y);
XX=1:N;
YY = interp1(X,Y,XX,'linear');
hold on
YY=round(YY);
plot(XX,YY,'*')
% 7. Define the topset region from which you want to remove bed elevations
% associated with channels. Be sure your line extends from x=0 to x=xmax
% and all x values are unique.
[Xtop,Ytop]=ginput;
Xtop=round(Xtop);
Ytop=round(Ytop);
XXtop=1:N;
YYtop = interp1(Xtop,Ytop,XXtop,'linear');
hold on
YYtop=round(YYtop);
plot(XXtop,YYtop,'o')
drawnow
% Make a vector of zeros and ones, with ones where YYtop is a NaN to
% control the loops below
ControlVec = isnan(YYtop);
% Extract the bed elevations and bed slopes of interest by setting all
% elevations and slopes seward of the region of interest to 0
for j = 1:row
    for i = 1:col
    if i > YY(j)
        ZZ(i,j) = NaN;
    end
    if ControlVec(j) ~= 1 && i < YYtop(j)
        ZZ(i,j) = NaN;
    end
    end
end
% Contour the bathymetry of the delta clinoform in the region of study
hold off
subplot(2,2,1); contour(dem,30);
subplot(2,2,2);[CS, H]= contour(ZZ,30);
%%
% 8. Calculate the aspect (dip direction), slope, and gradients (along the
% axes) of the delta foreset at every Delft3D cell. The reference vector
% converts the bathy elevation matric to actual geographic coordinates.
% The first number in the vector is the only important one; it gives the
% number of matrix entries per degree latitude.  Because our spacing is 25
% m, and there are 111000 meters per degree, the number of cells for us is
% 111000/25.
refvec = [111000/25 0 0];
[ASPECT, SLOPE, gradN, gradE] = gradientm(ZZ, refvec);
% Convert the aspect from a matrix to a column vector, while converting
% aspect to radians
k=0;
```

```
for i=1:col
    for j=1:row
        k=k+1;
        theta(k) = pi/180*ASPECT(i,j);
        dip(k) = SLOPE(i,j);
    end
end
% Remove NaNs
theta(isnan(theta)) = [];
dip(isnan(dip)) = [];
%Remove all slope data from the area of interest that are of a value less
%than what is observed in a foreset.
dimdip=size(dip);
increm = 0;
for counter=1:dimdip(2);
    if dip(counter) >= 0.008; %Modified from 0.08 to 1 by JAC 3/26/2014
        increm = increm+1;
        newdip(increm) = dip(counter);
        newtheta(increm)=theta(counter);
    end
end
newtheta=sort(newtheta);
% 9. Plot a rose diagram of clinoform dip direction:
subplot(2,2,3);
nbins = 36;
h=rose(newtheta,nbins);
view(90,-90)
% Define some constants
num=size(newtheta);
x=0;
y=0;
% Calculate the mean dip direction and dispersion (the statistics below are
% derived from Doornkamp and King, 1971, "Numerical Analysis in
% Geomorphology", p. 208-213)
% VERSION 2 (from Jones, 2006)
C = sum(cos(newtheta));
S = sum(sin(newtheta));
cd Y:\Cederberg\Stats\MatLabStatPrograms\Vector_Stats;
thetabar = VectMean_arctan(S,C); % function from Jones
R = sqrt((S/(num(2))^2 + (C/num(2))^2))
% Large Rbar = small variance and vice versa
s1 = sqrt(2*(1-R)); % Angular dispersion (in radians)as given by Doornkamp
                    % and King
AngularDispersionDeg=s1*(180/pi)%Angular Dispersion in degrees
% Be sure that dip magnitude is in degrees:
dipdegrees = newdip;
newtheta=newtheta';
title(['Mean dip direction =',num2str(thetabar)],'FontSize',8)
subplot(2,2,4);
histbin=[0:0.05:20];
hist(newdip,histbin);
avedipmag=mean(dipdegrees)
stdev = std(dipdegrees)
p50=prctile(dipdegrees, 50)

samples=length(dipdegrees);
text(50,500,['median dip magnitude =',num2str(p50)],'FontSize',8);
```

```
text(10,20,['mean dip magnitude =',num2str(avedipmag)],'FontSize',8);
text(10,100,['dip std dev =',num2str(stdev)],'FontSize',8);
%text(10,80,['p95 dip =',num2str(p95)],'FontSize',8);
%text(10,110,['Number of Samples =',num2str(samples)],'FontSize',8);
title('Mean Clinoform Bed Dip')
xlabel('dip (dg)')
ylabel('Frequency by Number')
```

Topset Roughness

```
%% Topset Roughness Code
% This code calculates the standard deviation of all elevation in the
% topset above 0.1m
%JAC 2014

clear all;close all
cd ('Y:\Cederberg\finalDeltas_data\20m10mm\')% RUN-SPECIFIC
%dts = 0; %Amount of base level change, in meters, in a single
%timestep(factoring in the MSF)Positive values relate to RBL Fall,
%negative to RBL Rise
%dts=0.007440475646880;%5m
dts=0.014880951293760;%10mm
load bedlevel.mat
[t,r,c]=size(data.Val);
tmax=532;
ZZ=cell(1,tmax);
stdev=zeros(1,tmax);
for n=1:tmax
    Z=[];
    disp(['Computing time slice ' num2str(n)])
    shore=-0.1-((i-1)*dts); %find the shoreline
    for i=1:r
        for j=1:c
            if data.Val(n,i,j)>(shore) & data.Val(n,i,j)<3 %Select points
                                                           %within the shoreline
                Z=[Z data.Val(n,i,j)];
            end

        end
    end
    ZZ{n}=Z;
    stdev(n)=std(ZZ{n}); %Calculate Std Dev
end
plot(stdev)
save('stdev','stdev')
```

Mean Grain Size and Topset Area of Each Delta Lobe

```
%% Average Grain Size of Lobes and Average Lobe Size
%Delineated lobes interactively with Matlab/Quickplot interface and
%calculate meand grain size and area of each delta lobe
%JAC 2014
close all
clear all
clc
%% This code is used for defining delta lobes in quickplot/matlab and calculating
% the average and D50 grain size of the lobe

%open quickplot through matlab using d3d_qp command
%navigate to run
d3d_qp
%% RUN SPECIFIC
tstep=217; %SET TIME STEP of interest
lyr=100;%number of strat layers
d3d_qp('openfile','H:\25mFinalRuns\8m10mmfinal\trim-8m_10mm_final.dat')
d3d_qp('selectfield','bed level in water level points')
d3d_qp('editt',tstep)
d3d_qp('loaddata')
d3d_qp('quickview')
%% User Action Required, click around the lobe
% Copy and paste as many times as needed to define all lobes
% Make sure to rename marked lines
a=impoly;%%Rename 'a' if needed
pos=getPosition(a);%%Rename 'a' if needed
xv=pos(:,1);
yv=pos(:,2);
X(:,:)=data.X(3:584,2:337);
Y(:,:)=data.Y(3:584,2:337);
IN=inpolygon(X,Y,xv,yv);
areapixA=nnz(IN);
volumepixA=areapixA*lyr;%multiply the area by the number to strat layers
%%RUN SPECIFIC
cd G:\CEDERBERG\Delft_Runs\12m0mmfinal
load strat_mm
for i=2:101
lobestrat(:,:,i)=IN.*strat(:,:,i);
end
SumStratX=sum(lobestrat);
SumStratX=squeeze(SumStratX);
SumStratY=sum(SumStratX);
SumStratY=squeeze(SumStratY);
SumStrat=sum(SumStratY);
AvgD50A=SumStrat/volumepixA;%%Rename 'AvgD50A' if needed
%% Lobe2
b=impoly;%%Rename 'a' if needed
pos=getPosition(b);%%Rename 'a' if needed
xv=pos(:,1);
yv=pos(:,2);
X(:,:)=data.X(3:584,2:337);
Y(:,:)=data.Y(3:584,2:337);
IN=inpolygon(X,Y,xv,yv);
areapixB=nnz(IN);
volumepixB=areapixB*lyr;%multiply the area by the number to strat layers
```

```
%%RUN SPECIFIC
%cd H:\25mFinalRuns\8m10mmfinal\
%load strat_mm.mat
for i=2:101
lobestrat(:,:,i)=IN.*strat(:,:,i);
end
SumStratX=sum(lobestrat);
SumStratX=squeeze(SumStratX);
SumStratY=sum(SumStratX);
SumStratY=squeeze(SumStratY);
SumStrat=sum(SumStratY);
AvgD50B=SumStrat/volumepixB;%%Rename 'AvgD50A' if needed
%% Lobe 3
c=impoly;%%Rename 'a' if needed
pos=getPosition(c);%%Rename 'a' if needed
xv=pos(:,1);
yv=pos(:,2);
X(:,:)=data.X(3:584,2:337);
Y(:,:)=data.Y(3:584,2:337);
IN=inpolygon(X,Y,xv,yv);
areapixC=nnz(IN);
volumepixC=areapixC*lyr;%multiply the area by the number to strat layers
%%RUN SPECIFIC
%cd H:\25mFinalRuns\8m10mmfinal\
%load strat_mm.mat
for i=2:101
lobestrat(:,:,i)=IN.*strat(:,:,i);
end
SumStratX=sum(lobestrat);
SumStratX=squeeze(SumStratX);
SumStratY=sum(SumStratX);
SumStratY=squeeze(SumStratY);
SumStrat=sum(SumStratY);
AvgD50C=SumStrat/volumepixC;%%Rename 'AvgD50A' if needed
```

```
%% Shoreline Extraction and Isoperimetric Quotient Calculation
%Added McGuffin's Base Level Fall adjustment
%APB June 14, 2012
%Modified by JAC 2014
%  Modified from the following:
%% Previous codes
%this m-file takes a cube of topography data from Delft3D output and
%converts each delta into a shoreline using the Open Angle Method (Shaw, et
%al, 2008).

%Code edited by APB and RLS 11/9/11
%Note:  When the delta has prograded to the edge of one of the open
%boundaries, this code will not compute the shoreline on the landward side
%of where the delta has prograded beyond the open boundary.
%%
% clear all;
% close all;
% clc
cd 'Y:\Cederberg\FinalDeltas_data\20m10mm'  %  for different runs, change the
%  run number in this line, and in line 74 of code.
%%
tmax=532;
%  1. Enter the number of time seps recorded for run and amount of base level fall in a time step(make sure to account for MSF)[RUN SPECIFIC]:
timeslices =532;% 1:tmax; %Range of timesteps recorded
%dts = 0; %Amount of base level change, in meters, in a single timestep(factoring in the MSF)Positive values relate to RBL Fall, negative to RBL Rise
%dts=0.007440475646880;%5mm
dts=0.014880951293760;%10mm
%%
%  2. Load bedlevel.mat "bed level in water level points" exported from
%  QUICKPLOT for all time steps:
load bedlevel; %
filename = 'temp';
areapix=cell(1,tmax);
Results.Area=ones(1,tmax);
Results.Perimeter=ones(1,tmax);
Results.IQ=ones(1,tmax);
FluvSurface=cell(1,tmax);
%%
%  3. Enter the initial time step where morphodynamic change begins to
%  occur, or the time step where you would like to begin
%  calculating the shoreline [RUN SPECIFIC]:
for i=timeslices;
    z=data.Val;
    m=length(z(:,1,1));
        disp(['Computing shoreline for ' filename ' time slice ' num2str(i)])
        ztemp=squeeze(z(i,:,:));
        [r,c]=size(ztemp);
        ztemp=ztemp(2:r-1,2:c-1); %the '-1' and '2' is to get rid of the collar of NaNs
        [r,c]=size(ztemp);
        mid=ceil(r/2);
        ztemp(mid-10:mid+10,1)=1;
        [r,c]=size(ztemp);
```

```
        [row,col]=size(ztemp);
        zz=ztemp<(-0.1-((i-1)*dts)); %  the land/water interface is defined as the -0.1 m contour
        if nansum(nansum(zz))<50
        shore{1,i} = 0;
        else
        n=90;
        cd 'H:\25mFinalRuns\ShorelineCode'
        sl=Seaangles2(zz,n); %this calls the OAM script written by John Shaw, et al 2008 GRL
        sl2=sparse(sl(2,:),sl(1,:),sl(3,:),r,c);
        sl2=sl2+0;
        angle = 25;
        c=contourc(sl2,[angle,angle]); %this is the NN degree OAM contour,
        % but the OAM method is imperfect and picks up other smaller,
        % artifical shorelines.  Thus, to find the real one we call contourc,
        % which exports the (x,y) for a given contour level then we sort
        % through that array and find the longest contour which is the shoreline
        sep=seplines(c);
        % sep=sep(:,2:length(sep(1,:)));  %this cuts off the first contour line
        % which is the border of the image and not the shoreline
        temp=sep(:,find(sep(1,:)==max(sep(1,:)))); %this returns the 3-row vector of the
        % longest contour line, which corresponds to the shoreline
        c=c(:,temp(2):temp(3));
        shoretemp=[c(1,:); c(2,:)];
        shore=shoretemp; %this is the x coord of the shoreline at time i
        % Plot the shoreline:
        x=shore(1,:);
        y=shore(2,:);
        % To see both the delta and the shoreline, add the delta to the
        % figure:
        plot(x,y,'o')
        hold on
        contour(ztemp)
        end
%  4.  Save the shoreline file:
cd 'Y:\Cederberg\FinalDeltas_data\20m5mm\Shoreline'
name=([filename(1:length(filename)-4) '_' num2str(i) '_OAM' num2str(angle) ]);
save(name,'shore')
%  5.  Calculate the area of the shoreline:
basin = zeros(row,col);
X = [];  %  determine the X,Y dimensions of the basin:
Y = [];
[rn,cn] = size(basin);
for j = 1:cn
    X(1:rn,j) = 1:rn;
    Y(1:rn,j) = j;
end
y=shore(1,:);
x=shore(2,:);
IN=inpolygon(X,Y,x,y); %this returns the logical "IN" matrix which is the
%  same size as X and Y with 1=yes this cell is within the shape, 0=no
%  this cell is outside the shape.
IN=+IN; %turns logical to numeric
FluvSurface{i}=IN;
total=sum(sum(IN));
```

```
areapix{i}=total;
DeltaArea = (total*(25*25))/(1000*1000);%  This is the area of the Delta [km^2]

%  6.   Calculate the perimeter of the shoreline:
sizextemp = size(x);
sizex  = sizextemp(2);
Perimeter = 0;
dist = zeros(1,sizex);
for k = 1:sizex-1;
    distx(k) = abs(x(k)*25 - x(k+1)*25);  %  horizontal distance [m]
    disty(k) = abs(y(k)*25 - y(k+1)*25);  %  vertical distance [m]
    if distx(k) == 0;
        dist(k) = disty(k);
    end
    if disty(k) == 0;
        dist(k) = distx(k);
    end
    if distx(k) ~= 0;
        if disty(k) ~=0;
            dist(k) = sqrt(distx(k)^2 + disty(k)^2);
        end
    end
    Perimeter = Perimeter + dist(k);  %  Perimeter recorded in [m]
end
%  Add in the distance along the beach!!!
DistBeach = abs(x(1)*25-x(sizex)*25);
PerimeterKM = (DistBeach+Perimeter)/1000  %  Perimeter length [km]
%  7.  Calculate the dimensionless Isoperimetric Quotient(IQ):
IQ(i) = (PerimeterKM^2)/(4*pi*DeltaArea)
Results.Area(1,i)=DeltaArea;
Results.Perimeter(1,i)=PerimeterKM;
Results.IQ(1,i)=IQ(i);
end
save('FluvialSurface','FluvSurface')
save('Results','Results')
save('areapix','areapix')
%  8.  Plot IQ through time:
figure(2)
plot(IQ)
axis([0 tmax 0 1]);
xlabel('Time Step');
ylabel('Isoperimetric Quotient');
```

Appendix C

Delft3D-Generated Internal Geometry of Simulated Deltas

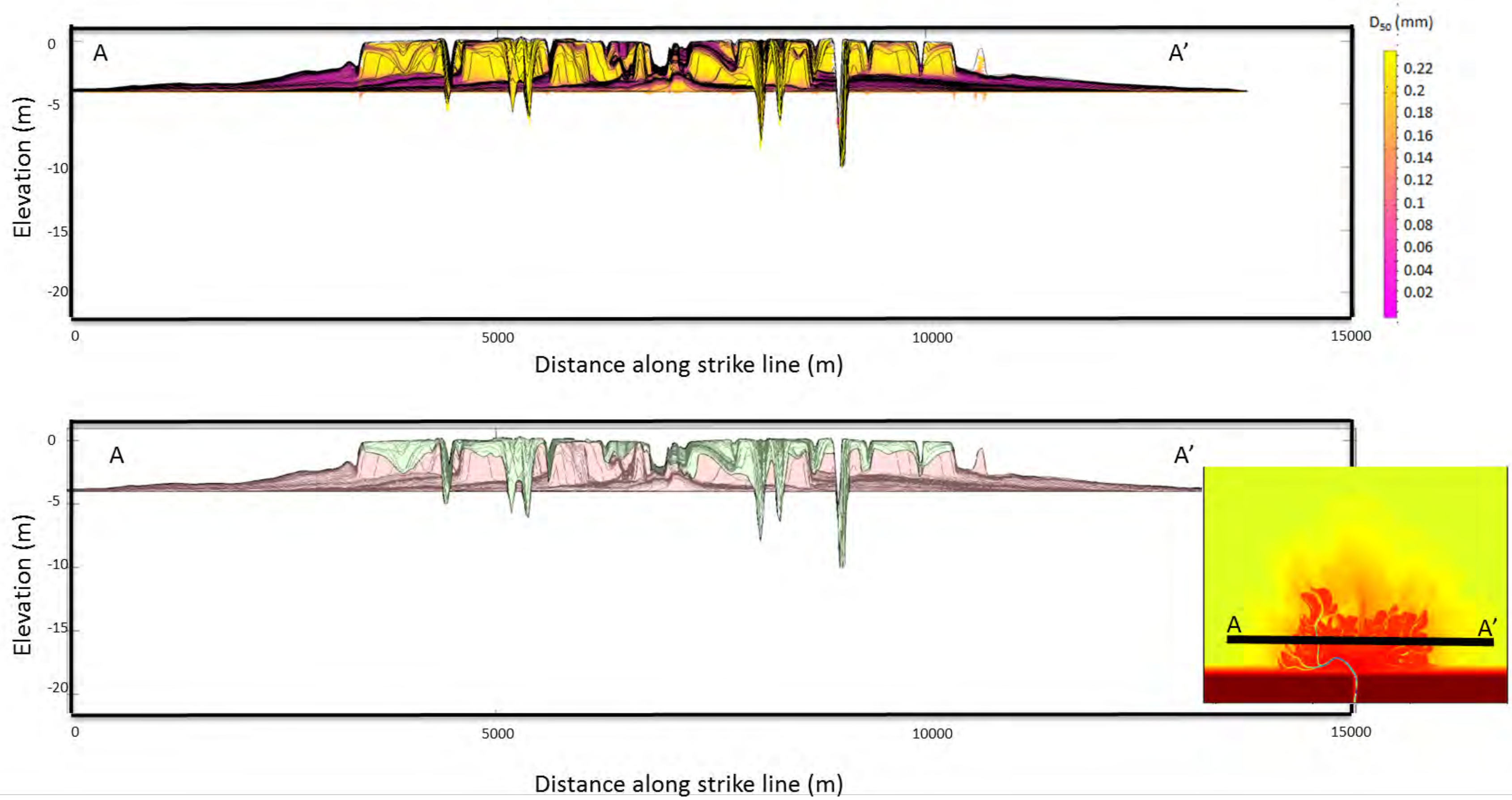

4m deep 0mm/yr RBLF. Upper image is Delft3D stratigraphy strike line with color representing D50 grain size. Yellow is coarse and pink is fine.
Black lines represent chronostratigraphic surfaces.
The bottom image shows the topset(green) and foreset(pink).

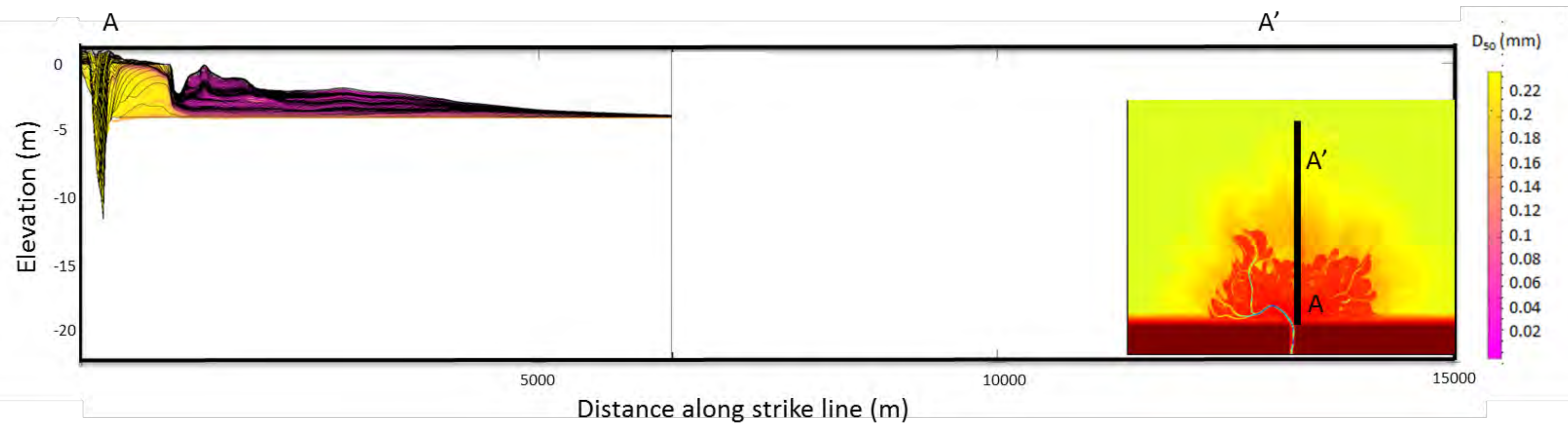

4m deep basin, 0mm/yr RBLF. Dip Line. Black lines are chronostratigraphic surfaces. Color indicates D_{50} grain size. Yellow is coarse and pink is fine.

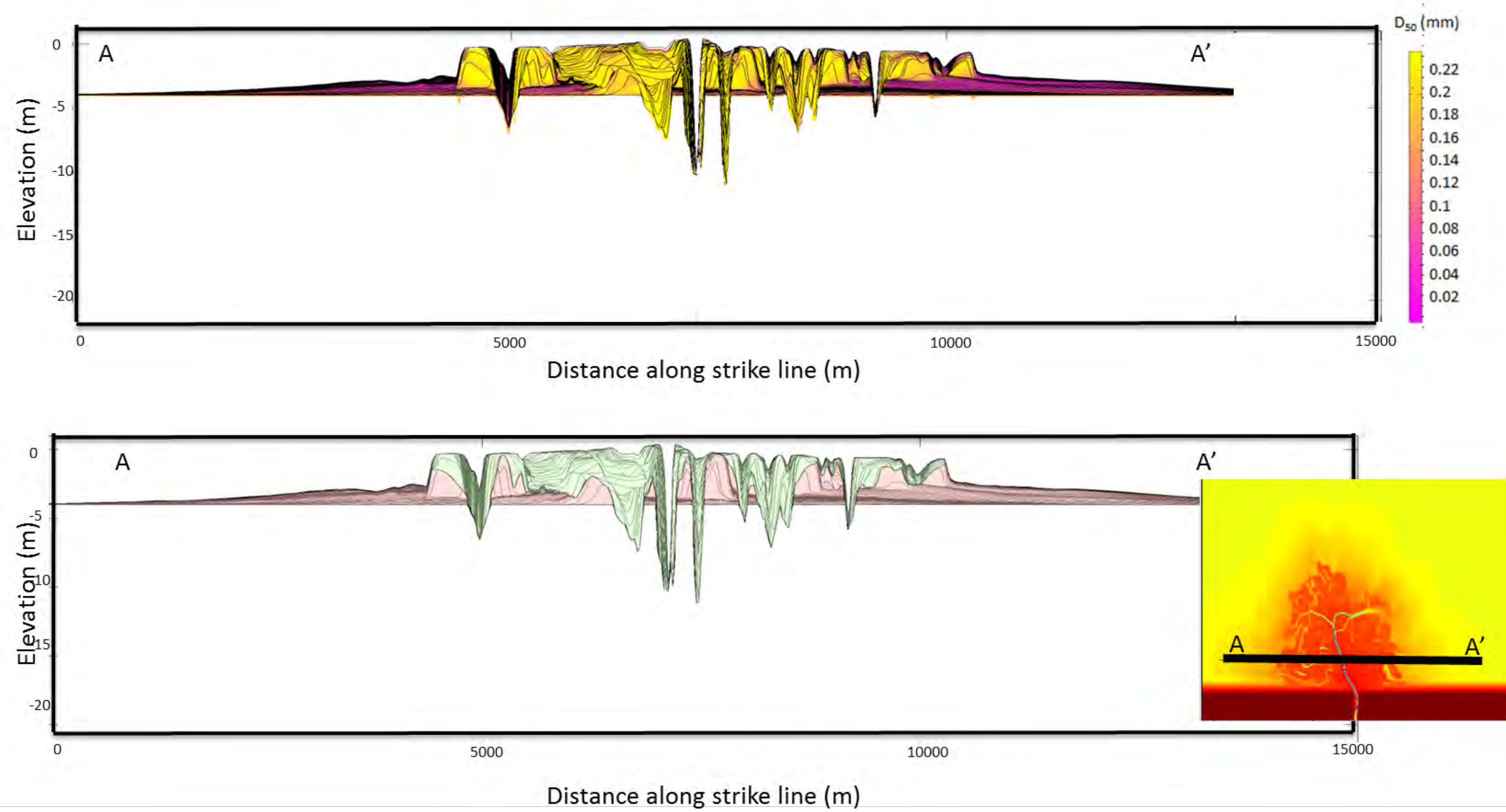

4m deep 5mm/yr RBLF. Upper image is Delft3D stratigraphy strike line with color representing D50 grain size. Yellow is coarse and pink is fine.
Black lines represent chronostratigraphic surfaces.
The bottom image shows the topset(green) and foreset(pink).

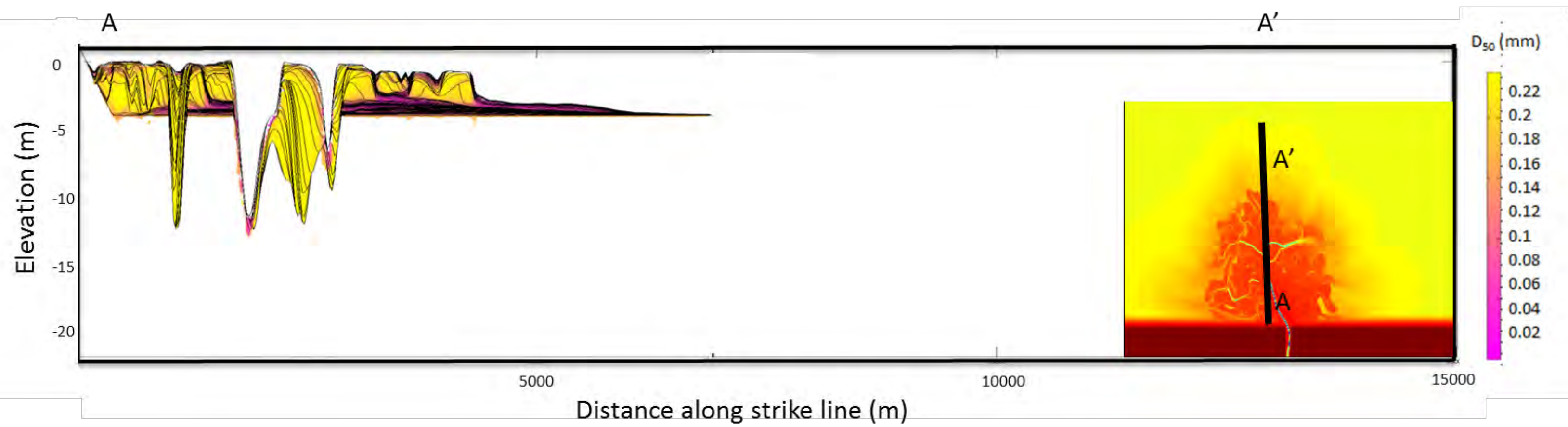

4m deep basin, 5mm/yr RBLF. Dip Line. Black lines are chronostratigraphic surfaces. Color indicates D_{50} grain size. Yellow is coarse and pink is fine.

2206

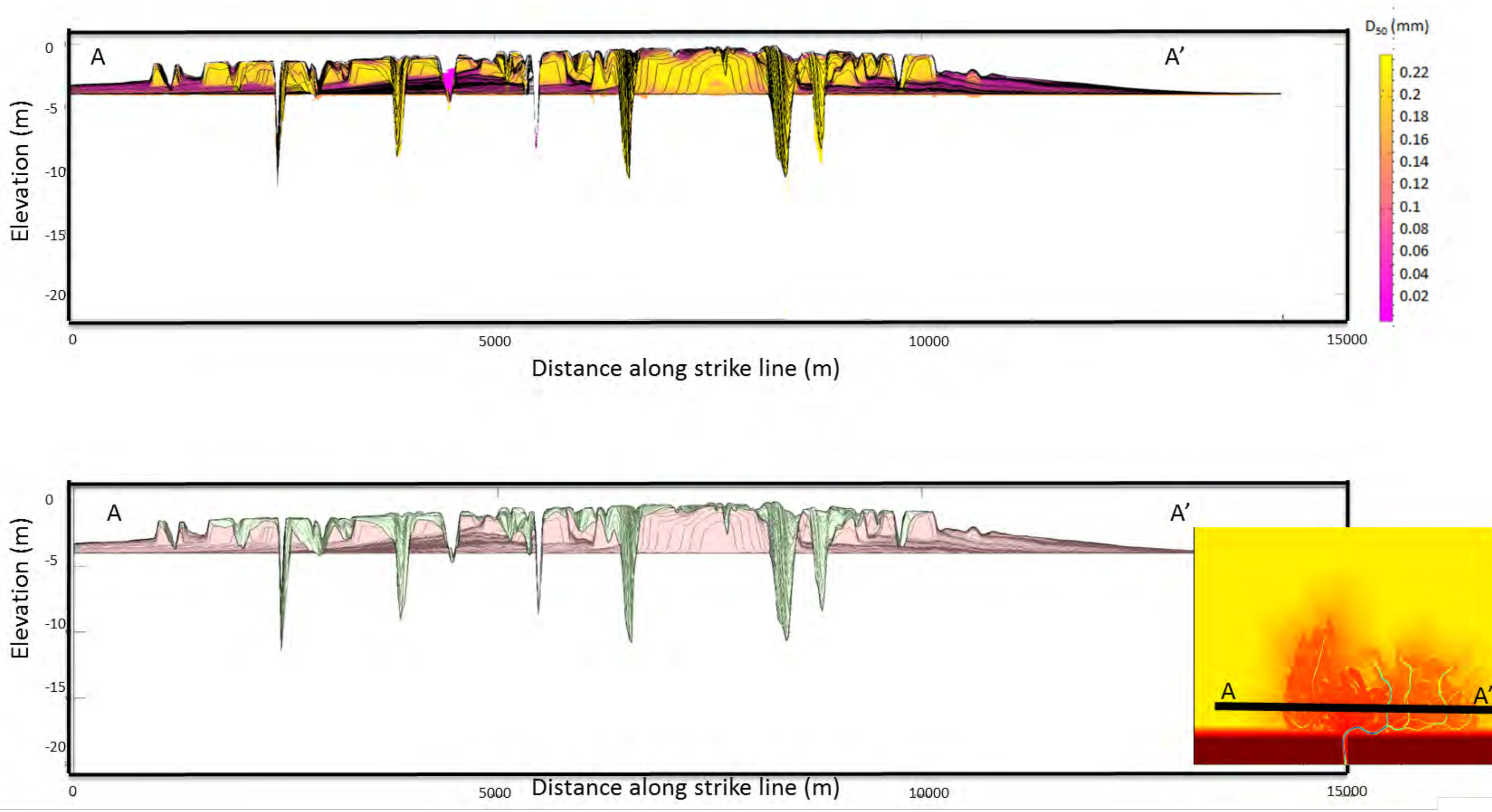

4m deep 10mm/yr RBLF. Upper image is Delft3D stratigraphy strike line with color representing D50 grain size. Yellow is coarse and pink is fine.
Black lines represent chronostratigraphic surfaces.
The bottom image shows the topset(green) and foreset(pink).

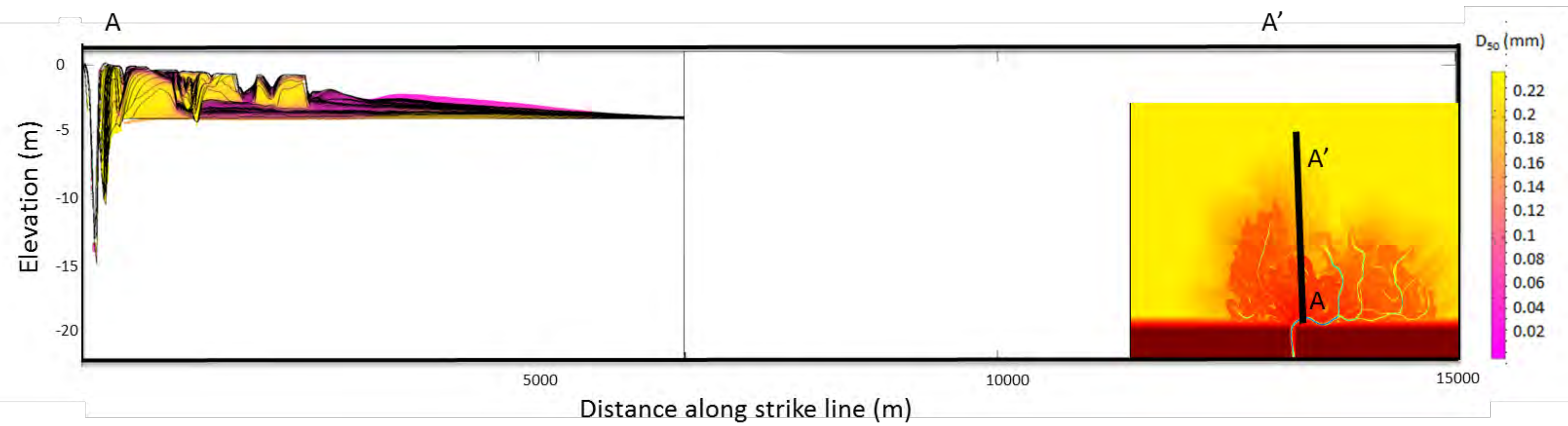

4m deep basin, 10mm/yr RBLF. Dip Line. Black lines are chronostratigraphic surfaces. Color indicates D_{50} grain size. Yellow is coarse and pink is fine.

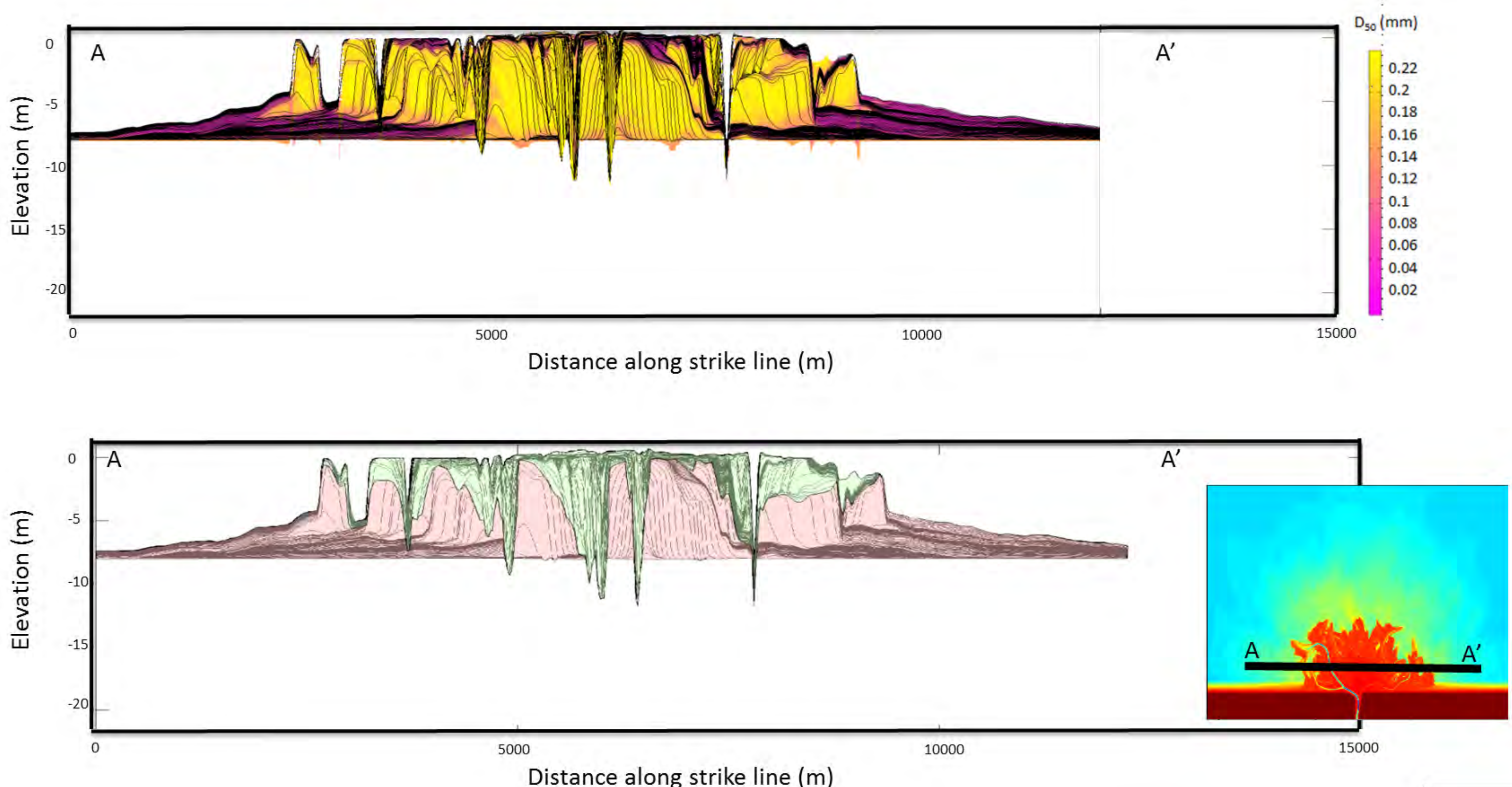

8m deep 0mm/yr RBLF. Upper image is Delft3D stratigraphy strike line with color representing D50 grain size. Yellow is coarse and pink is fine.
Black lines represent chronostratigraphic surfaces.
The bottom image shows the topset(green) and foreset(pink).

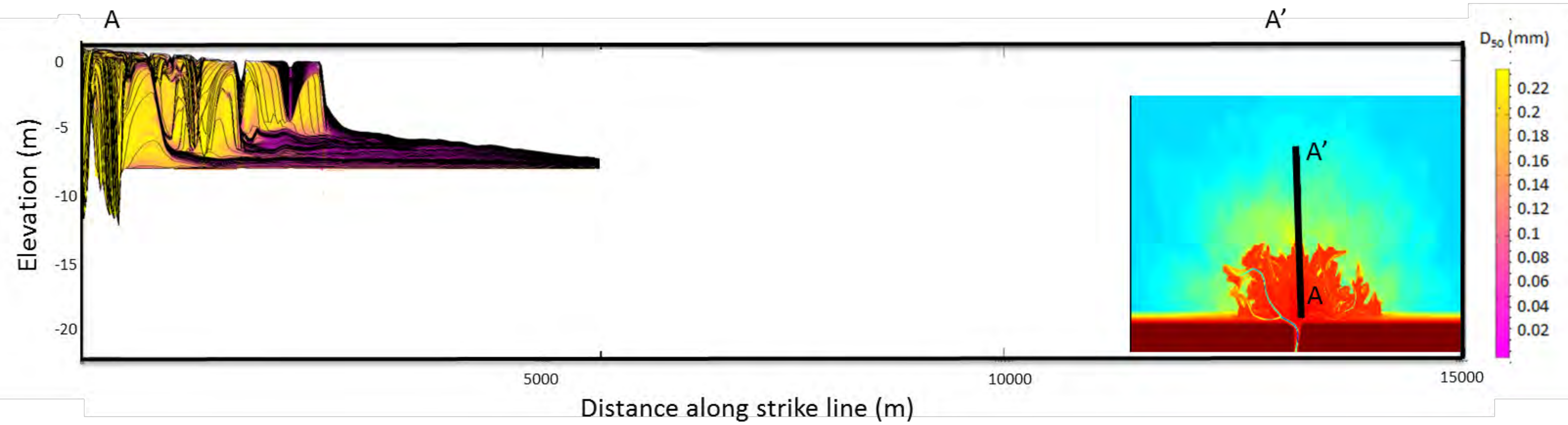

8m deep basin, 0mm/yr RBLF. Dip Line. Black lines are chronostratigraphic surfaces. Color indicates D_{50} grain size. Yellow is coarse and pink is fine.

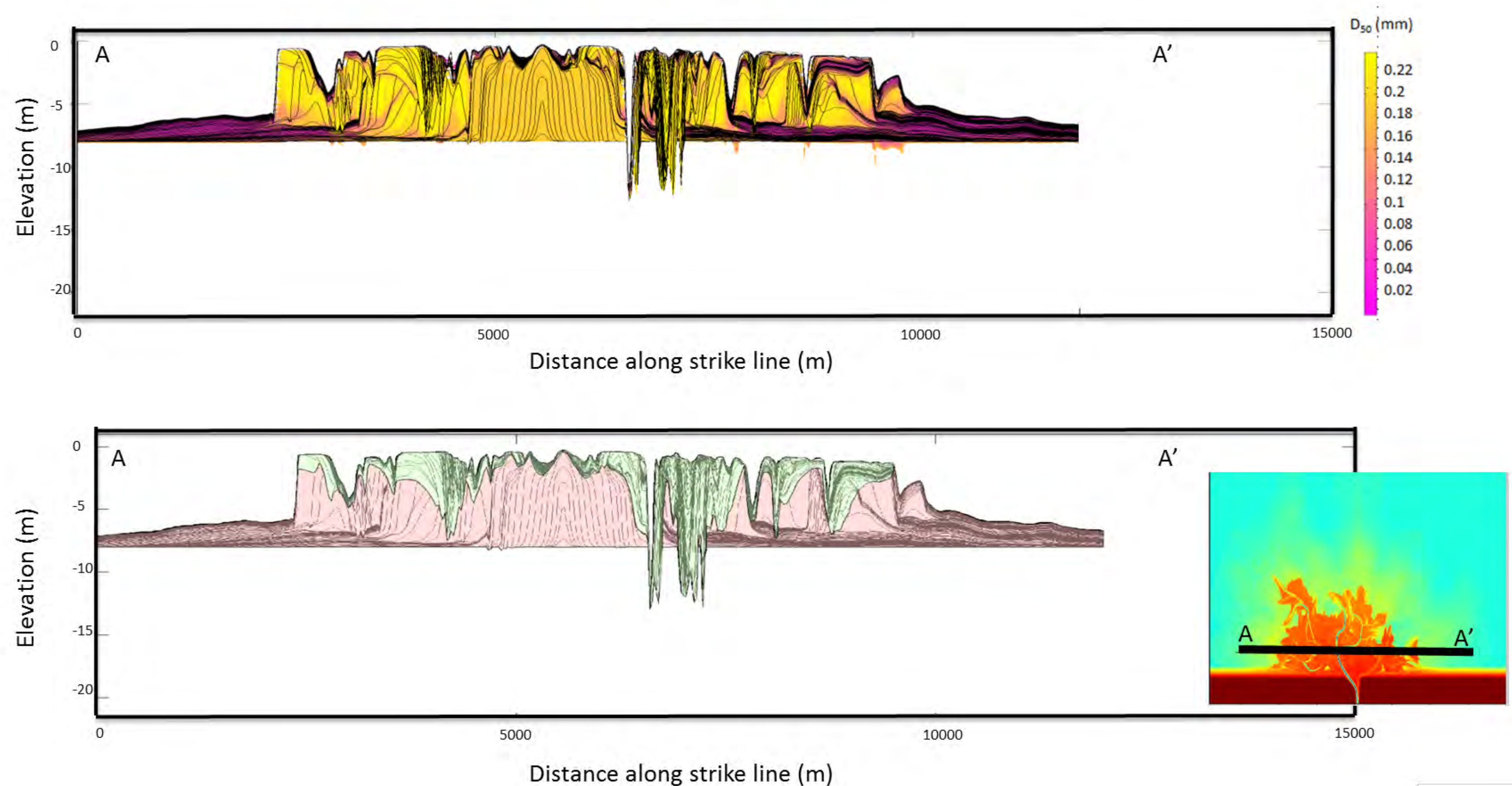

8m deep 5mm/yr RBLF. Upper image is Delft3D stratigraphy strike line with color representing D50 grain size. Yellow is coarse and pink is fine.
Black lines represent chronostratigraphic surfaces.
The bottom image shows the topset(green) and foreset(pink).

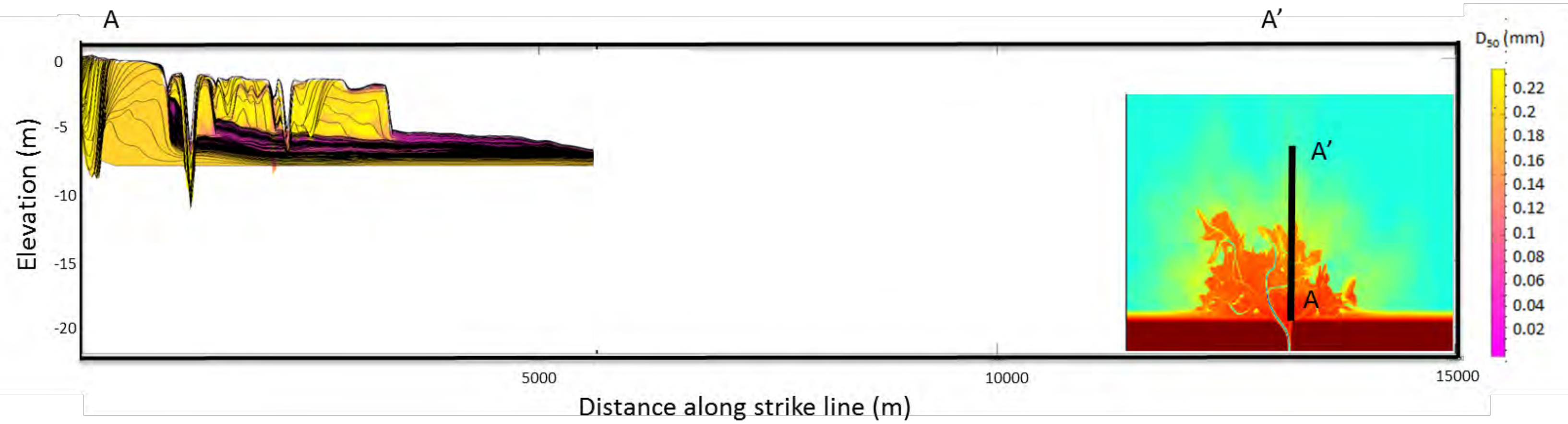

8m deep basin, 5mm/yr RBLF. Dip Line. Black lines are chronostratigraphic surfaces. Color indicates D_{50} grain size. Yellow is coarse and pink is fine.

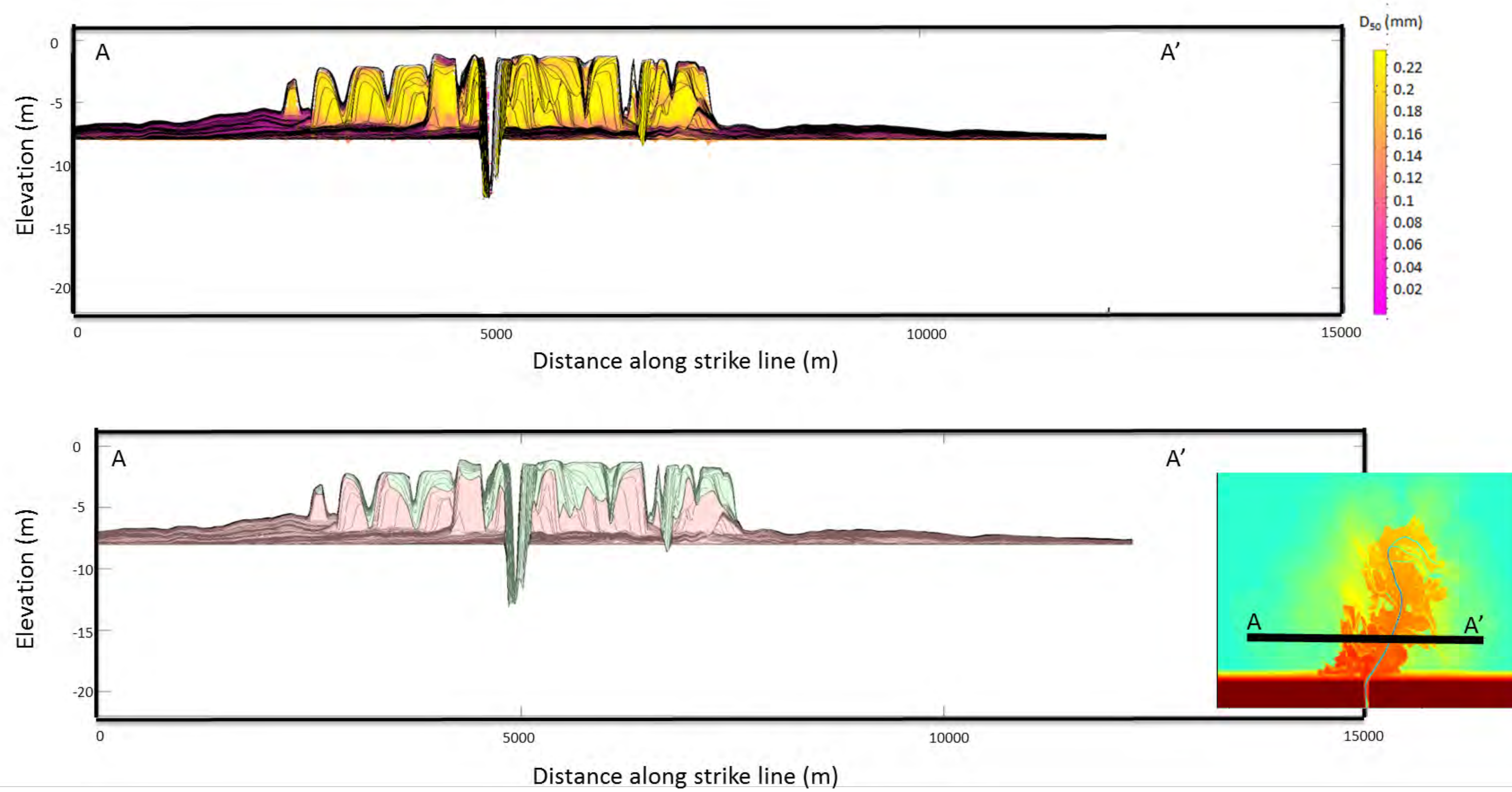

8m deep 10mm/yr RBLF. Upper image is Delft3D stratigraphy strike line with color representing D50 grain size. Yellow is coarse and pink is fine.
Black lines represent chronostratigraphic surfaces.
The bottom image shows the topset(green) and foreset(pink).

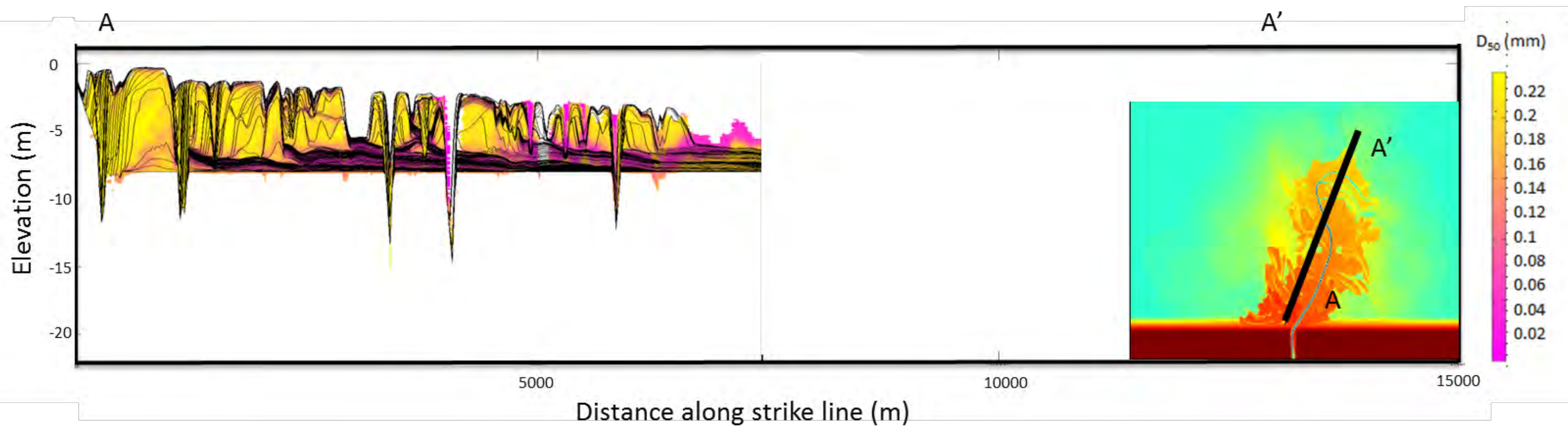

8m deep basin, 10mm/yr RBLF. Dip Line. Black lines are chronostratigraphic surfaces. Color indicates D_{50} grain size. Yellow is coarse and pink is fine.

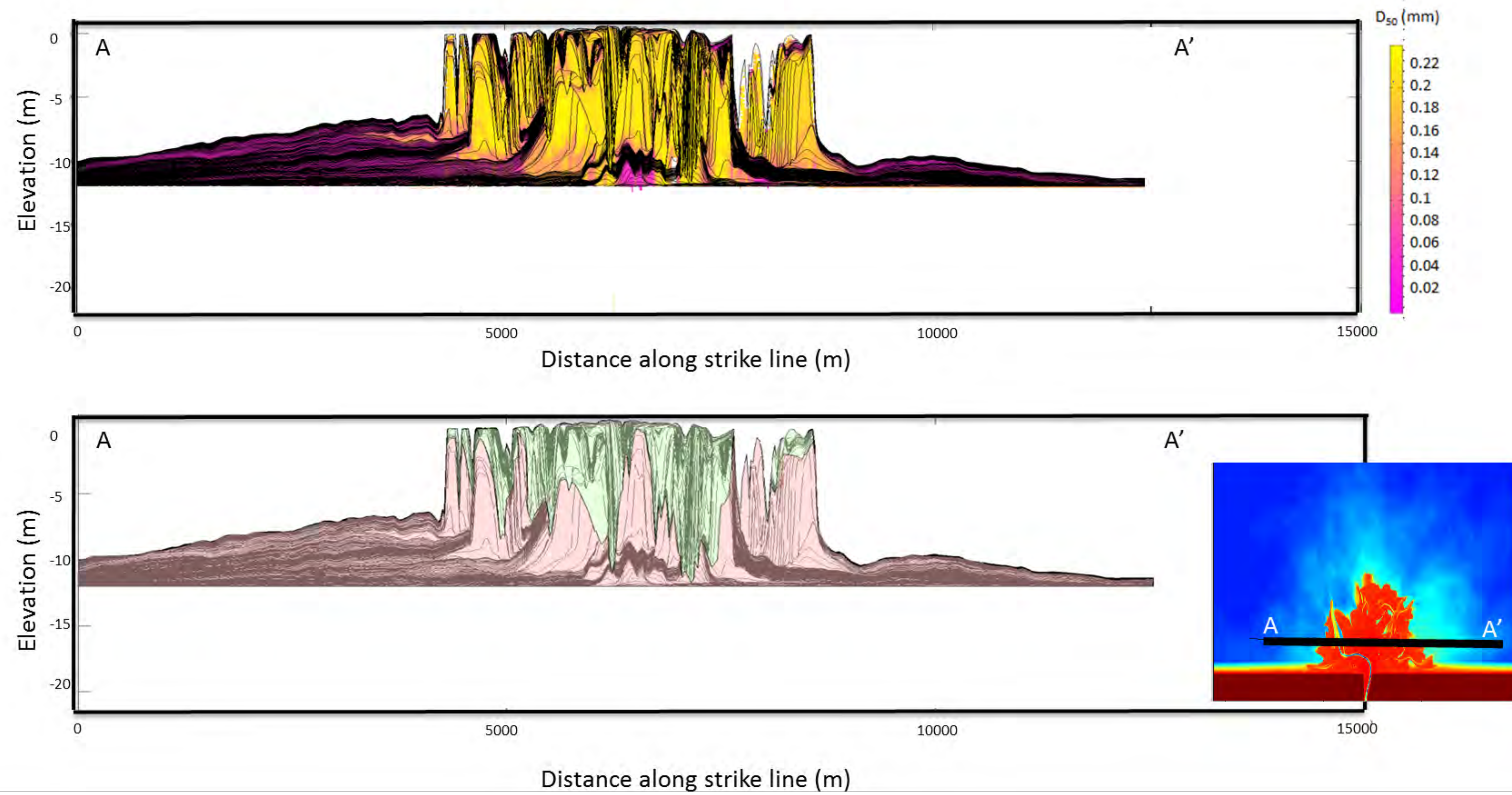

12m deep 0mm/yr RBLF. Upper image is Delft3D stratigraphy strike line with color representing D50 grain size. Yellow is coarse and pink is fine.
Black lines represent chronostratigraphic surfaces.
The bottom image shows the topset(green) and foreset(pink).

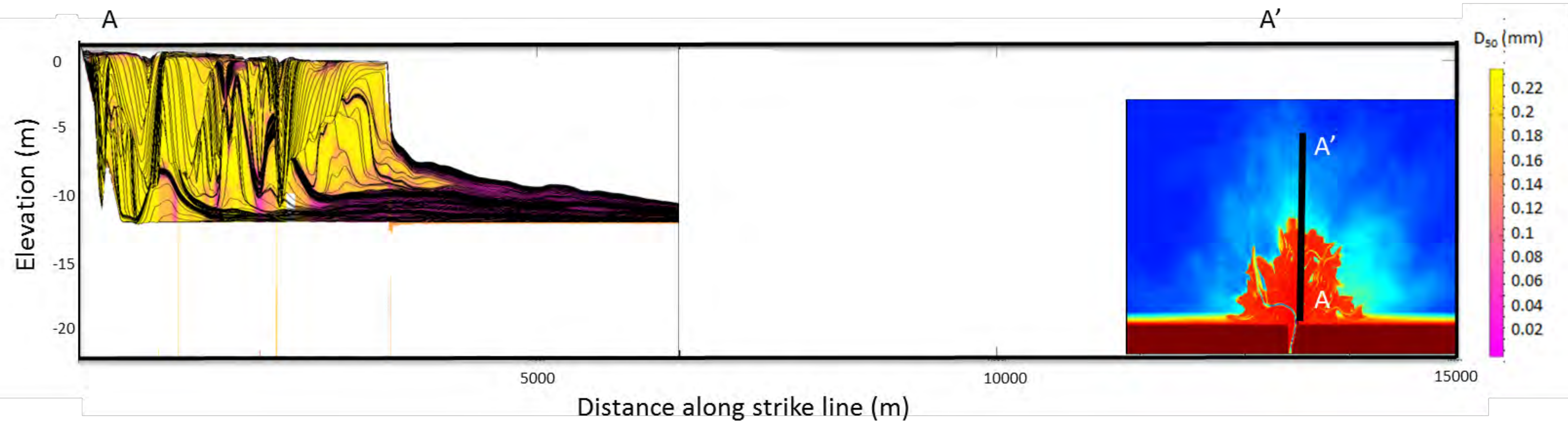

12m deep basin, 0mm/yr RBLF. Dip Line. Black lines are chronostratigraphic surfaces. Color indicates D_{50} grain size. Yellow is coarse and pink is fine.

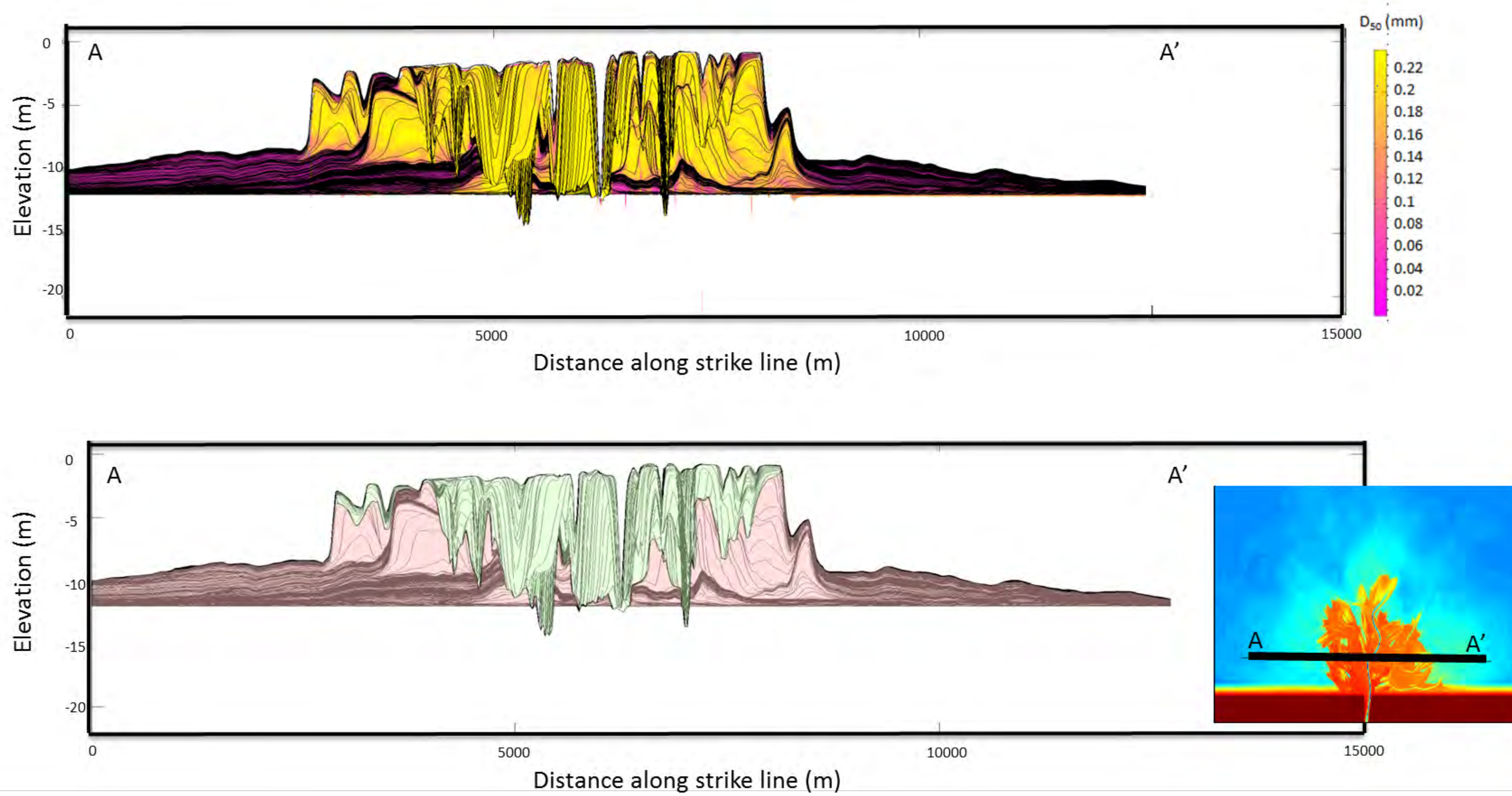

12m deep 5mm/yr RBLF. Upper image is Delft3D stratigraphy strike line with color representing D50 grain size. Yellow is coarse and pink is fine.
Black lines represent chronostratigraphic surfaces.
The bottom image shows the topset(green) and foreset(pink).

12m deep basin, 5mm/yr RBLF. Dip Line. Black lines are chronostratigraphic surfaces. Color indicates D_{50} grain size. Yellow is coarse and pink is fine.

2219

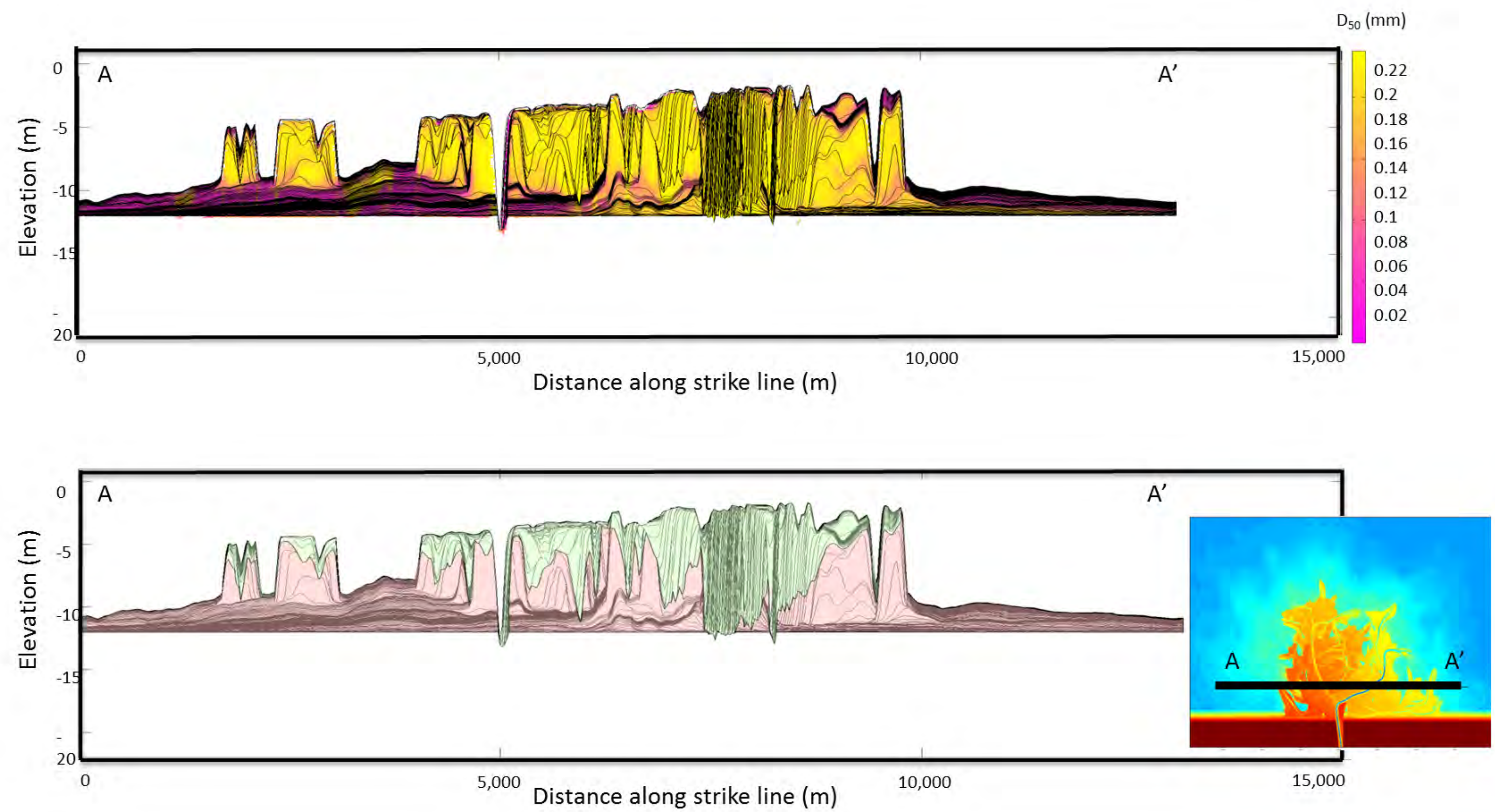

12m deep 10mm/yr RBLF. Upper image is Delft3D stratigraphy strike line with color representing D50 grain size. Yellow is coarse and pink is fine.
Black lines represent chronostratigraphic surfaces.
The bottom image shows the topset(green) and foreset(pink).

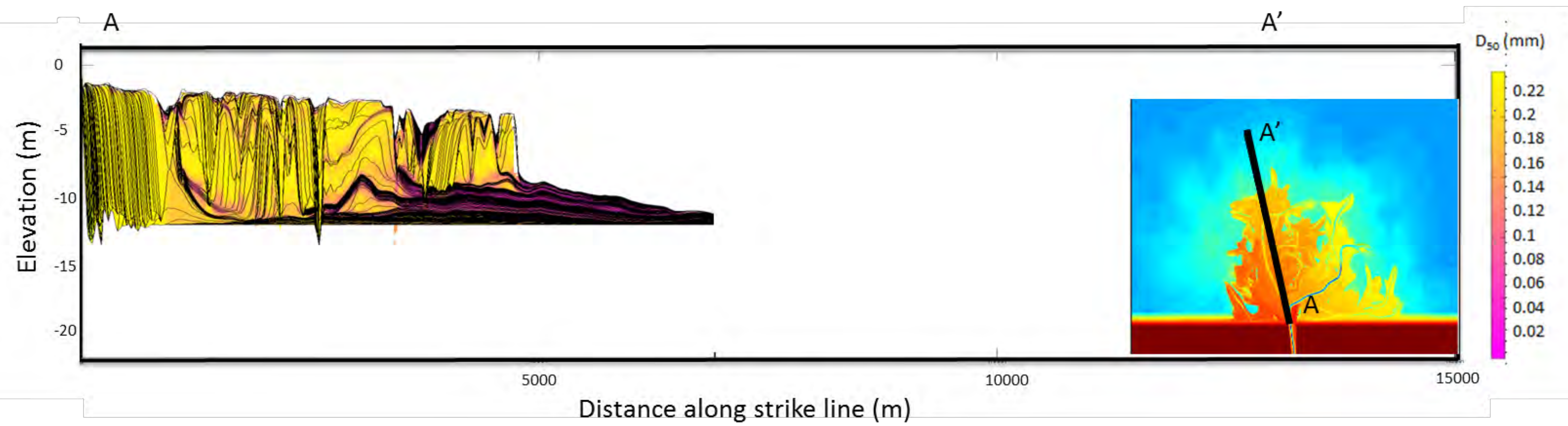

12m deep basin, 10mm/yr RBLF. Dip Line. Black lines are chronostratigraphic surfaces. Color indicates D_{50} grain size. Yellow is coarse and pink is fine.

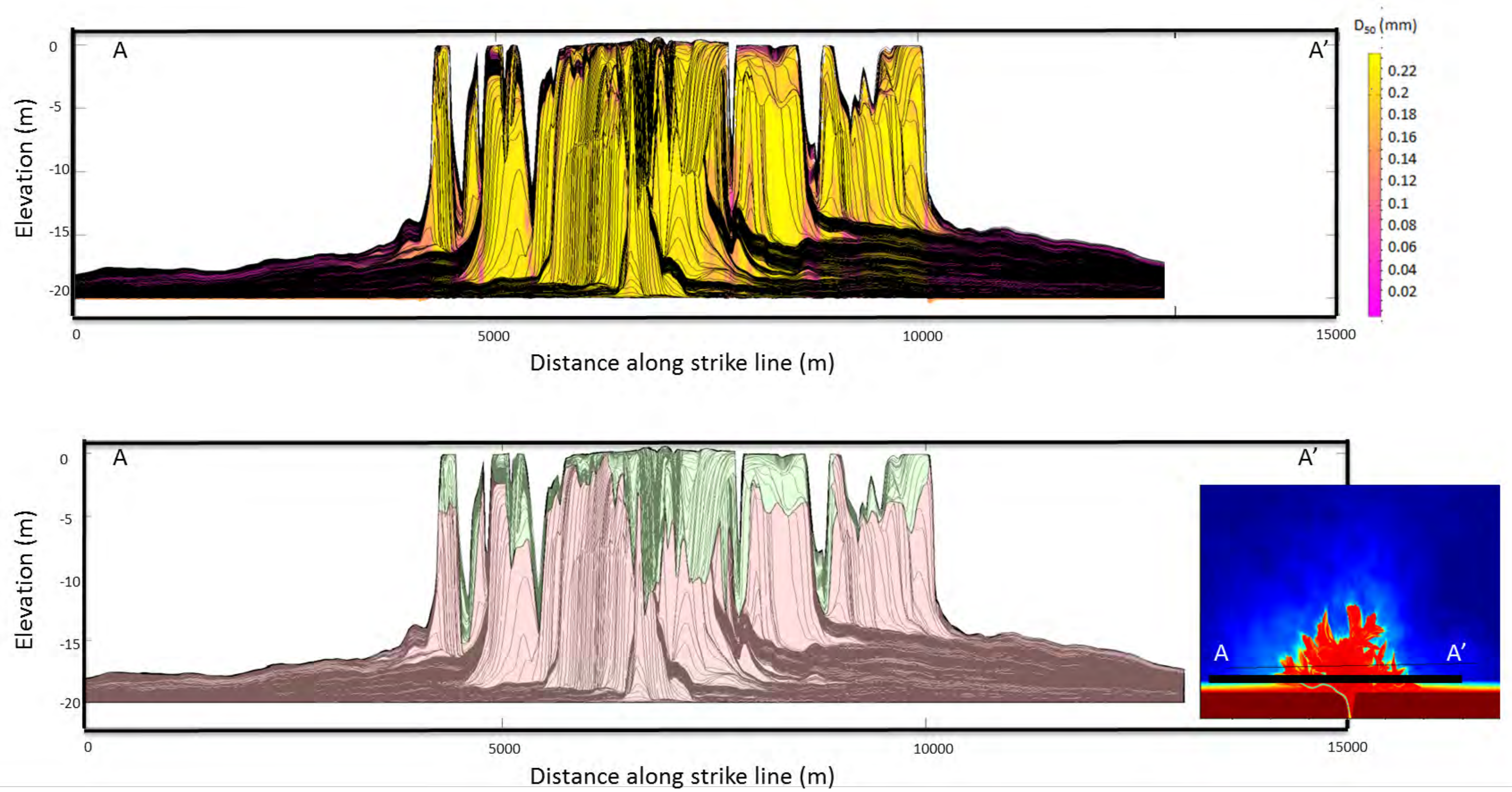

20m deep 0mm/yr RBLF. Upper image is Delft3D stratigraphy strike line with color representing D50 grain size. Yellow is coarse and pink is fine.
Black lines represent chronostratigraphic surfaces.
The bottom image shows the topset(green) and foreset(pink).

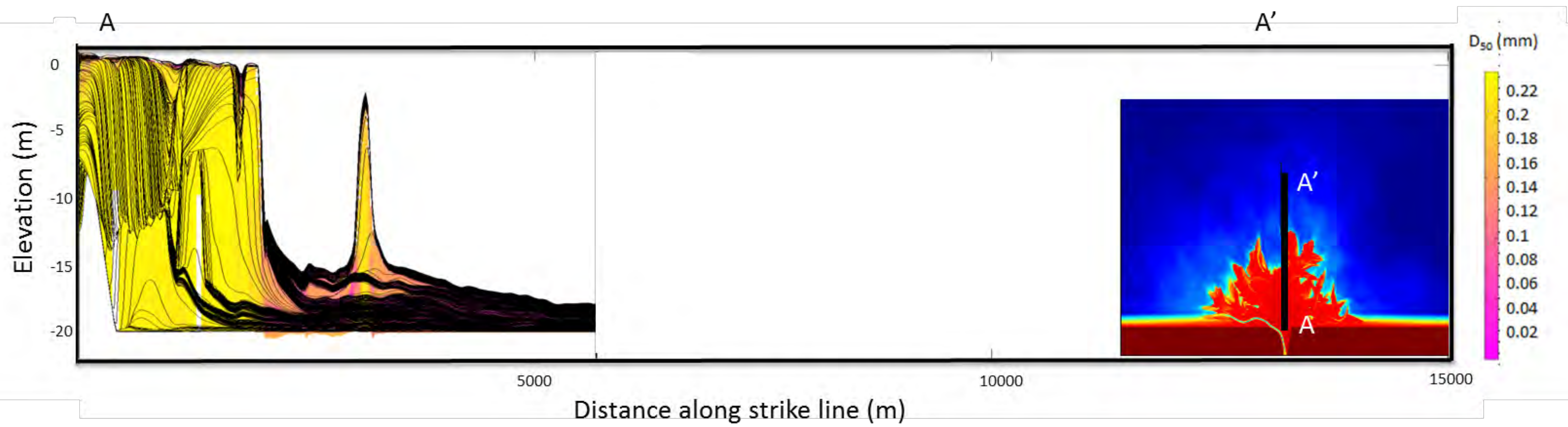

20m deep basin, 0mm/yr RBLF. Dip Line. Black lines are chronostratigraphic surfaces. Color indicates D_{50} grain size. Yellow is coarse and pink is fine.

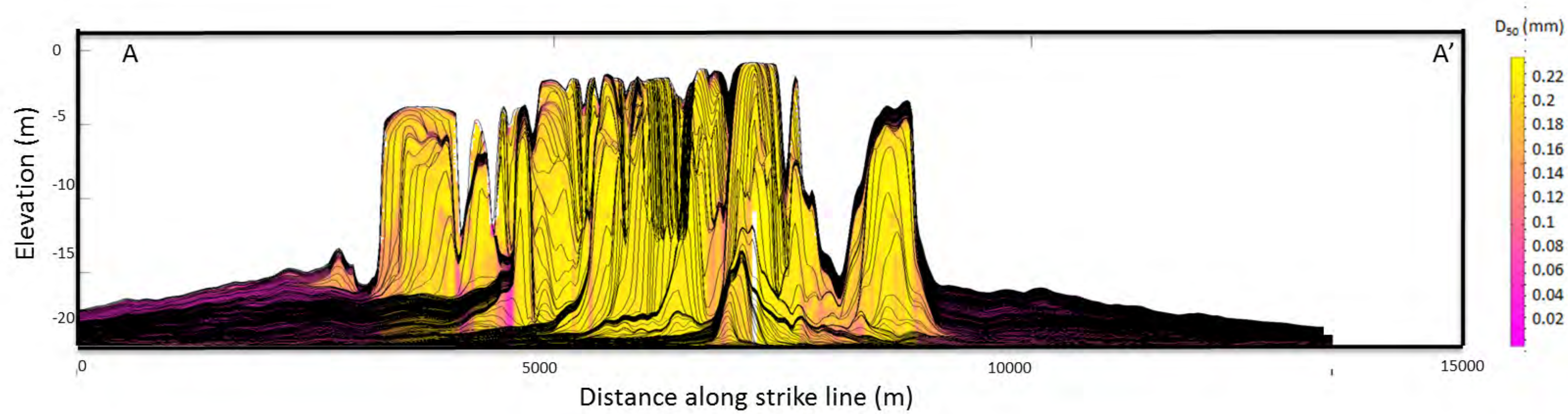

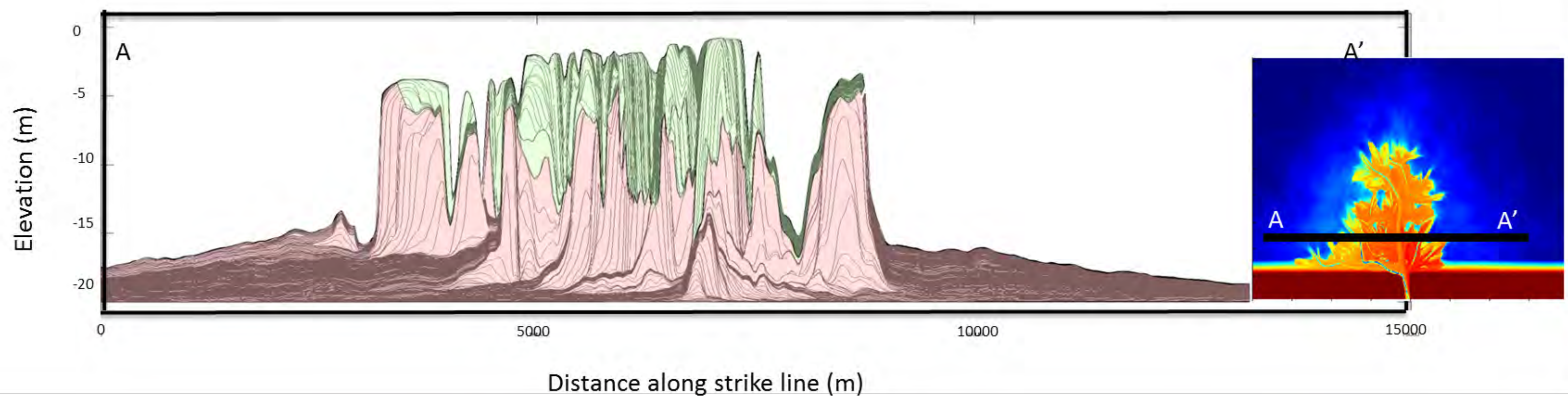

20m deep 5mm/yr RBLF. Upper image is Delft3D stratigraphy strike line with color representing D50 grain size. Yellow is coarse and pink is fine.
Black lines represent chronostratigraphic surfaces.
The bottom image shows the topset(green) and foreset(pink).

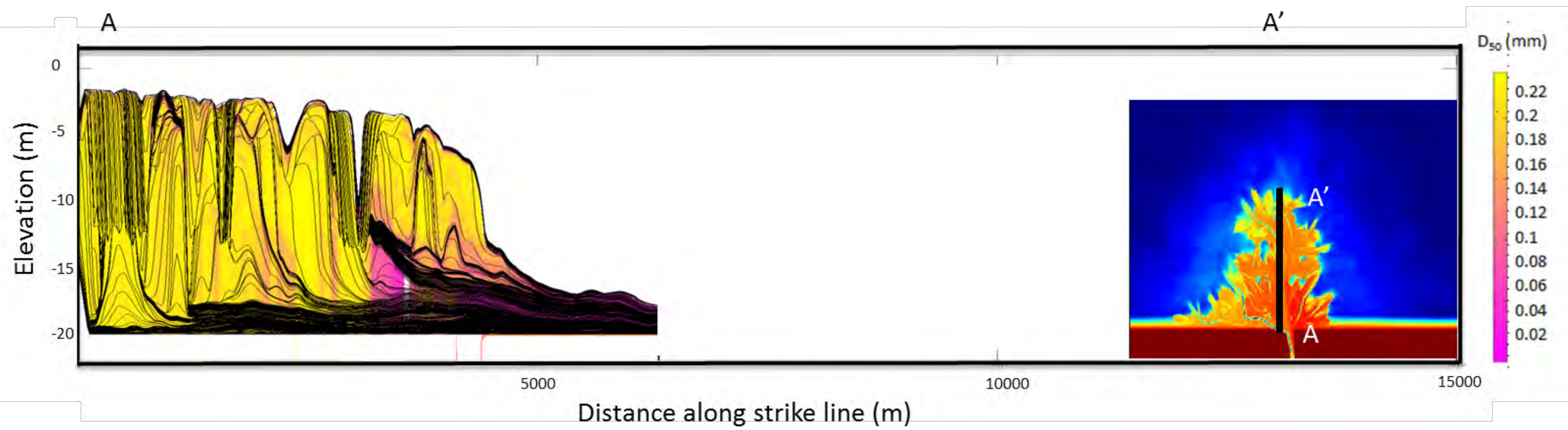

20m deep basin, 5mm/yr RBLF. Dip Line. Black lines are chronostratigraphic surfaces. Color indicates D_{50} grain size. Yellow is coarse and pink is fine.

2225

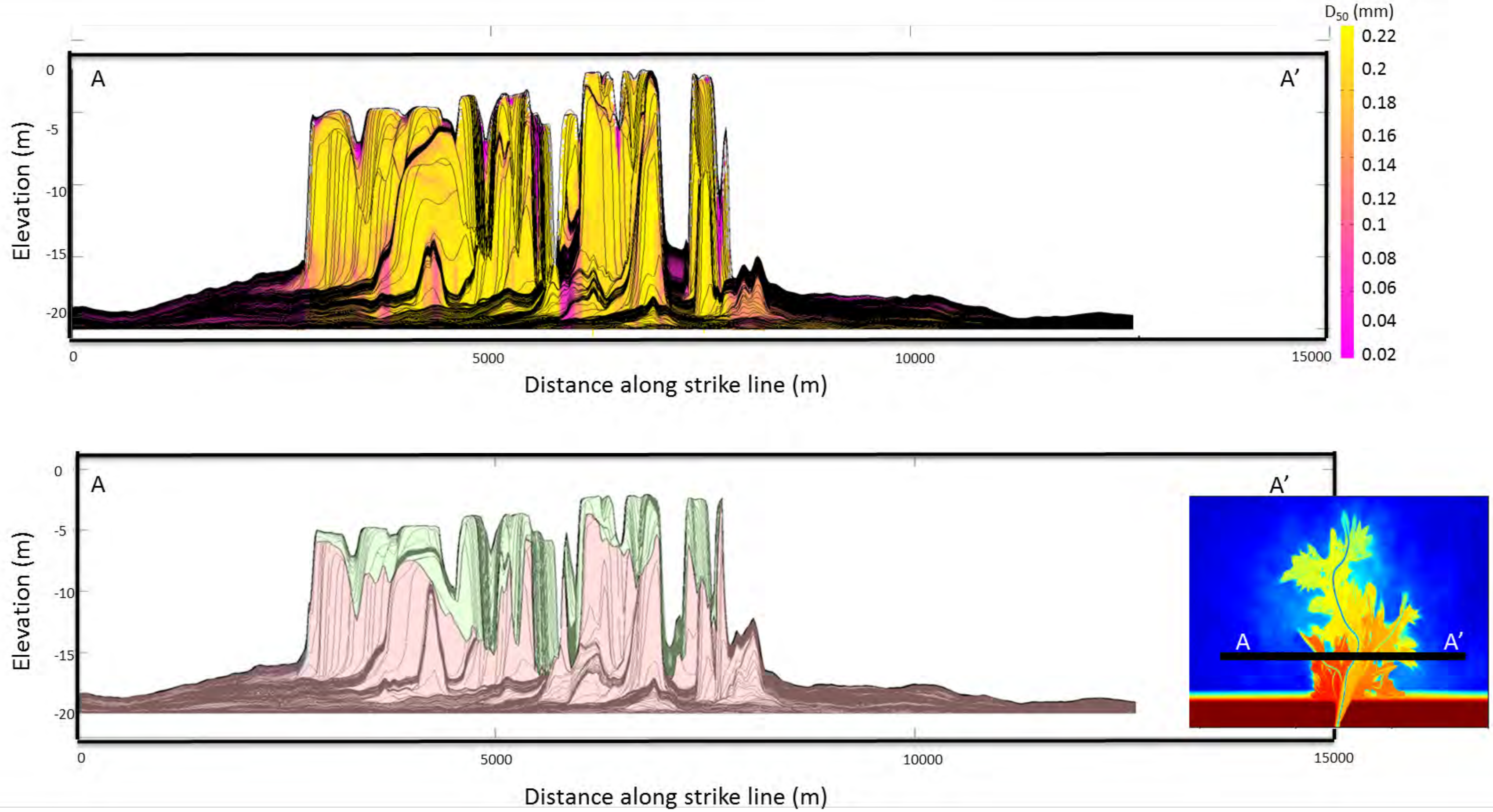

20m deep 10mm/yr RBLF. Upper image is Delft3D stratigraphy strike line with color representing D50 grain size. Yellow is coarse and pink is fine.
Black lines represent chronostratigraphic surfaces.
The bottom image shows the topset(green) and foreset(pink).

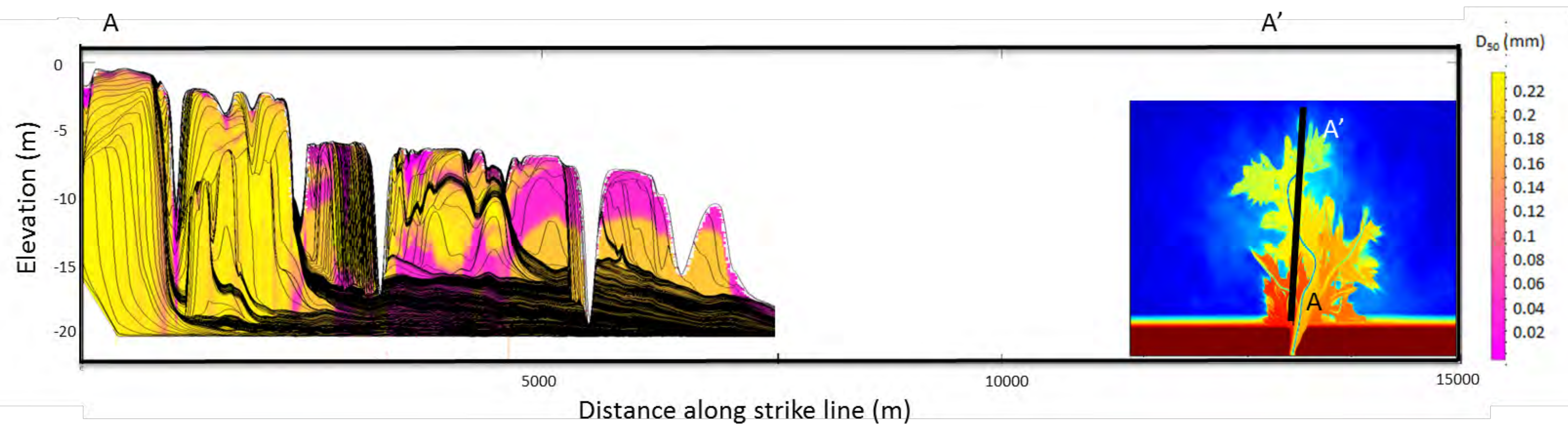

20m deep basin, 10mm/yr RBLF. Dip Line. Black lines are chronostratigraphic surfaces. Color indicates D_{50} grain size. Yellow is coarse and pink is fine.

Appendix D

Processed and Interpreted Ground Penetrating Radar Data From the Goose River Delta, Labrador, Canada

Aug3 Line19
Processing: Dewowed, Bandpass Filtered,
F-K(Stolt) Migration (v=0.6n/s), Depth Conversion
Clinoforms identified in blue

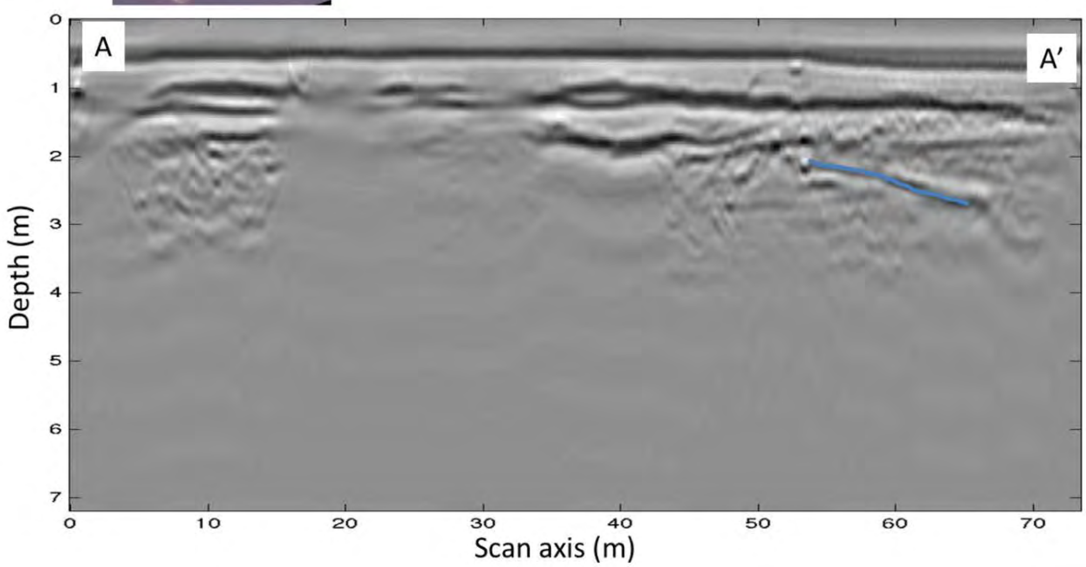

Aug3 Line21
Processing: Dewowed, Bandpass Filtered,
F-K(Stolt) Migration (v=0.6n/s), Depth Conversion
Clinoforms identified in blue

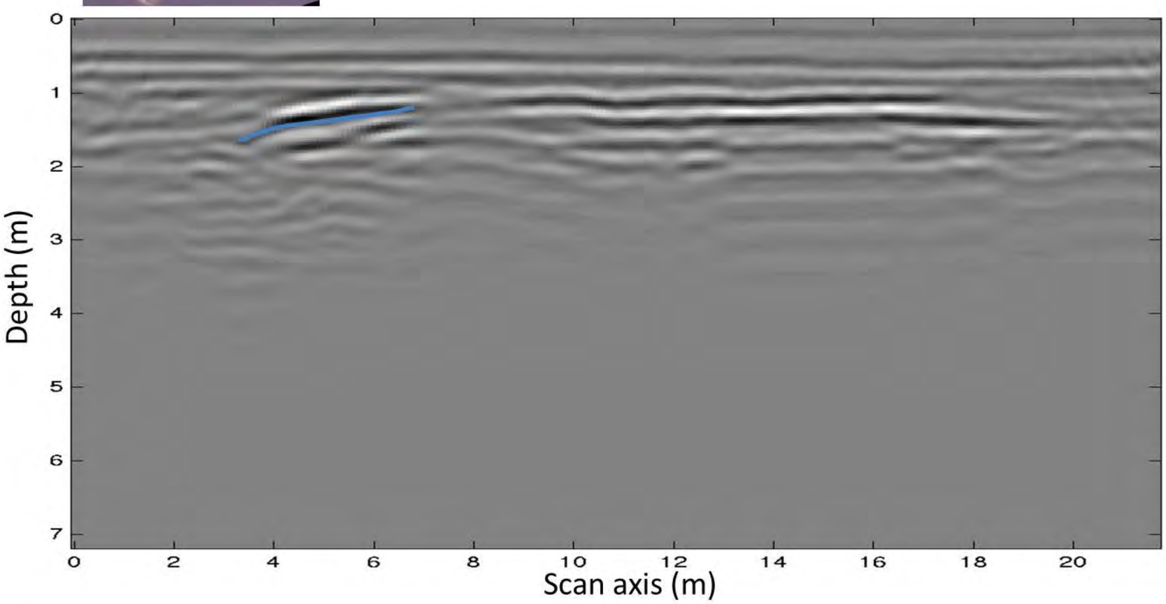

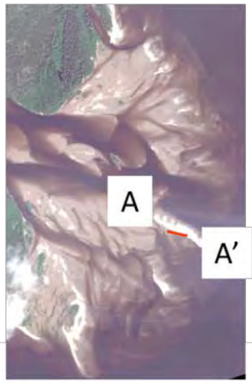

Aug3 Line22

Processing: Dewowed, Bandpass Filtered,

F-K(Stolt) Migration (v=0.6n/s), Depth Conversion

Clinoforms identified in blue

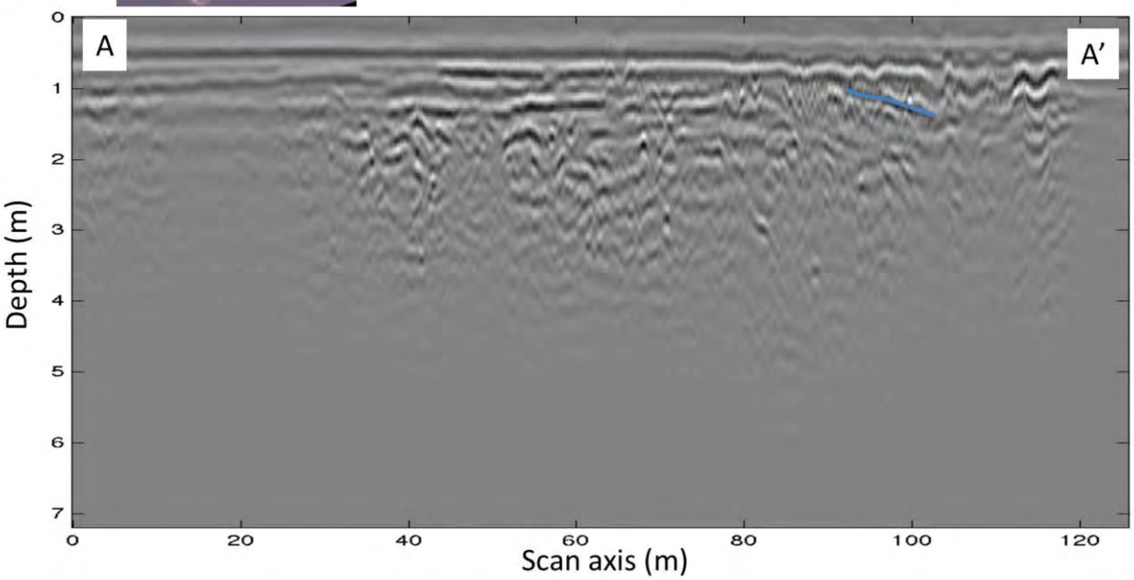

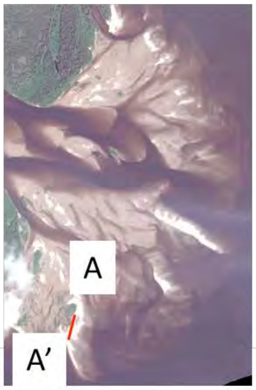

Aug3 Line27
Processing: Dewowed, Bandpass Filtered,
F-K(Stolt) Migration (v=0.6n/s), Depth Conversion
Clinoforms identified in blue

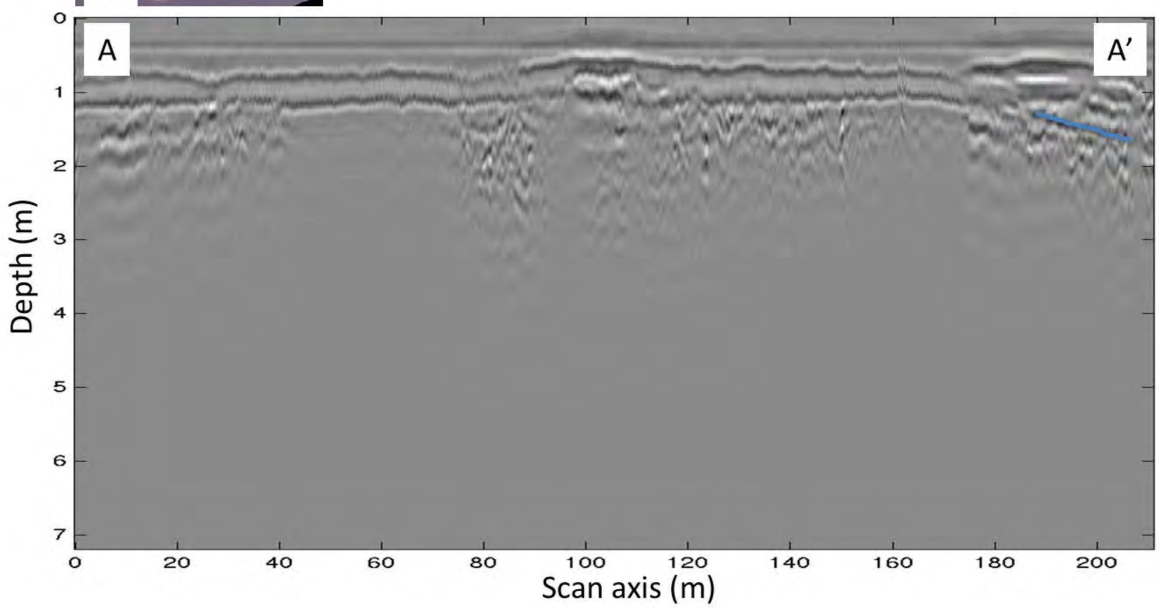

2235

Aug3 Line28
Processing: Dewowed, Bandpass Filtered,
F-K(Stolt) Migration (v=0.6n/s), Depth Conversion
Clinoforms identified in blue

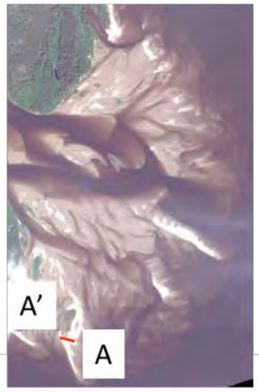

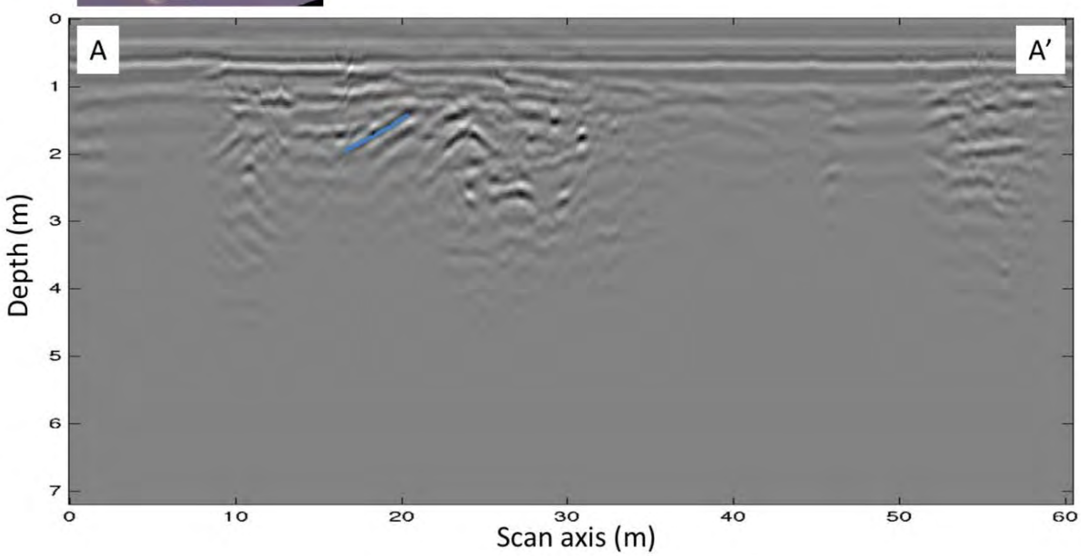

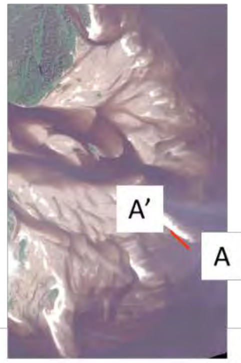

Aug4 Line32
Processing: Dewowed, Bandpass Filtered,
F-K(Stolt) Migration (v=0.6n/s), Depth Conversion
Clinoforms identified in blue

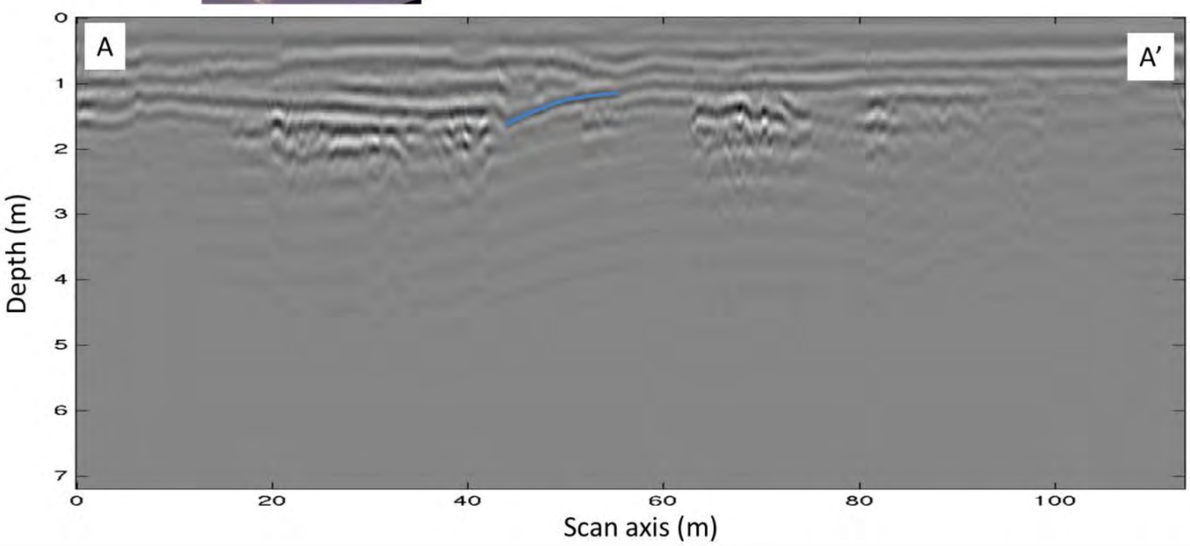

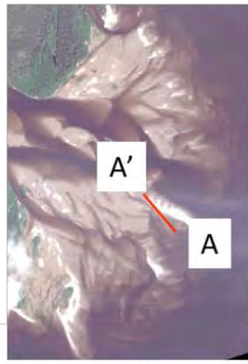

Aug4 Line37
Processing: Dewowed, Bandpass Filtered,
F-K(Stolt) Migration (v=0.6n/s), Depth Conversion
Clinoforms identified in blue

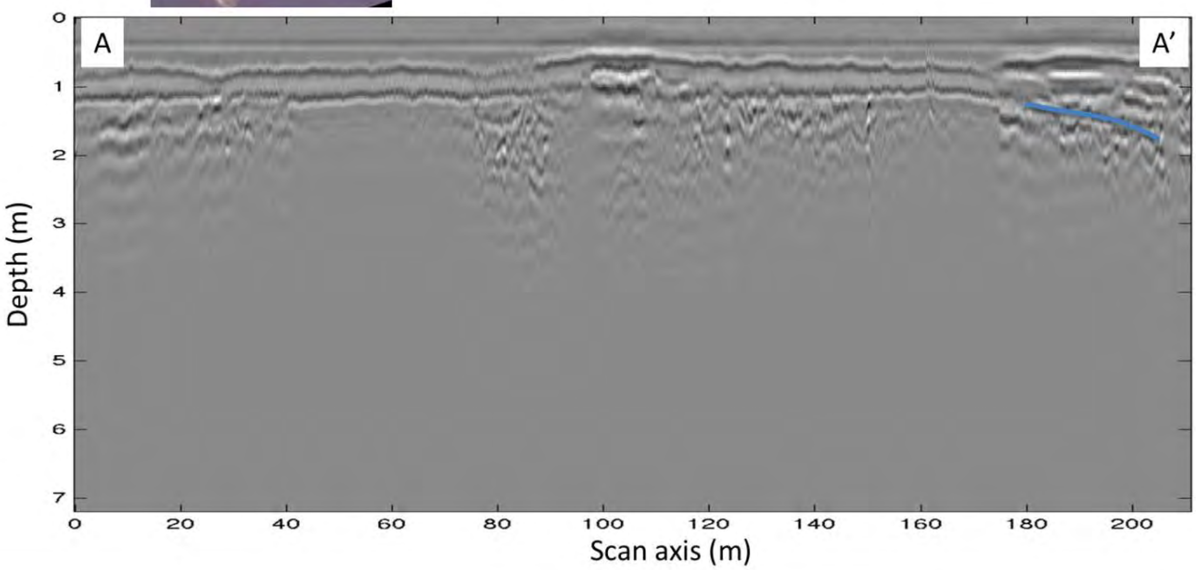

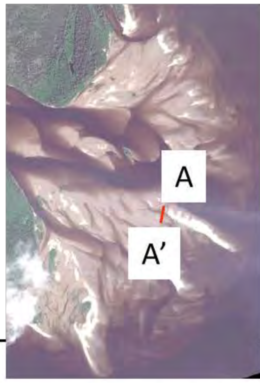

Aug4 Line38
Processing: Dewowed, Bandpass Filtered,
F-K(Stolt) Migration (v=0.6n/s), Depth Conversion
Clinoforms identified in blue

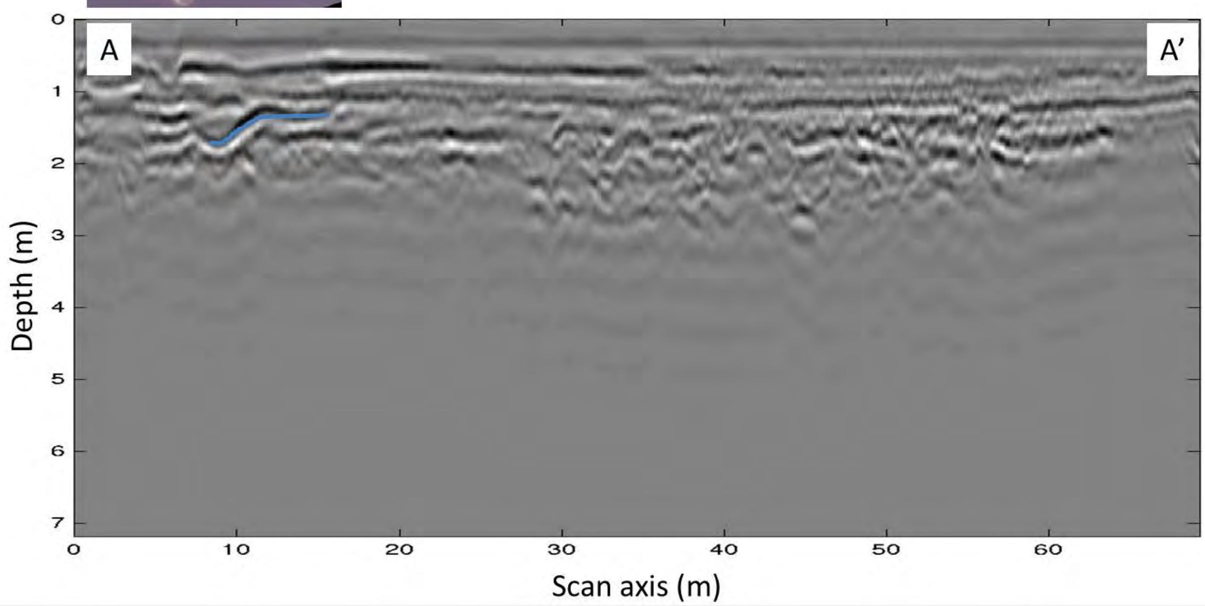

Aug4 Line39
Processing: Dewowed, Bandpass Filtered,
F-K(Stolt) Migration (v=0.6n/s), Depth Conversion
Clinoforms identified in blue

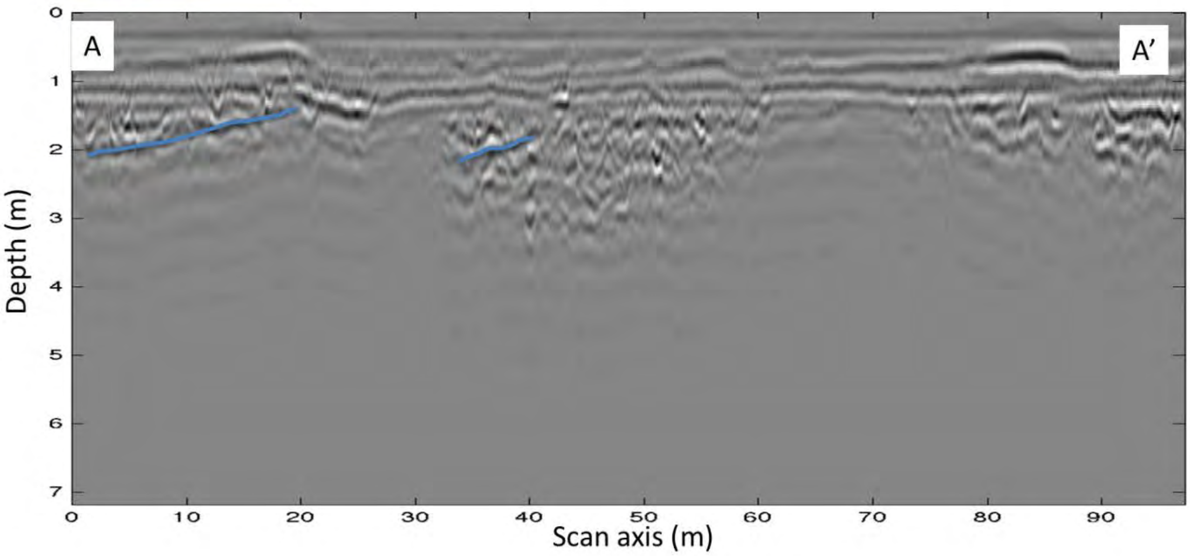

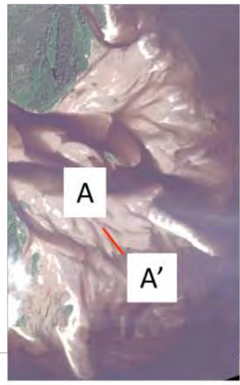

Aug4 Line42
Processing: Dewowed, Bandpass Filtered,
F-K(Stolt) Migration (v=0.6n/s), Depth Conversion
Clinoforms identified in blue

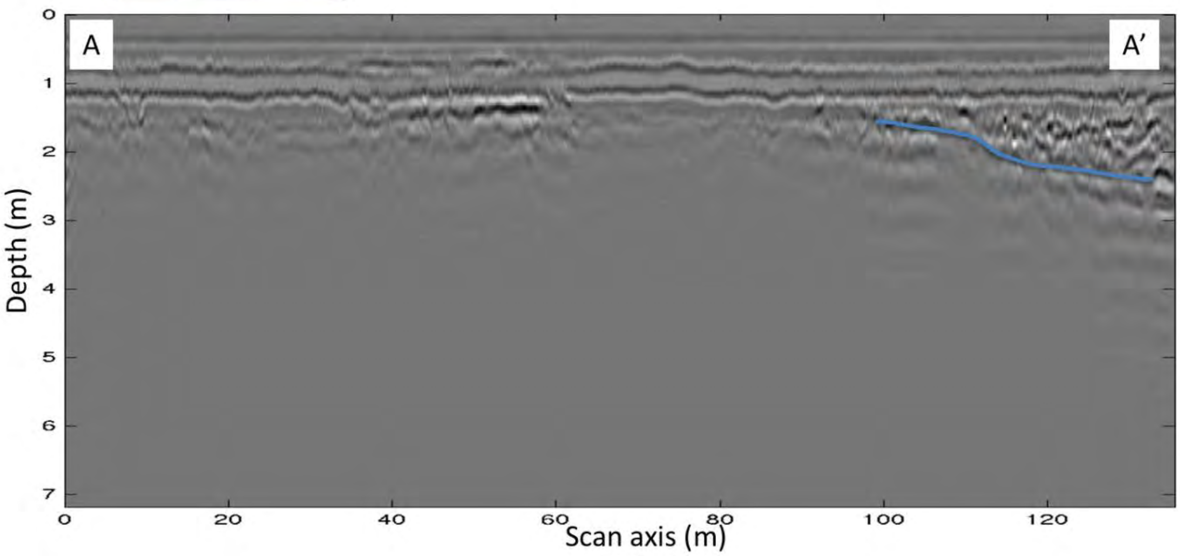

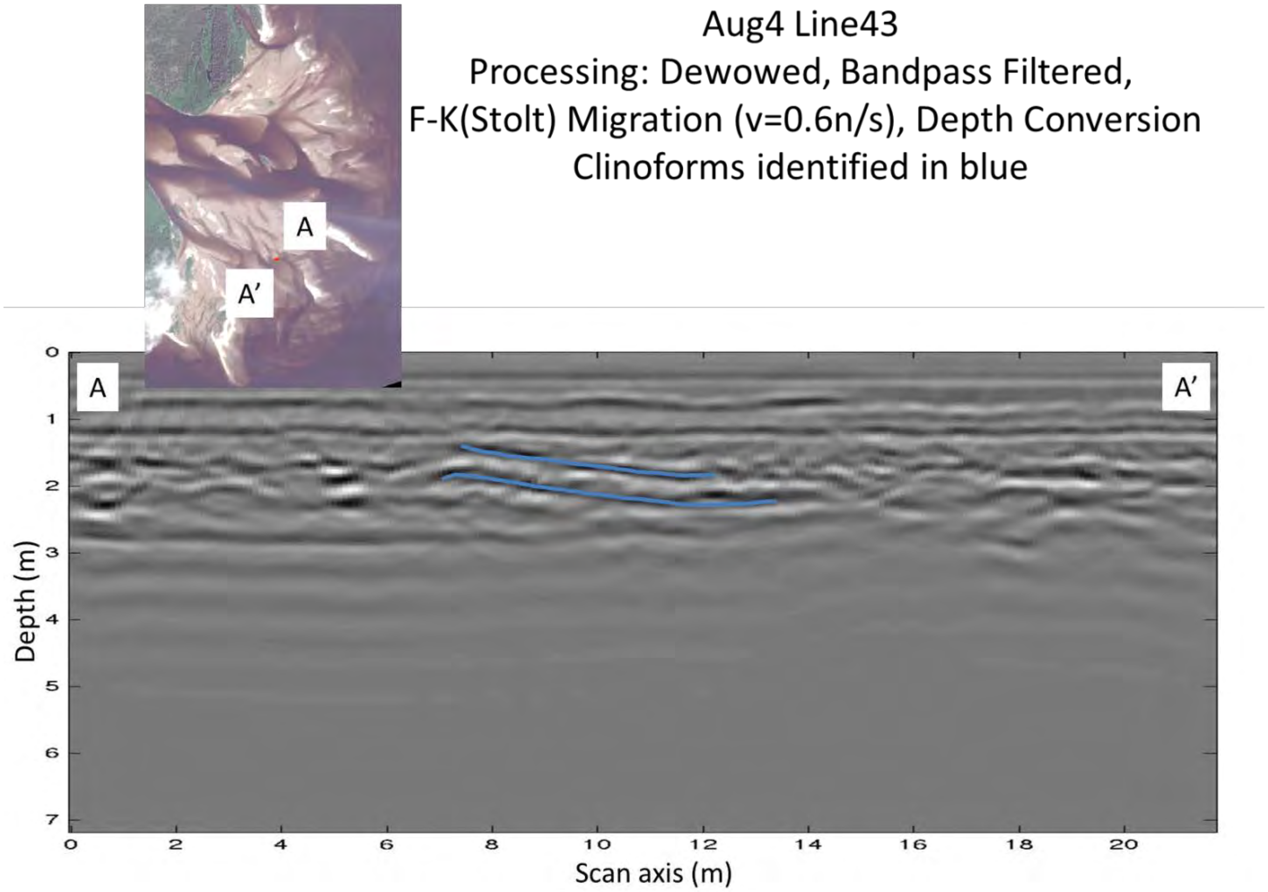
Aug4 Line43
Processing: Dewowed, Bandpass Filtered,
F-K(Stolt) Migration (v=0.6n/s), Depth Conversion
Clinoforms identified in blue
A
A'
A
A'
Depth (m)
Scan axis (m)
0
1
2
3
4
5
6
7
0
2
4
6
8
10
12
14
16
18
20

Aug4 Line44
Processing: Dewowed, Bandpass Filtered,
F-K(Stolt) Migration (v=0.6n/s), Depth Conversion
Clinoforms identified in blue

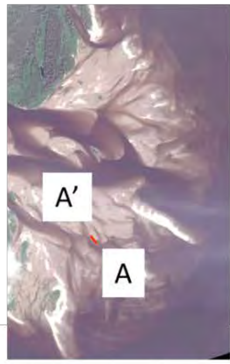

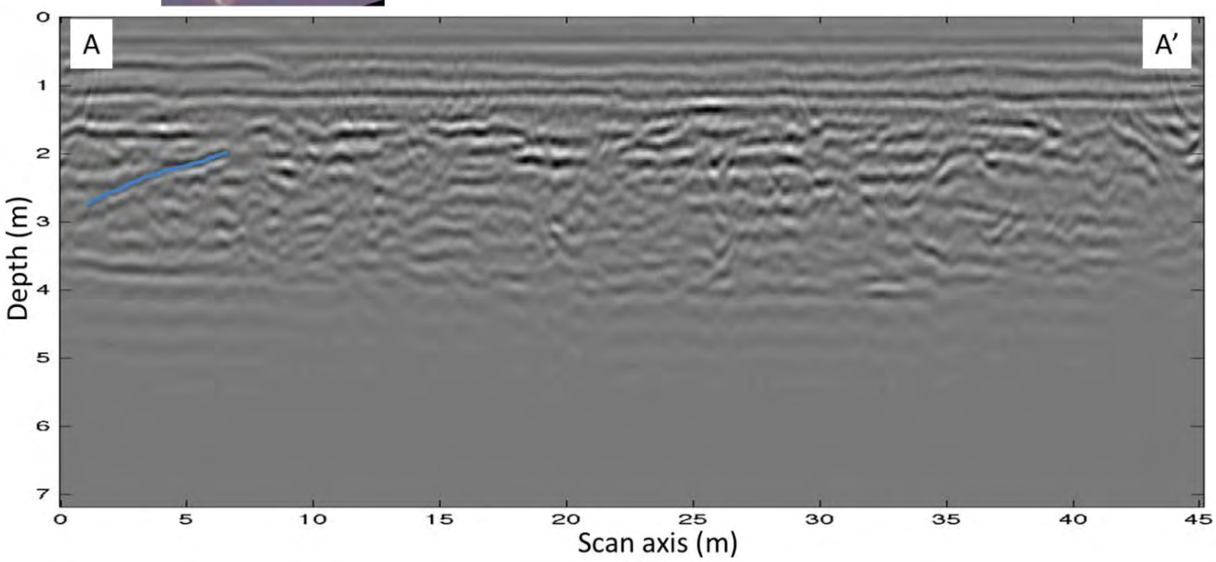

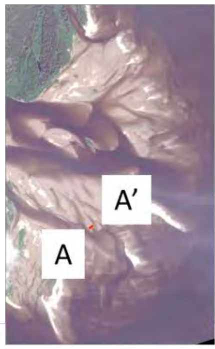

Aug4 Line45

Processing: Dewowed, Bandpass Filtered,

F-K(Stolt) Migration (v=0.6n/s), Depth Conversion

Clinoforms identified in blue

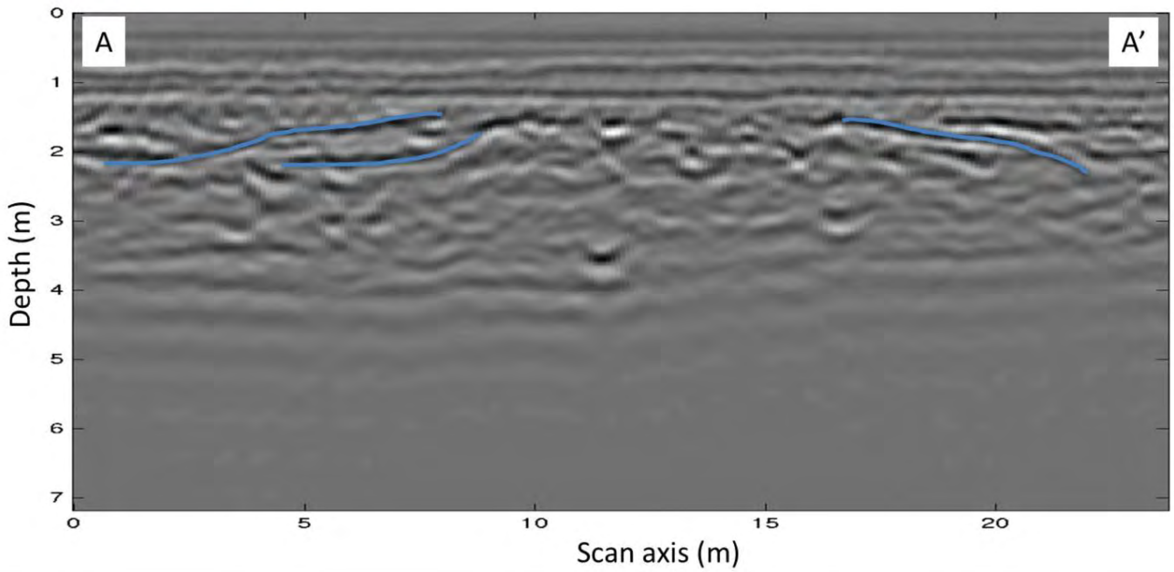

Aug4 Line46
Processing: Dewowed, Bandpass Filtered,
F-K(Stolt) Migration (v=0.6n/s), Depth Conversion
Clinoforms identified in blue

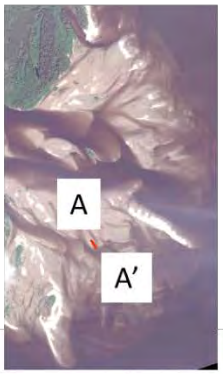

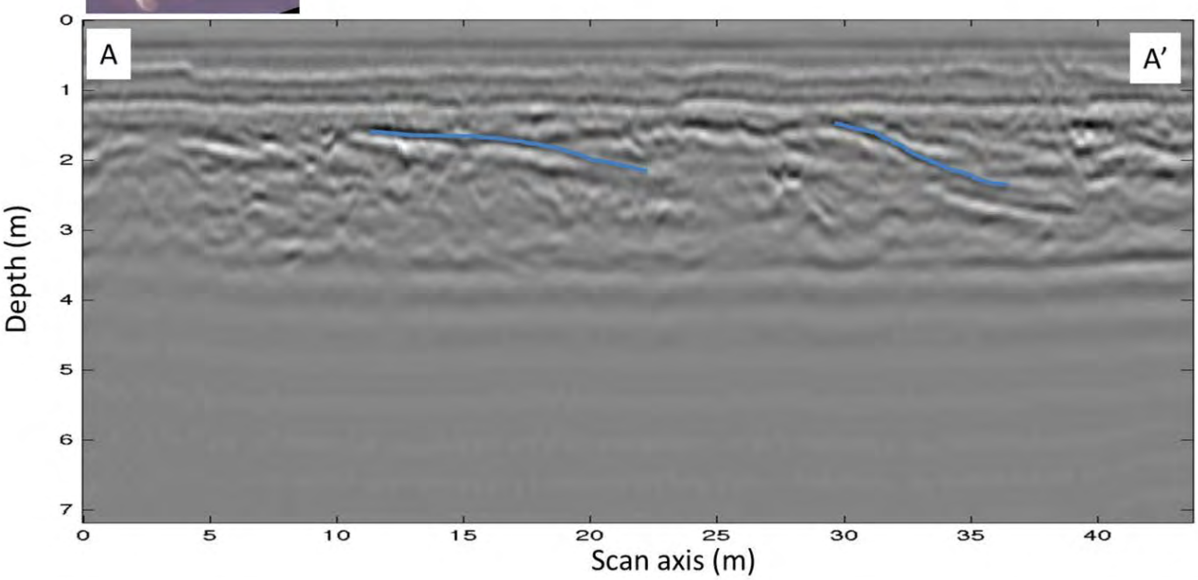

Aug4 Line47
Processing: Dewowed, Bandpass Filtered,
F-K(Stolt) Migration (v=0.6n/s), Depth Conversion
Clinoforms identified in blue

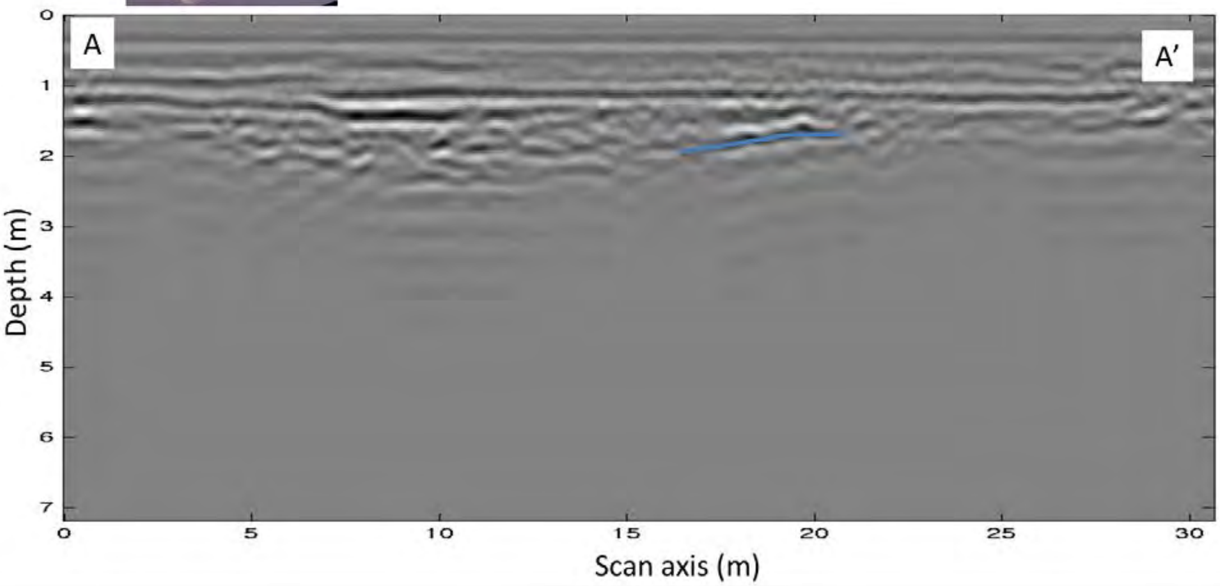

Aug4 Line59
Processing: Dewowed, Bandpass Filtered,
F-K(Stolt) Migration (v=0.6n/s), Depth Conversion
Clinoforms identified in blue

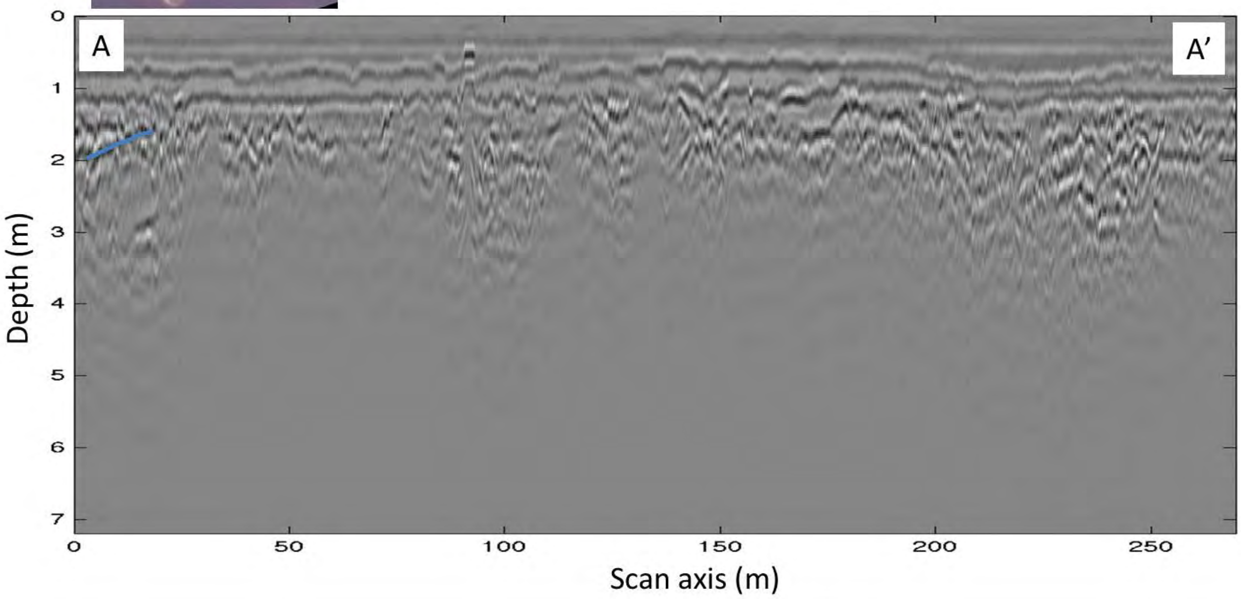

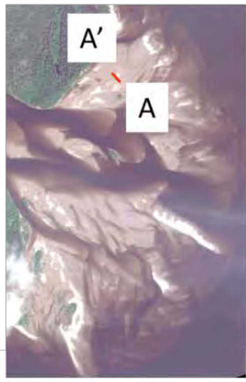

Aug4 Line62
Processing: Dewowed, Bandpass Filtered,
F-K(Stolt) Migration (v=0.6n/s), Depth Conversion
Clinoforms identified in blue

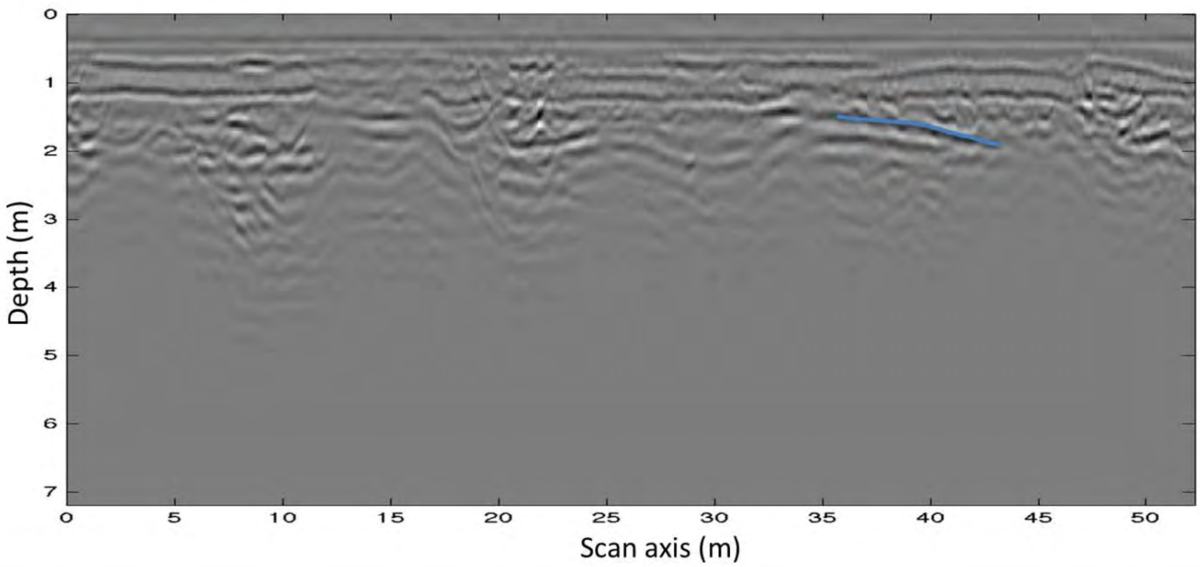

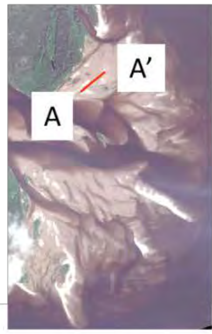

Aug4 Line67
Processing: Dewowed, Bandpass Filtered,
F-K(Stolt) Migration (v=0.6n/s), Depth Conversion
Clinoforms identified in blue

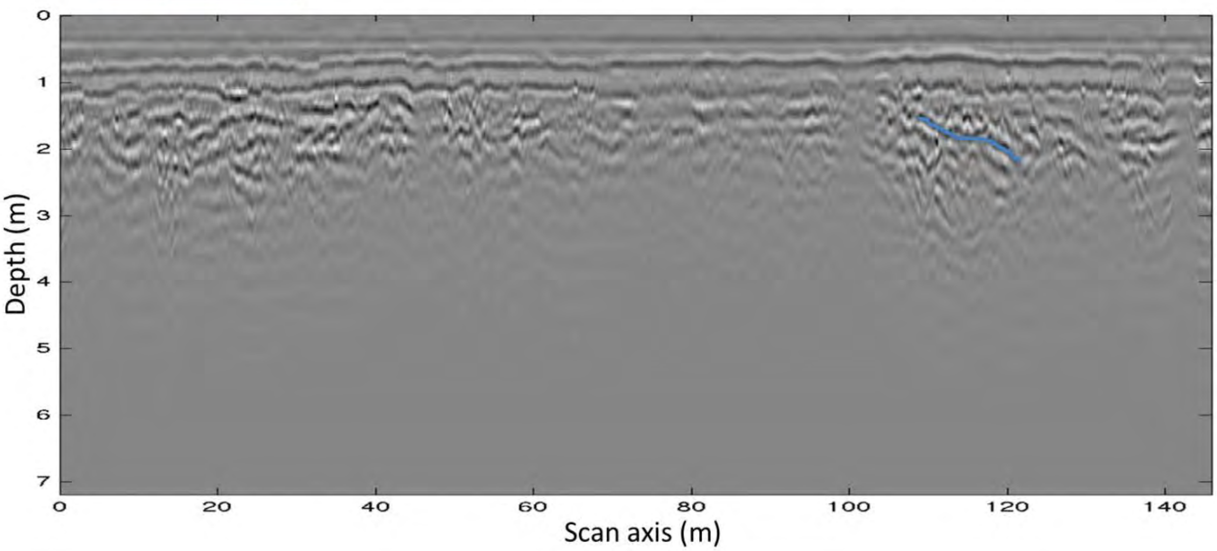

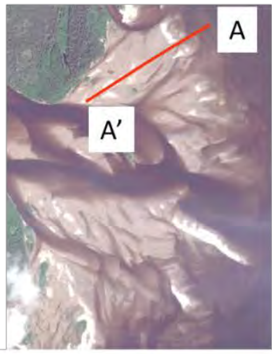

Aug5 Line00
Processing: Dewowed, Bandpass Filtered,
F-K(Stolt) Migration (v=0.6n/s), Depth Conversion
Clinoforms identified in blue

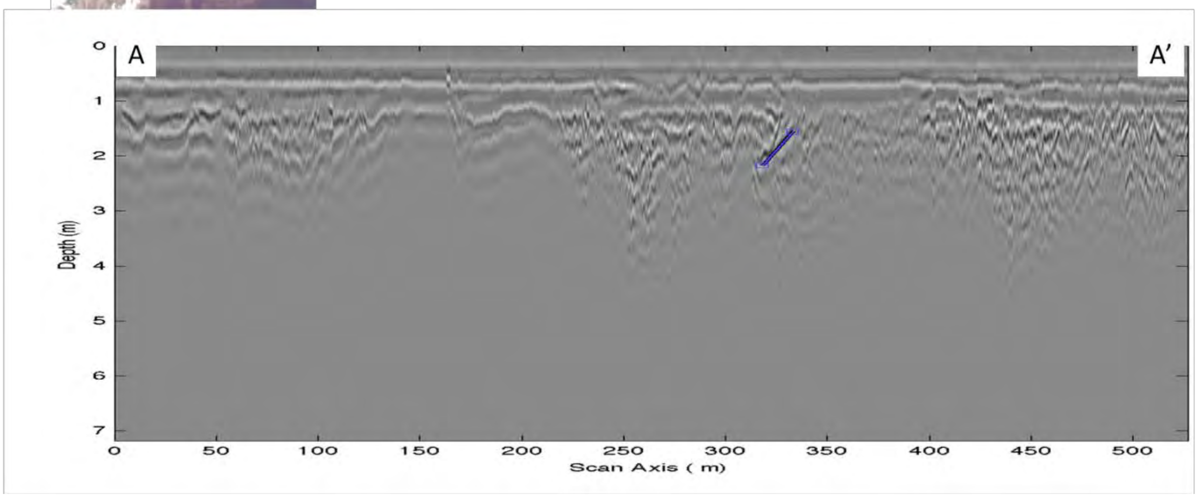

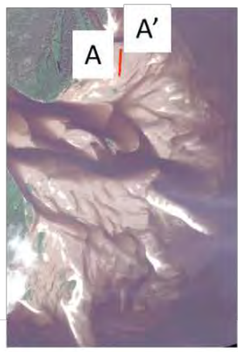

Aug5 Line10
Processing: Dewowed, Bandpass Filtered,
F-K(Stolt) Migration (v=0.6n/s), Depth Conversion
Clinoforms identified in blue

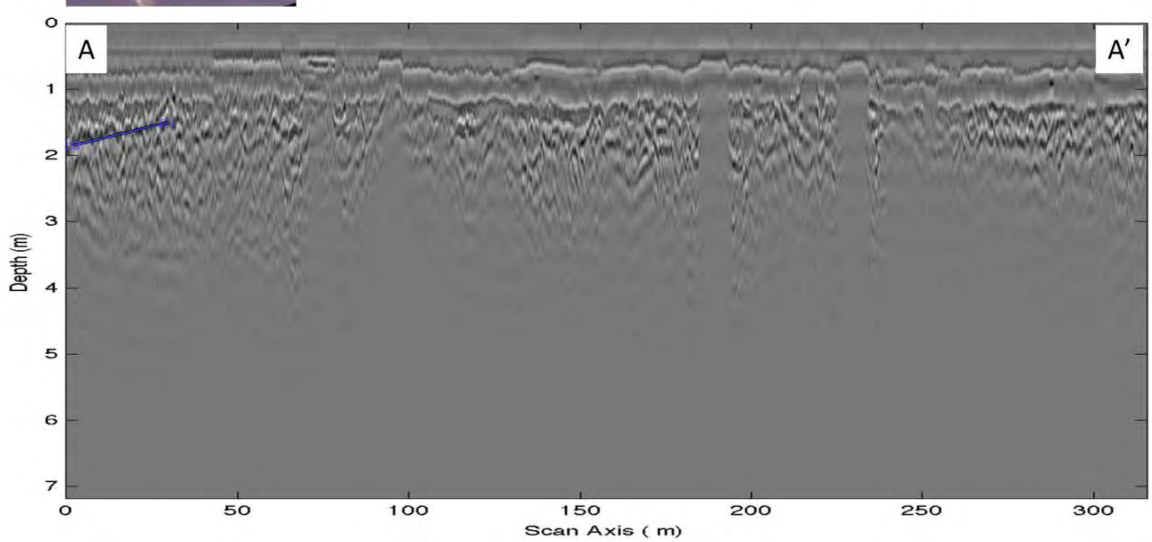

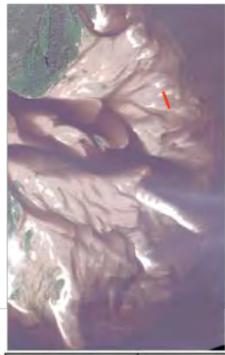

Aug5 Line14
Processing: Dewowed, Bandpass Filtered,
F-K(Stolt) Migration (v=0.6n/s), Depth Conversion
Clinoforms identified in blue

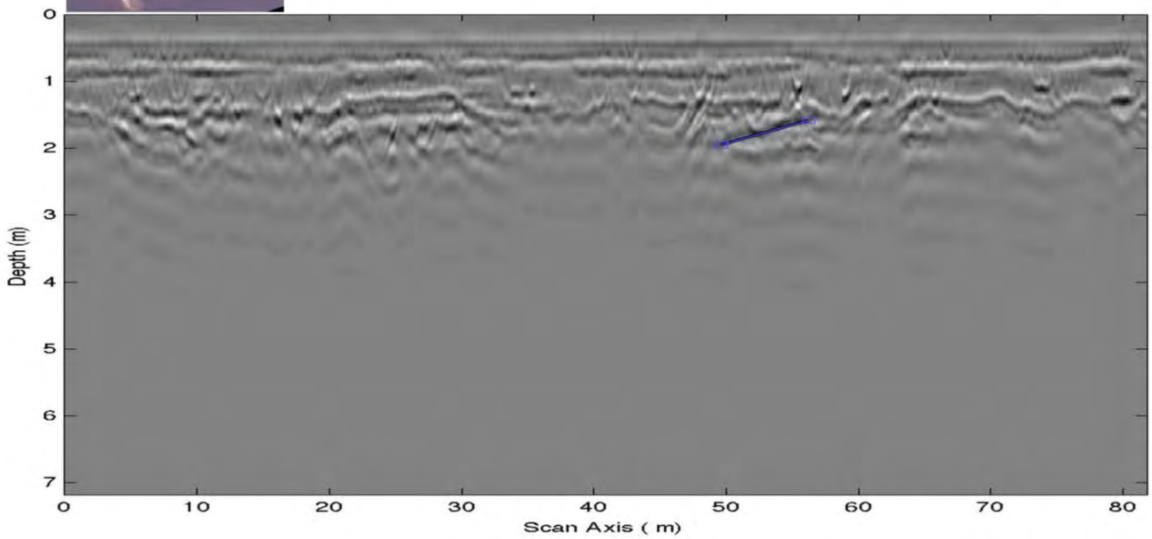

2256

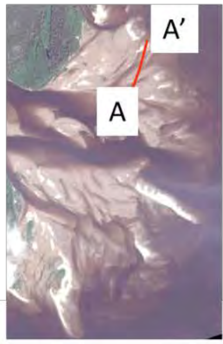

Aug5 Line18
Processing: Dewowed, Bandpass Filtered,
F-K(Stolt) Migration (v=0.6n/s), Depth Conversion
Clinoforms identified in blue

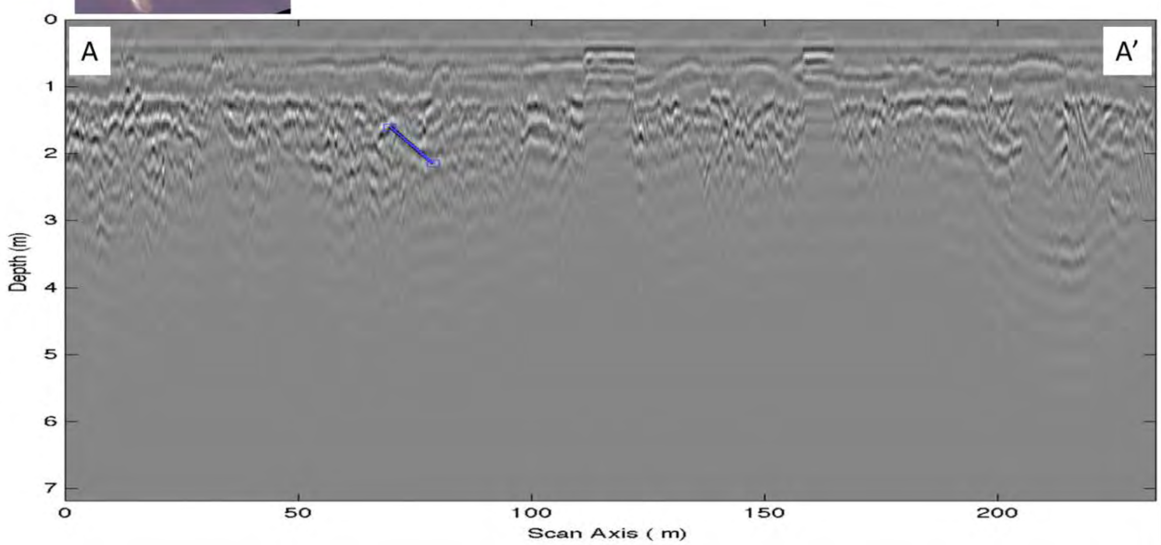

2257

Aug5 Line20
Processing: Dewowed, Bandpass Filtered,
F-K(Stolt) Migration (v=0.6n/s), Depth Conversion
Clinoforms identified in blue

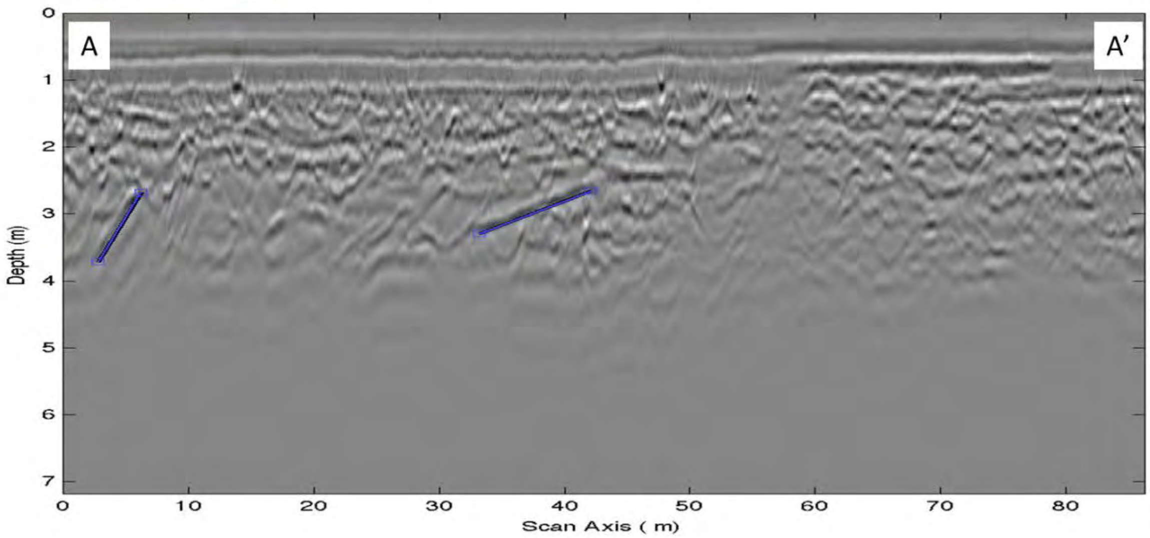

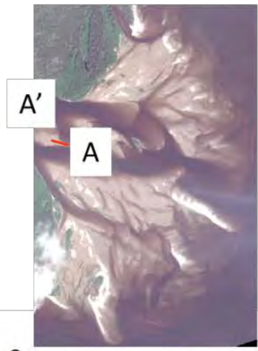

Aug5 Line25
Processing: Dewowed, Bandpass Filtered,
F-K(Stolt) Migration (v=0.6n/s), Depth Conversion
Clinoforms identified in blue

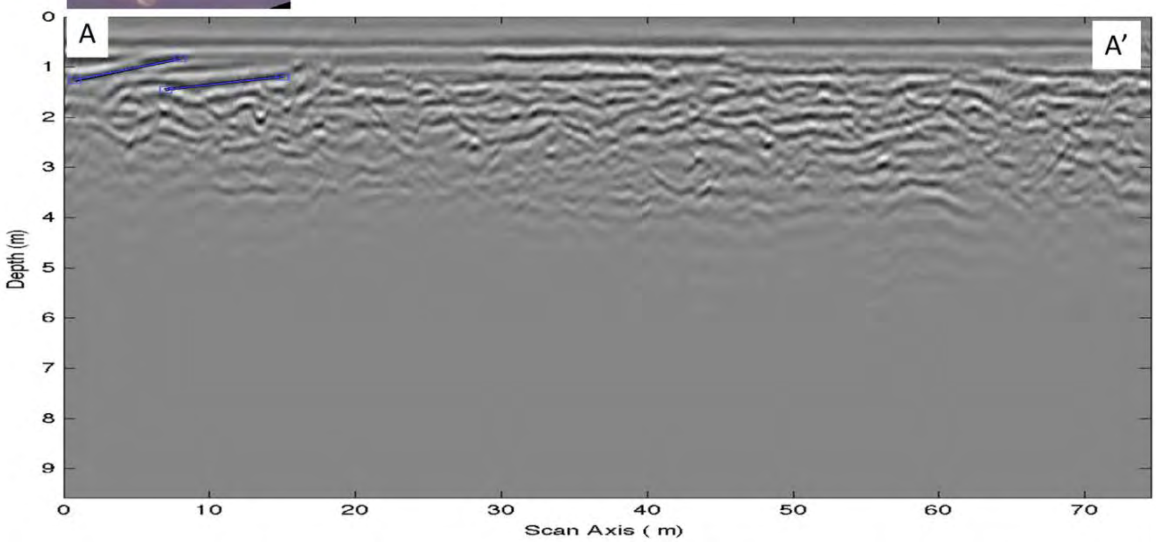

2259

Aug5 Line27
Processing: Dewowed, Bandpass Filtered,
F-K(Stolt) Migration (v=0.6n/s), Depth Conversion
Clinoforms identified in blue

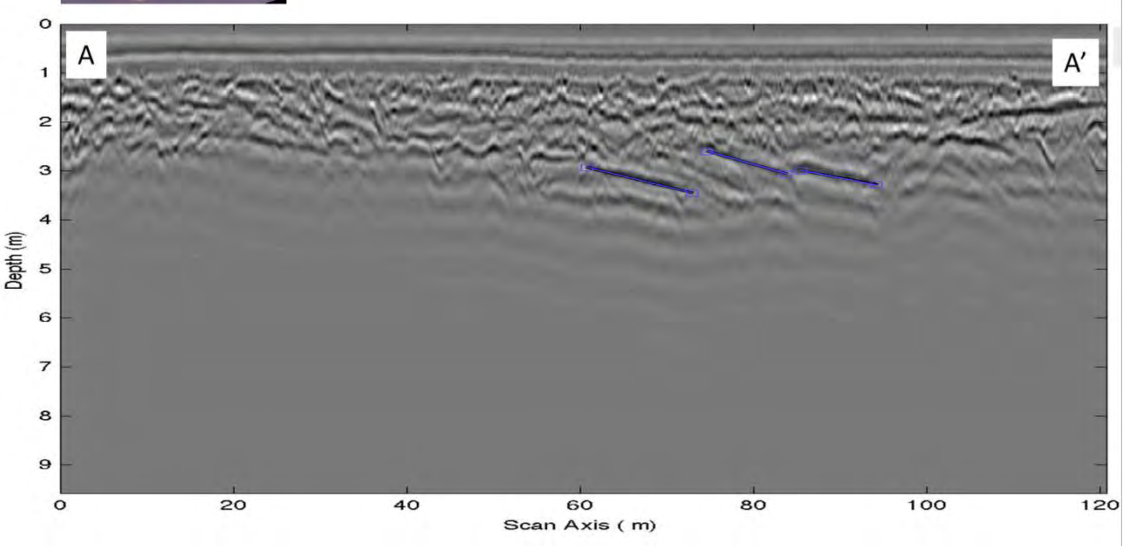

Aug5 Line04
Processing: Dewowed, Bandpass Filtered,
F-K(Stolt) Migration (v=0.6n/s), Depth Conversion
Clinoforms identified in blue

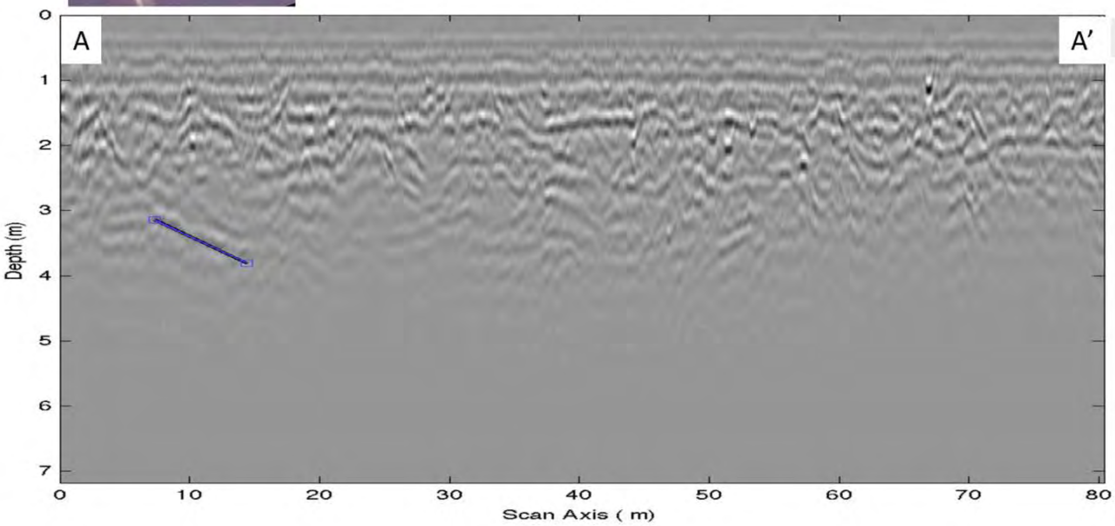

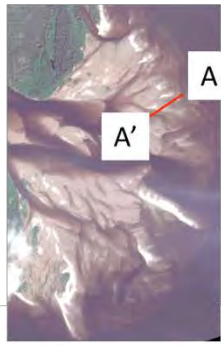

Aug5 Line12
Processing: Dewowed, Bandpass Filtered,
F-K(Stolt) Migration (v=0.6n/s), Depth Conversion
Clinoforms identified in blue

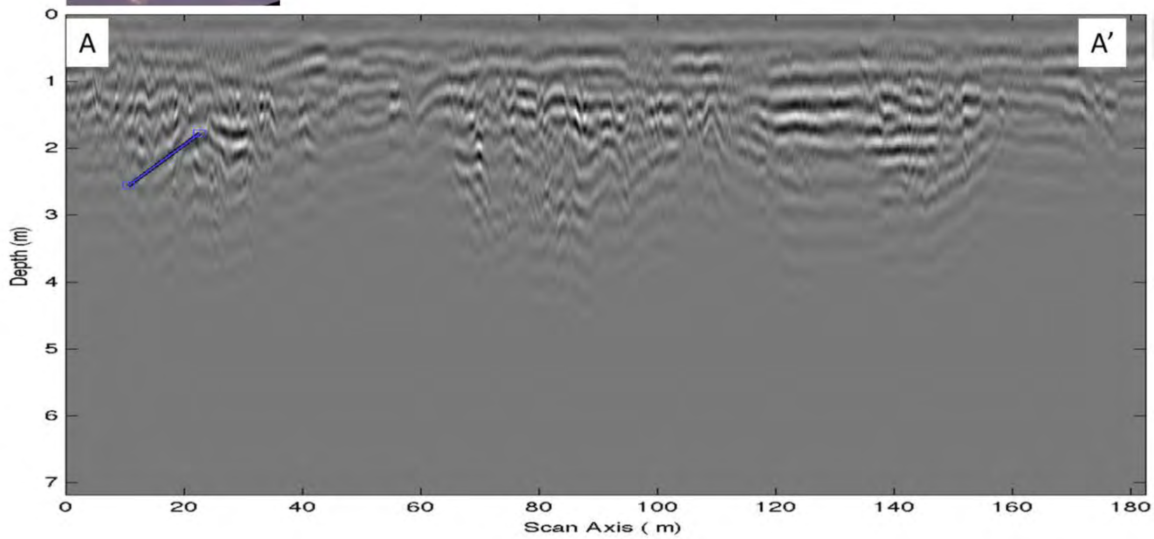

Aug5 Line13
Processing: Dewowed, Bandpass Filtered,
F-K(Stolt) Migration (v=0.6n/s), Depth Conversion
Clinoforms identified in blue

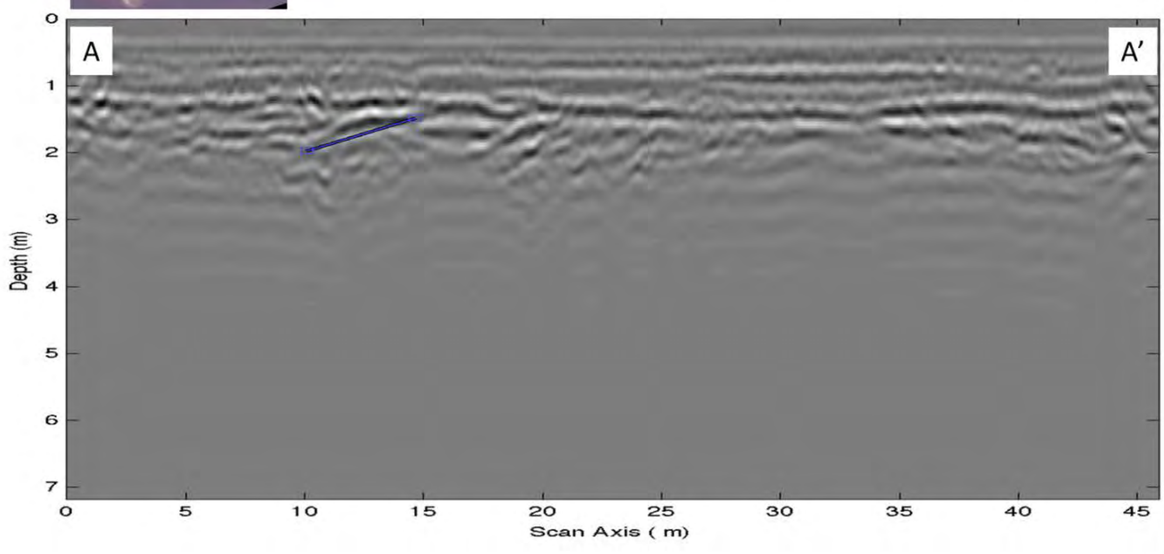

2263

Aug5 Line17
Processing: Dewowed, Bandpass Filtered,
F-K(Stolt) Migration (v=0.6n/s), Depth Conversion
Clinoforms identified in blue

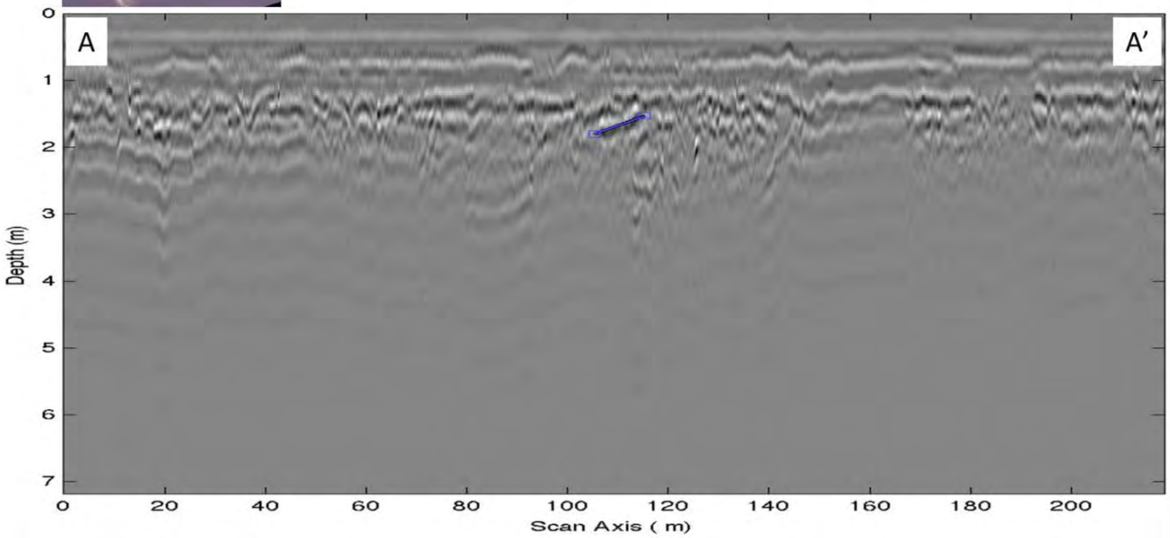

2264

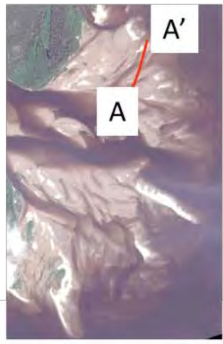

Aug5 Line18
Processing: Dewowed, Bandpass Filtered,
F-K(Stolt) Migration (v=0.6n/s), Depth Conversion
Clinoforms identified in blue

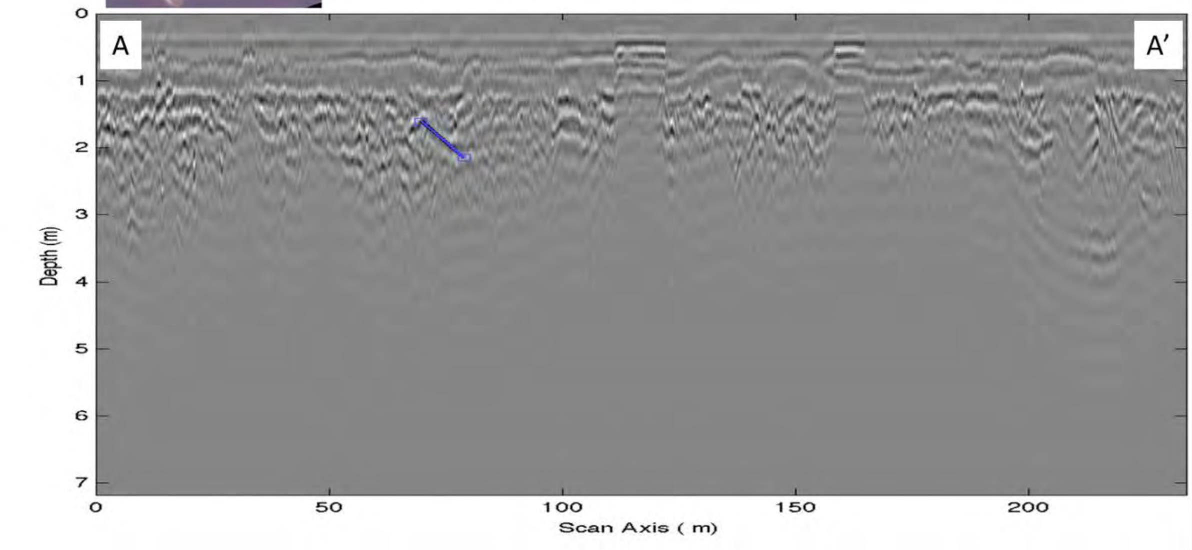

Aug5 Line19
Processing: Dewowed, Bandpass Filtered,
F-K(Stolt) Migration (v=0.6n/s), Depth Conversion
Clinoforms identified in blue

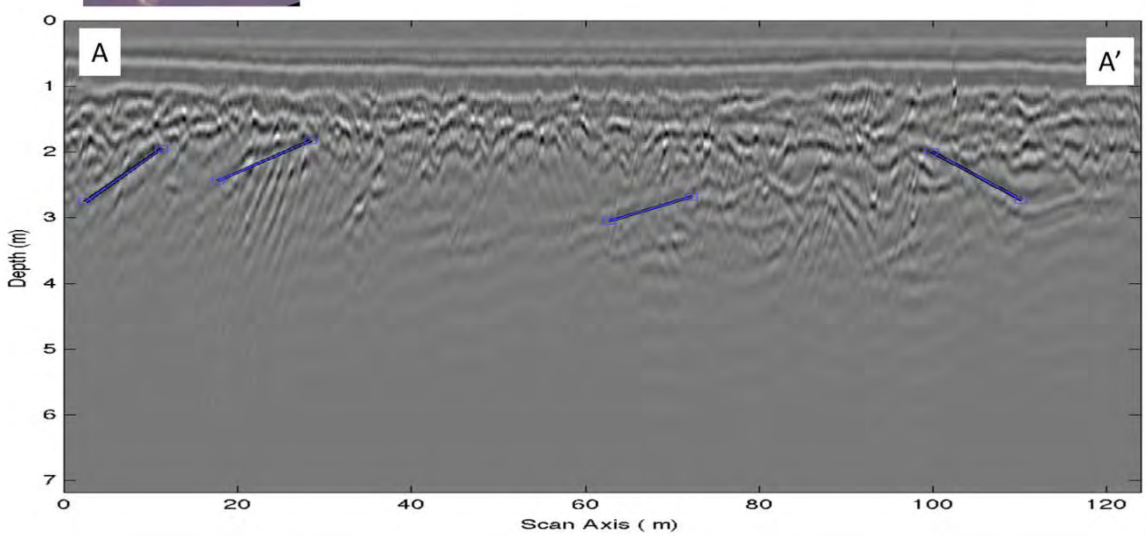

Aug5 Line24
Processing: Dewowed, Bandpass Filtered,
F-K(Stolt) Migration (v=0.6n/s), Depth Conversion
Clinoforms identified in blue

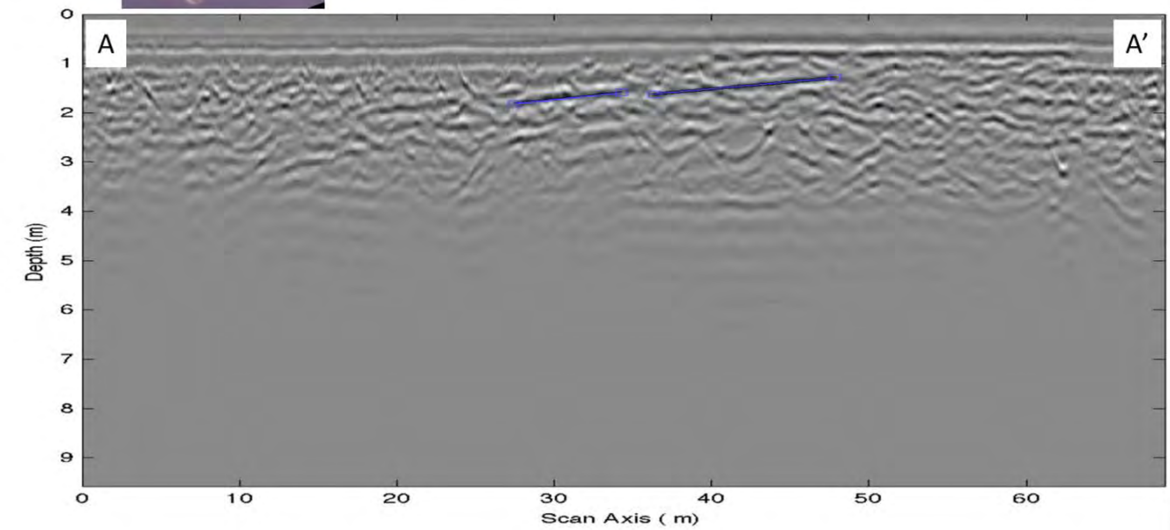

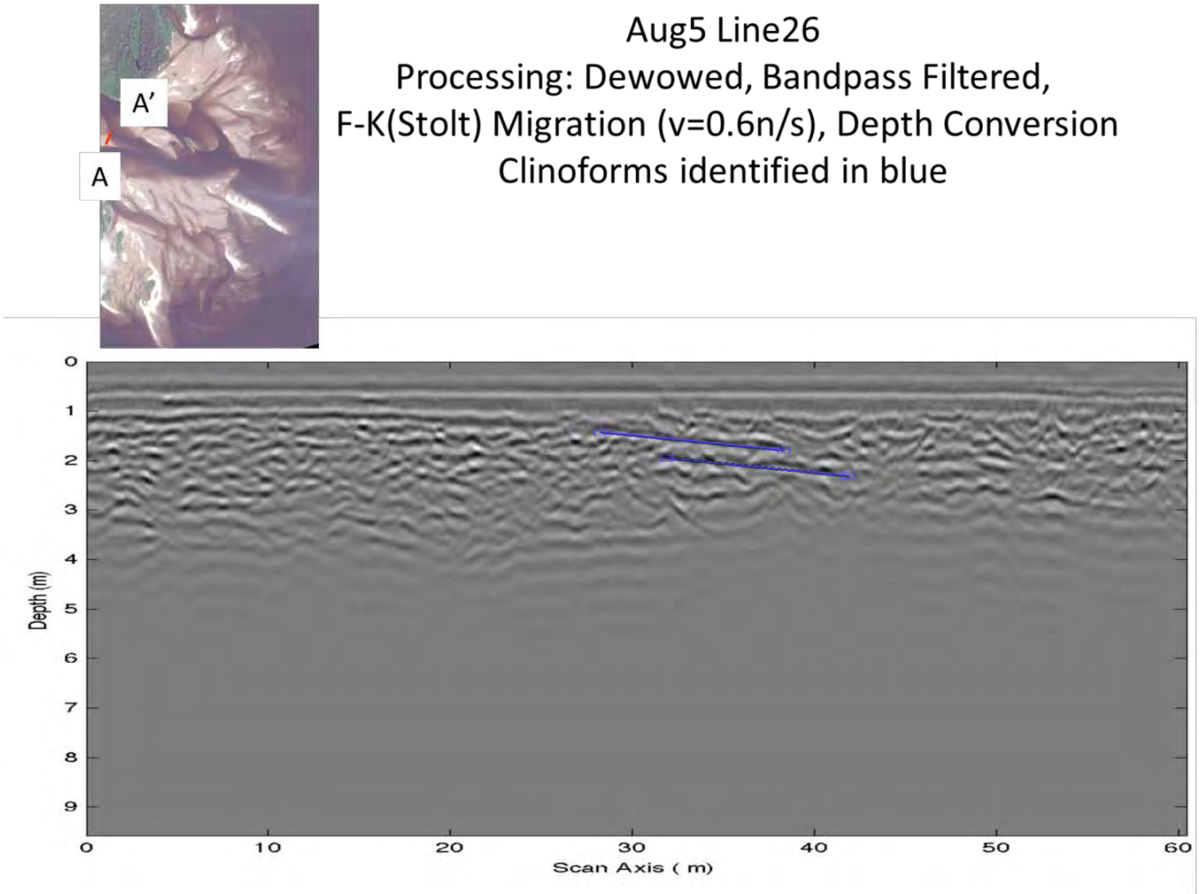
A'
A
Aug5 Line26
Processing: Dewowed, Bandpass Filtered,
F-K(Stolt) Migration (v=0.6n/s), Depth Conversion
Clinoforms identified in blue
Depth (m)
Scan Axis (m)
0
1
2
3
4
5
6
7
8
9
0
10
20
30
40
50
60